NTNU

Norwegian University of
Science and Technology

Control Strategy for AHC Offshore Crane Systems

Solveig Steinsland

Master of Science in Industrial Cybernetics
Submission date: June 2016
Supervisor: Thor Inge Fossen, ITK

Norwegian University of Science and Technology
Department of Engineering Cybernetics

Preface

This is a master's thesis in the course TTK4900 - Engineering Cybernetics, NTNU, which is part of the master's degree programme, Industrial Cybernetics. It was carried out during the fourth semester of this program and corresponds to 30 credits. This thesis was suggested by MacGregor Norway AS, and was defined in cooperation with professor of guidance, navigation and control at Department of Engineering Cybernetics, Thor Inge Fossen. It is an investigation of MacGregor's AHC offshore crane and its control system strategy. The challenge was inspiring and rewarding even though I lacked some of the most relevant subjects regarding the topic. Hence a considerable part of the material had to be learned throughout the semester.

First of all I would like to thank Professor Thor Inge Fossen for his kind and magnificent guidance and supervision during this semester. I would also like to thank discipline lead, Software, Børge Mosgren, project engineer Georg Hafslund and discipline lead, E&I, Maj Paulsen in MacGregor Norway AS for their guidance and contribution in this thesis. Student colleague Emilie Laache deserves plenty of recognition for supporting me in many ways during the whole process of creating this master's thesis. Last but not least my husband, Simon Reinhardtsen, has supported me in a skillful and excellent manner for which I am beyond words grateful.

Trondheim, 2016-06-10

Solveig Steinsland

Abstract

This master's thesis presents a mathematical model of MacGregor's AHC offshore crane and examines control strategies for the crane system. This crane is placed on ships and is designed for safe and accurate offshore and deepwater subsea lifting operations. The objective of the crane is to compensate for the wave impact. Today MacGregor compensate for wave influence in heave direction using the wire only. This decision could be questioned considering the the impact the waves have on the xy-plane, especially when the crane carries out difficult tasks that require high precision. Hence the objective of this thesis is to investigate the possibility of compensating for the movements in the xy-plane with the intention of increasing the value and usability of the crane.

In order to achieve the objective it was necessary to model the crane mathematically and implement it in MATLAB. The next objective was to suggest a variety of control strategies and identify which was most beneficial to the purposes of the crane. In the interest of keeping MacGregor's existing wire compensating system in the future, the heave movements are compensated by the wire only. The control system is compensating for the wave influence on xy-plane and due to the slowness of the crane, the design becomes crucial. Since the desired tasks are specified in the operational space and require precise control of the crane tip motion, it was decided to use operational space control methods. Four different operational space controller methods were chosen and compared. The first two controllers, Jacobian inverse control and Jacobian transpose control, are intuitive and nonmodel–based. The last two controllers, PD control with gravity compensation and Inverse dynamics control, were model–based which meant that the mathematical models were included in the control system. The results implies that the two first controllers, that were nonmodel-based, were not able to compensate for the wave movement in the surge and sway direction , and therefore not recommended for MacGregor. On the other hand, the two last model-based controllers behaved unexpectedly satisfying. Further investigation remains before any certain conclusions can be made, but this thesis provides a solid foundation.

Because there has been no prior investigation of this, a critical approach to the result is appropriate. There are several aspects concerning the outcome that can be associated with uncertainty including some simplifications of the system, potential errors in the crane specifications and not least the fact that it is a theoretical approach. Regardless I am confident they will provide MacGregor with ideas and inspiration on how to improve their system.

Sammendrag

Denne masteroppgaven studerer modellering av og kontrollerstrategi for MacGregor sitt AHC offshore kransystem. Denne kranen er plassert på skip, og er utformet for sikker og nøyaktig offshore og dypvannsløfteoperasjoner. Formålet med kranen er å kompensere for bølgepåvirkningene. I dag kompenserer MacGregor kun for bølgepåvirkningene i z-retning ved hjelp av wire. På grunn av bølgenes påvirkning på xy-planet, spesielt i krevende høypresisjonsoppgaver, kan man stille spørsmål ved denne avgjørelsen. Målet med denne oppgaven er derfor å undersøke muligheten for å kompensere for bevegelser i xy-planet med den hensikt å øke verdien og brukervennlighet til kranen.

For å oppnå formålet var det nødvendig å modellere kranen matematisk og implementere den i MATLAB. Deretter måtte en undersøkelse av kontrollstrategier utføres. Med mål om å beholde MacGregors eksisterende wire kompenserende system kompenseres for bølgepåvirkningene i z-retning med wire. Kontrollsystemet kompenserer for bølgepåvirkningene på xy-planet og, på grunn av kranens treghet, ble utformingen avgjørende. Siden de ønskede oppgaver er spesifisert i arbeidsrommet og krever presis kontroll av bevegelsene til krantuppen, ble det besluttet å bruke arbeidsrom kontrollmetoder. Fire ulike arbeidsrom kontrolleremetoder ble valgt og sammenlignet. De to første kontrollerne, Jacobian inverse control og Jacobian transpose control, var intuitive og ikke modellbaserte. De to siste kontrollerne, PD control with gravity compensation og Inverse dynamics control var modellbaserte, som betydde at de matematiske modellene ble inkludert i kontrollsystemet. Resultatene antyder at de to første kontrollerne, som ikke var modellbaserte, ikke var i stand til å kompensere for bølgepåvirkningene i x og y retning. Dermed ble ikke disse anbefalt for MacGregor. På den annen siden oppførte de to siste modellbaserte kontrollerne seg overraskende tilfredsstillende. Det gjenstår flere studier og arbeid før noen endelig konklusjon kan fattes, men denne avhandlingen gir et solid fundament.

På grunn av manglende studier på området anbefales en kritisk tilnærming til oppgavens resultat. Det er flere faktorer som kan stille spørsmål ved troverdigheten til denne oppgaven. Systemet har visse forenklinger som kan påvirke resultatet, det kan finnes feil i kranspesifikasjonene og det faktum at dette er en teoretisk oppgave kan påvirke utfallet annerledes enn om den fysiske kranen var blitt testet. Uansett er jeg sikker på at oppgaven vil gi MacGregor ideer og inspirasjon til hvordan de kan forbedre deres kontrollsystem.

Contents

List of Figures

List of Tables

Abbreviations

DOF	Degrees of freedom
AHC	Active heave compensation
HPU	Hydraulic power unit
MRU	Motion reference unit
AC	Alternating current
EOM	Equations of Motion
PD	Proportional–derivative

1 Introduction

This chapter explains the motivation for this master's thesis, presents a survey of previous work, describes the problem and defines the limitation for the project. In the end an overview of the entire report is displayed.

1.1 Background and motivation

When it comes to offshore installations there are several challenging factors to consider. The severe sea conditions make it difficult to handle even the smallest tasks. Offshore cranes are often required to handle sensitive payloads without damaging anything or endanger the work environment. The cranes must therefore be designed carefully to perform as desired.

Figure 1.1: MacGregor's AHC offshore crane operating under rough weather conditions. Reproduced with kind permission from MacGregor.

MacGregor Norway AS is a part of the Finnish company Cargotec and has offices in Kristiansand, Norway. They deliver equipment for handling marine cargoes and offshore payloads in addition to their equipment service. Because the active heave compensated (AHC) offshore crane investigated in this thesis is custom made, it is flexible in its use (see Figure 1.1).

This thesis will examine MacGregor's active boost type of AHC subsea crane, which is placed on ships and is designed for safe and accurate offshore and deepwater subsea lifting operations. The crane's objective is to compensate for the wave impact on the crane in heave direction. This function is in use when the most sensitive and important tasks are done. Figure 1.1 illustrates the importance of an advanced and precise control system in order to achieve a desired outcome.

In 2014 and 2015 I worked as a summer intern for MacGregor and it was during this time they asked me to write this thesis. MacGregor's motivation for giving me this thesis is to investigate whether the control system for their offshore crane can be improved. In addition the time spent in their software department made me reflect on their existing system. Their hydraulic nonlinear offshore crane system has made them decide to exclusively compensate with the wire, compensating for wave impact on heave only, because the slowness of the crane makes it hard to compensate for the fast-moving waves. Additionally they argue with the natural water dampening on the payload when placed on the bottom of the ocean. Despite these factors I have decided to investigate whether they should compensate for the wave impact on the xy-plane or not. My purpose with this investigation is to:

- Increase the crane's operative hours
- Widen the number of applications in which can use the compensation system
- Ensure a more safe and accurate payload handling

In this thesis I will examine if MacGregor can increase the value of their offshore cranes by implementing a more complex compensating system.

1.2 Previous work

There has never been done any investigation on whether MacGregor should control their AHC offshore cranes in all of the degrees of freedom, which is the reason they asked me to do it. However a former NTNU student in the Department of Marine Technology, Pål Guttorm Syvertsen, has studied the same crane investigated in this thesis. Even though he had a different objective he also described the crane mathematically. His thesis has been of inspiration in the mathematical part, although there has been made some adjustments.

1.3 Contribution and scope

MacGregor challenged me to find ways of improving their crane system for the Active Boost type AHC offshore crane for my master's thesis. The problem defining this master's thesis is:

Is it beneficial to compensate for the wave impact on a offshore crane placed on a ship in surge and sway direction in addition to the existing AHC system? If so, what controller strategy is the best choice in regard to efficiency, safety and cost?

In order to answer these questions the crane system will be mathematically modeled and different controller designs will be implemented to achieve a desirable result. The work needed to be done in this thesis is therefore:

- Literature study on modeling and control of robot manipulators
- Describe the crane specifications
- Derive a mathematical model for an active heave compensated (AHC) crane onboard a ship and implement it in MATLAB/Simulink
- Investigate methods for controlling the AHC offshore crane and its payload. The ship motions in surge and sway should be minimized during heave compensation
- Implement and simulate the different controller strategies and compare them
- Which controller strategy should be recommended for the company in regard to stability, efficiency and cost?

The natural step after reading this thesis is to compare the recommended control system design with MacGregor's existing control system, and try to implement it in their system. Subsequent the choice of controller design becomes crucial. First of all the controller must be applicable for the company. Secondly the improvements must be efficient enough to be appreciated and implemented despite its cost. Safety of the personnel and the equipment must also be taken into consideration.

1.4 Project limitations

On the grounds that there were limited time for this thesis and other physical restrictions, the following simplifications and limitations were set

- The cable is modeled as stiff when it actually is flexible
- The crane is modeled as a rigid-body system though the crane is softer than a rigid body
- The drum is simplified
- Friction is neglected
- Dimensions may have some deviations from the actual crane
- The whole process is done in MATLAB/Simulink and not inside a real life crane

The last bullet is of course vital. There were on the other hand significant advantages to simply implement and tune the different controllers on my own computer in Trondheim. In this way I could avoid destroying expensive offshore cranes, it was faster than doing it in a physical crane and I was able to benefit from the knowledge at NTNU. Figure 1.2 shows the pier in Kristiansand where some of their cranes are produced. As one can see from the picture it would have been risky trying out new control system designs there.

Figure 1.2: The pier in Kristiansand where some of their cranes are produced. As the picture illustrates it would have been risky testing out new control system designs here. Reproduced with kind permission from Mac-Gregor.

These limitations were necessary to set in order to achieve any useful result through this one-semester thesis, and are important to keep in mind while reading this thesis in order to get a proper perspective.

1.5 Organization

Figure 1.3 gives an overview of the crane system investigated. It shows the system's components and where to find it in the report. As displayed the control system compensates for the deviations in surge, x, and sway, y, direction. The wire drum compensates for the deviations in heave, z, direction.

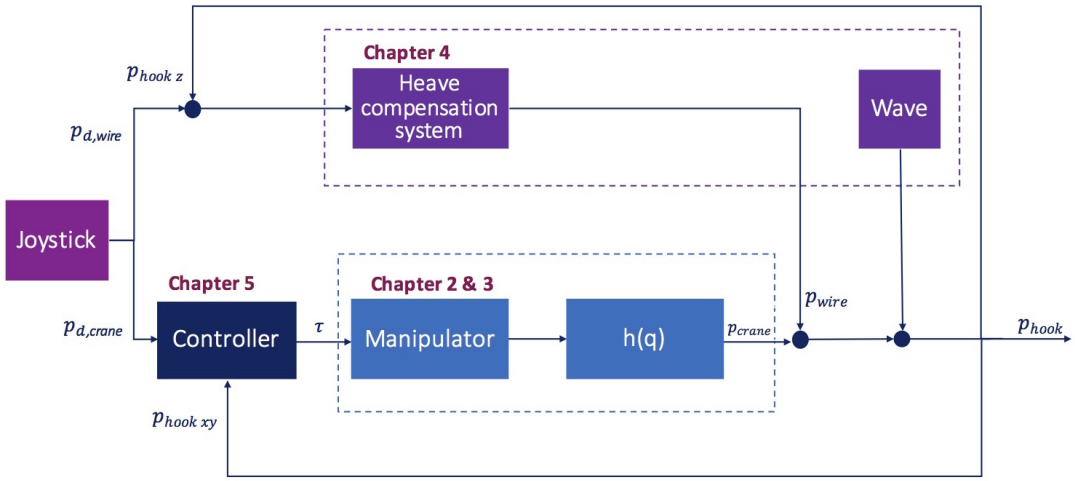

Figure 1.3: A description of the overall system examined in this thesis. The z-position of the hook is controlled by the wire compensating system (upper part of the figure), while the xy-position is controlled by the chosen control system strategy.

Chapter 2 contains notations and definitions for this thesis, a description of the crane investigated and the mathematical derivations of the crane. The last part of the mathematical modeling of the crane is derived in Chapter 3 and it gives the equations of motion. All of these mathematical derivations were implemented in the Simulink system as illustrated in Figure 1.3.

Chapter 4 includes the heave compensation system and the irregular wave disturbance affecting the crane on all of the degrees of freedom.

The controller strategies are presented in Chapter 5 and these are compensating for the

wave influence upon the xy-plane. Four different operational space controller systems are presented and all of the choices made in the controlling part are included. The simulations of these controllers in addition to the heave compensating part and a robustness analysis are included in the results chapter (6).

Closing discussions, a conclusion, advice for further studies and recommendations for MacGregor are included in the conclusion chapter(7).

2 Crane Modeling

The objective of this chapter is to describe and mathematically derive the crane investigated. At first some notations and definitions are included. Later on the different specifications of the crane are presented. The rest of this chapter contains relevant mathematical definitions and derivations such as position and orientation, rotation matrices, homogeneous transformations and kinematics.

2.1 Notations and definitions

In robot modeling theory several different notations are used. For that reason it's important to establish notations before investigating further. The table before Chapter 1, named Abbreviations, shows the different abbreviations used later on in the thesis. Figure 2.1 illustrates the crane on board a ship and the ship's six degrees of freedom. Table 2.2 shows the crane's six degrees of freedom and it's notations while Table 2.1 includes the motion variables vectors. Some mathematically abbreviations were used in this thesis for simplicity's sake and are included in Table 2.3.

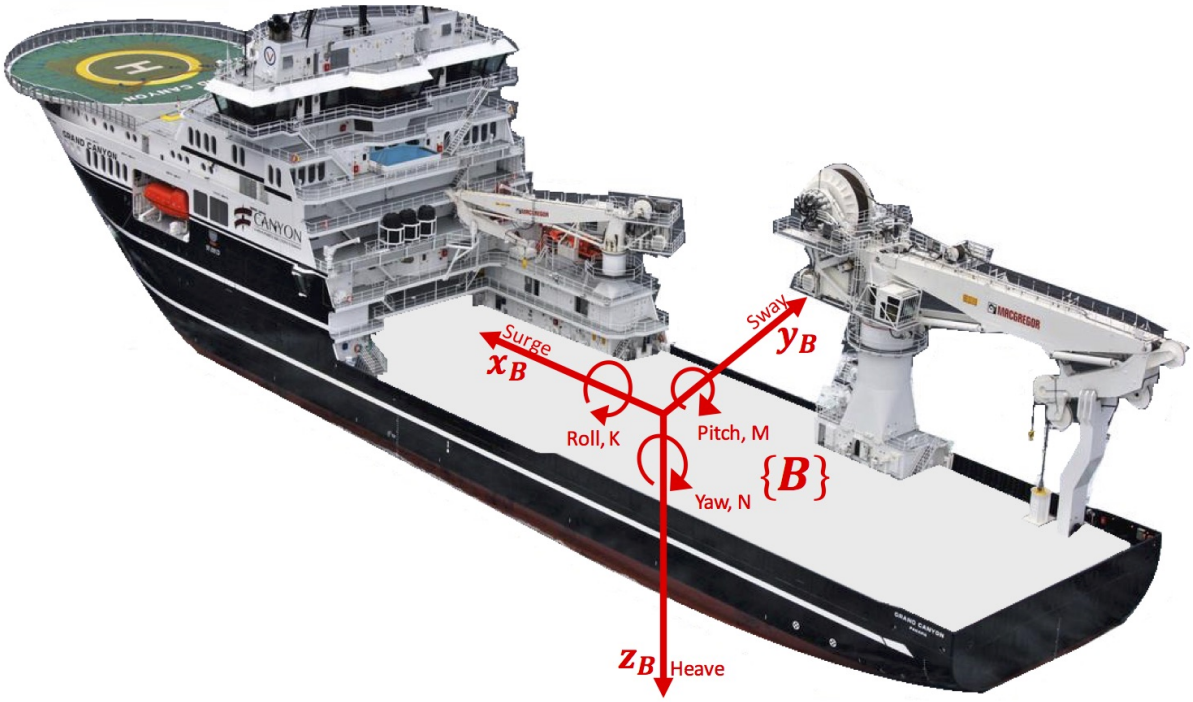

Figure 2.1: The crane on board a ship with the ship's motion in six degrees of freedom.

Table 2.1: Motion variables vectors used in thesis.

NED Position:	$\boldsymbol{p}^n = \begin{bmatrix} x \\ y \\ z \end{bmatrix}$	Orientation (Euler angles):	$\boldsymbol{\theta}_b^o = \begin{bmatrix} \boldsymbol{\phi} \\ \boldsymbol{\theta} \\ \boldsymbol{\psi} \end{bmatrix}$
Body-fixed linear velocity:	$\boldsymbol{v}^f = \begin{bmatrix} u \\ v \\ w \end{bmatrix}$	Body-fixed angular velocity:	$\boldsymbol{\omega} = \begin{bmatrix} p \\ q \\ r \end{bmatrix}$
Body-fixed force:	$\boldsymbol{f}_b^b = \begin{bmatrix} X \\ Y \\ Z \end{bmatrix}$	Body-fixed moment:	$\boldsymbol{m}_b^n = \begin{bmatrix} K \\ M \\ N \end{bmatrix}$

$\boldsymbol{q}_i$ represents the robot manipulator variable and the set of joint variables are represented as $\boldsymbol{q} = [q_1, q_2, ..., q_n]^T$. For the crane investigated there are three joint variables, q_1, q_2 and q_3 which give the vector $\boldsymbol{q} = [q_1\ q_2\ q_3]^T$. These joint variables can be seen in the following section in Figure 2.3. The coordinate system are written as $O_i - x_i y_i z_i$ where i defines the frame number and x_i, y_i and z_i are the corresponding unit vectors. The $O_0 - x_0 y_0 z_0$ frame is termed **base frame** and the frame attached to the end effector is called the **end effector frame**.

Figure 2.2: MacGregor's crane with it's end effector labeled. Reproduced with kind permission from Mac-Gregor.

End effector is specified according to the task the robot shall execute. For material handling tasks, the end effector is constituted by a gripper of proper shape and dimensions determined by the object to grasp. In this thesis the end effector is specified to be the crane tip illustrated in Figure 2.2.

Table 2.2: Notations of the crane's six DOF variables.

Degree of Freedom	**Forces and moments**	**Linear angular velocities**	**Position and Euler angles**
Surge, translation in the x-direction	X	u	x
Sway, translation in the y-direction	Y	v	y
Heave, translation in the z-direction	Z	w	z
Roll, rotation about the x-axis	K	p	ϕ
Pitch, rotation about the y-axis	M	q	θ
Yaw, rotation about the z-axis	N	r	ψ

Table 2.3: Mathematical abbreviations and simplifications used in thesis.

c_1	$=$	$\cos(q_1)$
s_1	$=$	$\sin(q_1)$
c_2	$=$	$\cos(q_2)$
s_2	$=$	$\sin(q_2)$
c_3	$=$	$\cos(q_3)$
s_3	$=$	$\sin(q_3)$
c_{23}	$=$	$\cos(q_2 + q_3)$
s_{23}	$=$	$\sin(q_2 + q_3)$
$\sin(\alpha + \beta)$	$=$	$\sin(\alpha)\cos(\beta) + \cos(\alpha)\sin(\beta)$
$\cos(\alpha + \beta)$	$=$	$\cos(\alpha)\cos(\beta) - \sin(\alpha)\sin(\beta)$
1	$=$	$\sin^2(\alpha) + \cos^2(\alpha)$

2.2 Crane design

This section presents different specifications of the crane that are the basis for the mathematical modeling and the simulation. It includes a description of the crane, the actuators used and the cranes limitations.

2.2.1 Crane description

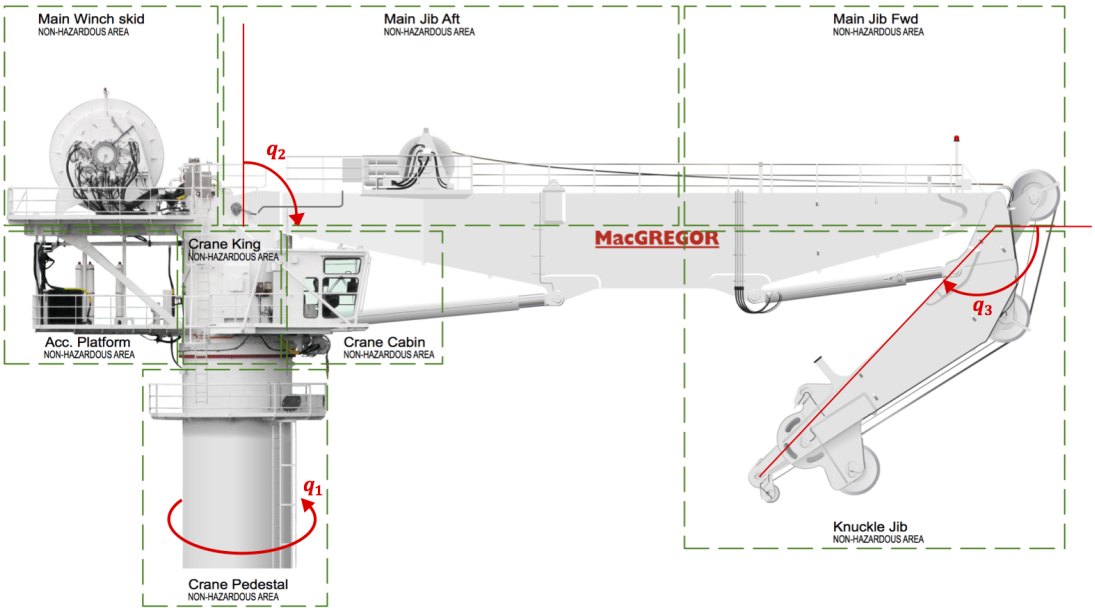

Figure 2.3: A description of MacGregor's AHC active boost crane (HMC 3568 LKO) with the three revolute joints q_1, q_2 and q_3. Reproduced with kind permission from MacGregor.

The crane investigated is MacGregor's HMC 3568 LKO crane. It is an active heave compensated crane uses the AHC technique, which reduces the influence of wave disturbance upon the offshore operation. The goal is for the payload to be motionless with regard to the seabed when difficult and sensitive tasks are to be done (Scantrol, 2015). MacGregor uses Kongsberg Maritime's MRU H to detect the ships motions in all directions. The datasheet for this MRU is included in Appendix C. They have a control system programmed in Siemens SIMATIC STEP 7 to calculate how the system should react to the movements. Unfortunately MacGregor did not have any satisfying description document of this control system which is why it is not included in this thesis. Hence this thesis will investigate the control system for the crane with clean slates. The control system's

design is essential to the cranes performance and should be optimized in an intelligent way. With this in mind the objective of this thesis is clear. Figure 2.3 shows this crane and now the structure of the crane will be described.

A manipulator, like the crane investigated, can either be structured as an open kinematic chain or as a closed kinematic chain. A closed kinematic chain is when a sequence of links forms a loop, which is not the case for this crane. On the other hand the open kinematic chain is defined as one sequence of links connecting the two ends of the chain which is the case for the crane investigated.

The joints between the links are essential for a manipulator to be mobile and they can either be revolute or prismatic. For an open kinematic chain both the revolute and the prismatic joint gives a single degree of mobility and one degree of freedom(DOF). The revolute joint is rotational and the prismatic joint is linear which means that the rotational joint is often preferred because of it's reliability and compactness. The crane presented in this thesis has an anthropomorphic geometry which consists of three revolute joints (Crowder, 2016). Since all of the joints are revolute this structure is the most dexterous one. The three joints can be seen in Figure 2.3 and Figure 2.4 as q_1, q_2 and q_3.

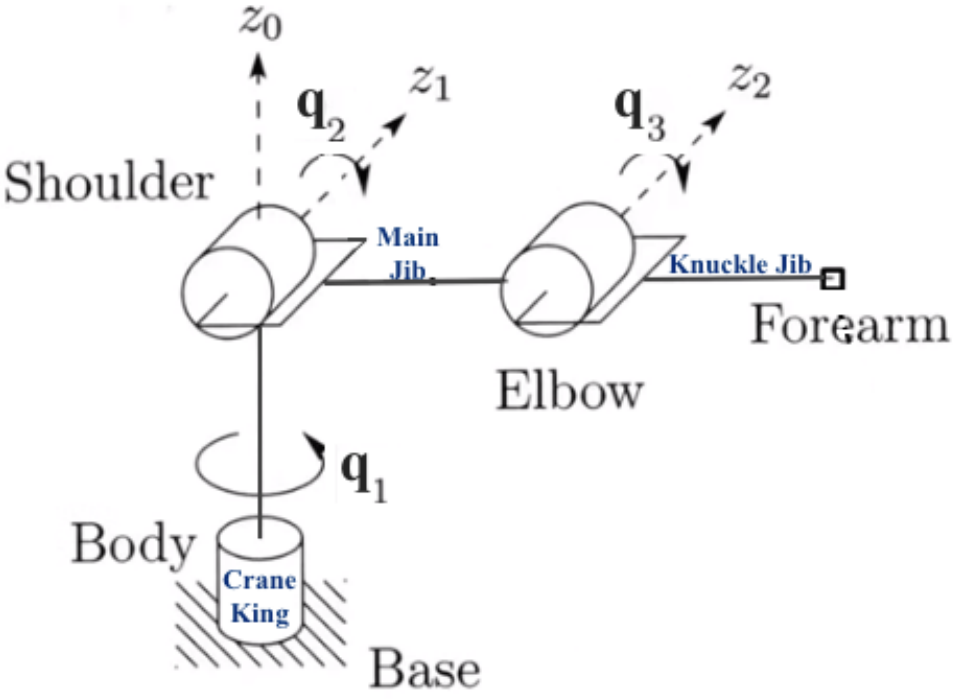

Figure 2.4: The crane's three revolute joints, q_1, q_2 and q_3. As the drawing illustrates the first joint is perpendicular on the two other joints.

The revolute axis of joint q_1 is orthogonal to the axes of q_2 and q_3 which are in parallel. In the offshore crane industry the link between q_2 and q_3 is called the main jib and the link between q_3 and the end effector is called the knuckle jib due to its similarity to the human leg. In robot manipulator theory joint q_2 is called shoulder joint and q_3 elbow joint due to its similarity to the human arm where the main jib is the arm and the knuckle jib is the forearm. For the crane investigated the joints movement are actuated by a hydraulic power unit.

In a three dimensional space an object is required to have six DOF, three for positioning and three for orientation. If more available DOF the manipulator is said to be redundant (Sciavicco and Siciliano, 1996). This system has these six degrees of freedom so it is not redundant.

The dimensions of the HMC 3568 LKO crane needed to model it was found by investigating the AutoCAD drawing illustrated in appendix A and are shown in Table 2.4 and in Appendix B.

Table 2.4: The crane dimensions used in this thesis.

Length, king	l_1	9.3 m
Length, main jib	l_2	24.0 m
Length, knuckle jib	l_3	13.3 m
Radius, king	r_1	1.8 m
Height, main jib	h_2	2.0 m
Height, knuckle jib	h_3	1.5 m
Depth, main jib	d_2	1.9 m
Depth, main jib	d_3	1.0 m
Mass, king	m_1	168.5 kg
Mass, main jib	m_2	130.0 kg
Mass, knuckle jib	m_3	69.5 kg

Now some of the basic information is given in order to derive the mathematical model of the crane. The following section gives information of the power given to the defined joint angles and it's limitations. The section after gives information of the physical joint angle limitations.

2.2.2 Actuators

There are four electrical motors all operating their own hydraulic pump on the HPU. Each and one of these motors are 550 kW AC motors driven by a 690 Voltage AC three phase supply. The motors run at 1 789 rpm loaded and are described further in the datasheet in Appendix D. The torque limitations are defined by these four electrical motors and can be calculated like this (**?**)

$$\tau = \frac{P_W \cdot 9.549}{n} \qquad \Rightarrow \qquad \tau = \frac{550\text{kW} \cdot 9.549}{1789\text{rpm}} = 2.936\text{kNm}, \tag{2.1}$$

where τ = torque [Nm], P_W = power [W] and n = revolution per minute [rpm]

These torque limitations were set in as limitation on each of the three torque variables (τ_1, τ_2 and τ_3) in the controllers with a saturation block.

2.2.3 Crane limitations

The crane's physical limitations is given in Table 2.5. As the results in Appendix E are showing the limitations would only affect controller 1 and 2. As a consequence of the bad behavior of the these controllers and little time the limitations were not included in the Simulink file.

Table 2.5: Crane limitations.

Joint	**Orientation [deg]**	**Angular velocity [deg/s]**	**Angular acceleration [deg/s^2]**
1	[0, 360]	6	2
2	[0, 86]	1	0.5
3	[-155, -37]	2	1

2.3 Position and orientation

A rigid body is completely described in space by its position and orientation with respect to a reference frame. Figure 2.5 illustrates the crane system with it's different joint angles and coordinate systems. Here $\{O\}$ represent the reference frame with $\boldsymbol{x}_0$, $\boldsymbol{y}_0$ and $\boldsymbol{z}_0$ as unit vectors.

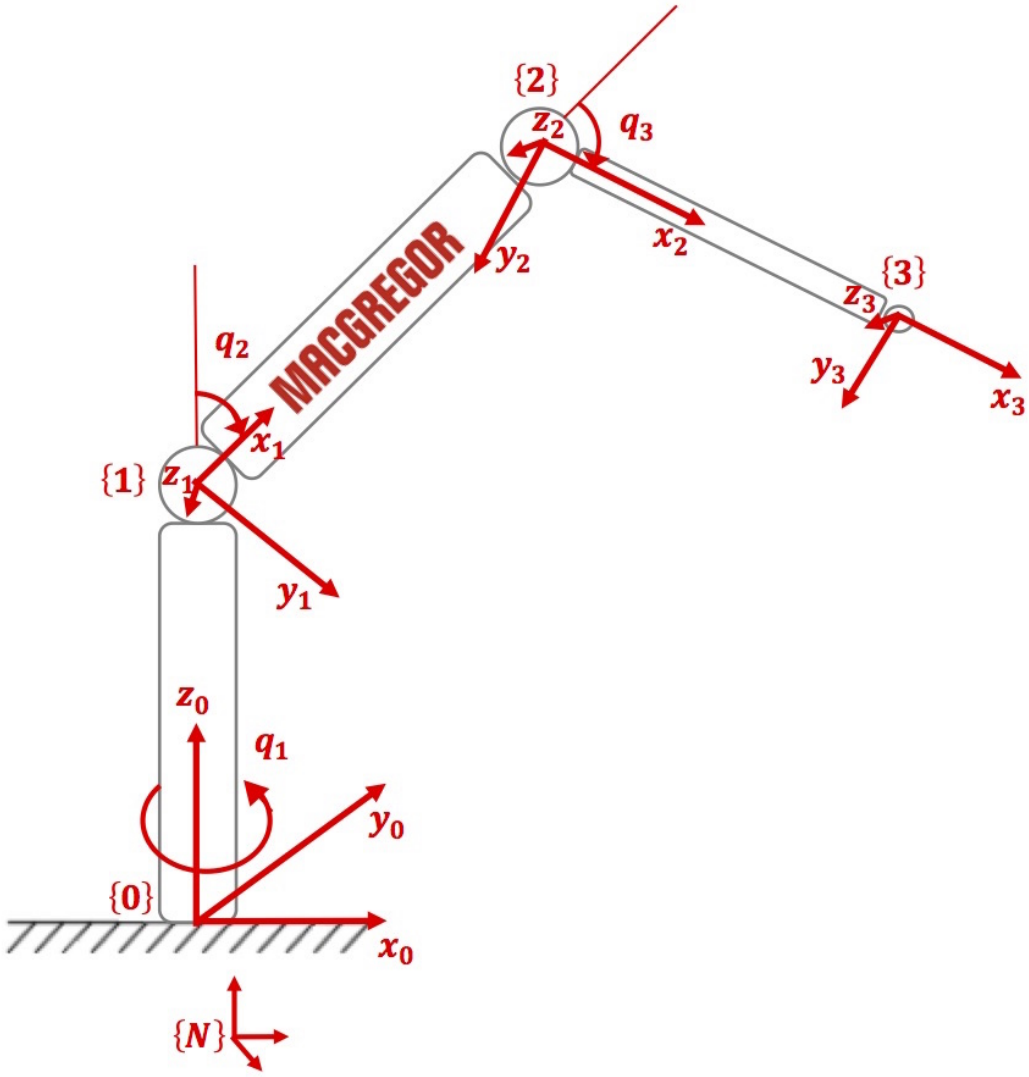

Figure 2.5: The crane with the different joints and frames. Frame $\{0\}$ is called the base frame while frame $\{3\}$ is the end effector frame.

The position of a point at the rigid body, O', is then defined:

$$\boldsymbol{o'} = o'_x\boldsymbol{x} + o'_y\boldsymbol{y} + o'_z\boldsymbol{z}, \qquad \boldsymbol{o'} = \begin{bmatrix} o'_x \\ o'_y \\ o'_z \end{bmatrix} \tag{2.2}$$

The orientation with respect to the reference frame can be expressed by the vectors x', y' and z':

$$\boldsymbol{x'} = x'_x\boldsymbol{x} + x'_y\boldsymbol{y} + x'_z\boldsymbol{z} \tag{2.3}$$

$$\boldsymbol{y'} = y'_x\boldsymbol{x} + y'_y\boldsymbol{y} + y'_z\boldsymbol{z} \tag{2.4}$$

$$\boldsymbol{z'} = z'_x\boldsymbol{x} + z'_y\boldsymbol{y} + z'_z\boldsymbol{z} \tag{2.5}$$

MacGregor's crane's end effector position can be given by the $6x1$ vector $\boldsymbol{x}$, where the three first elements are the $\boldsymbol{p}$ vector which represent the position and the three last elements are the orientation vector $\boldsymbol{\Theta}$ which represent the orientation (see Table 2.1).

$$\boldsymbol{p} = \begin{bmatrix} x \\ y \\ z \end{bmatrix} \quad \text{and} \quad \boldsymbol{\Theta} = \begin{bmatrix} \phi \\ \theta \\ \psi \end{bmatrix} \quad \text{giving} \quad \boldsymbol{x} = \begin{bmatrix} \boldsymbol{p} \\ \boldsymbol{\Theta} \end{bmatrix} \tag{2.6}$$

Figure 2.6 illustrates the six DOF of the ship and is included here as well in order to understand the end effector's six DOF. The surge is the first element, x, sway is the second element, y, and heave is the third element of $\boldsymbol{p}$, z. Roll (rotation about x-axis) is the first element, K , pitch (rotation about y-axis) is the second element, M, and yaw (rotation about z-axis) is the third element, N, of $\boldsymbol{\theta}$.

In other words $\boldsymbol{x}$ is defined in the space where the crane operations are specified in, hence it's called operation space. Workspace, which is a subcategory of operation space, is illustrated in Figure 2.7. This is described by the end effector when all the joints execute all possible motions.

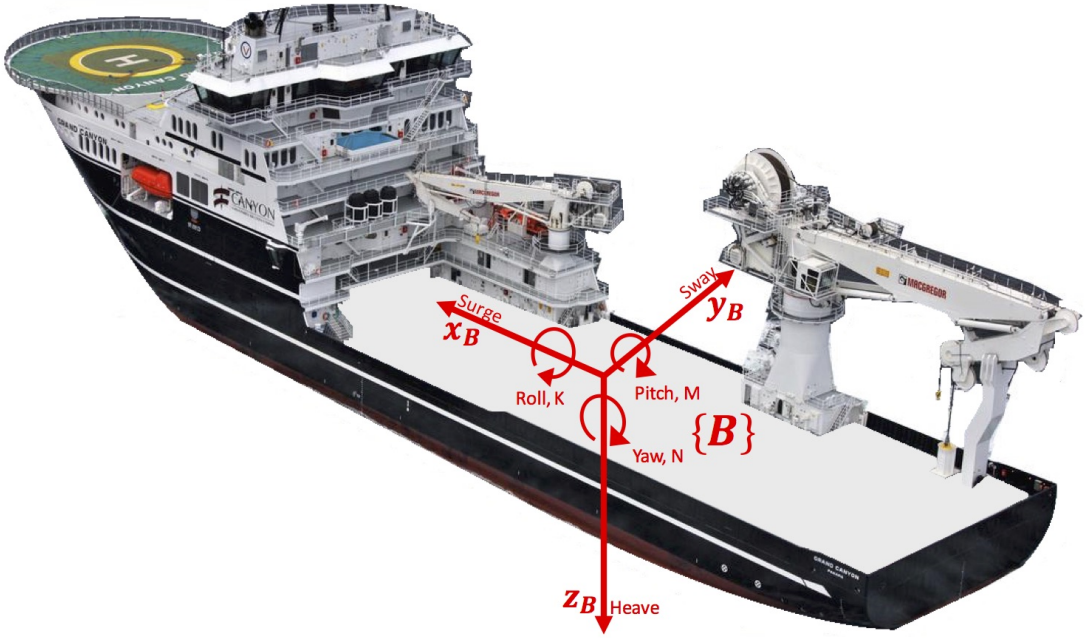

Figure 2.6: The crane on board a ship with the ship's motion in six degrees of freedom.

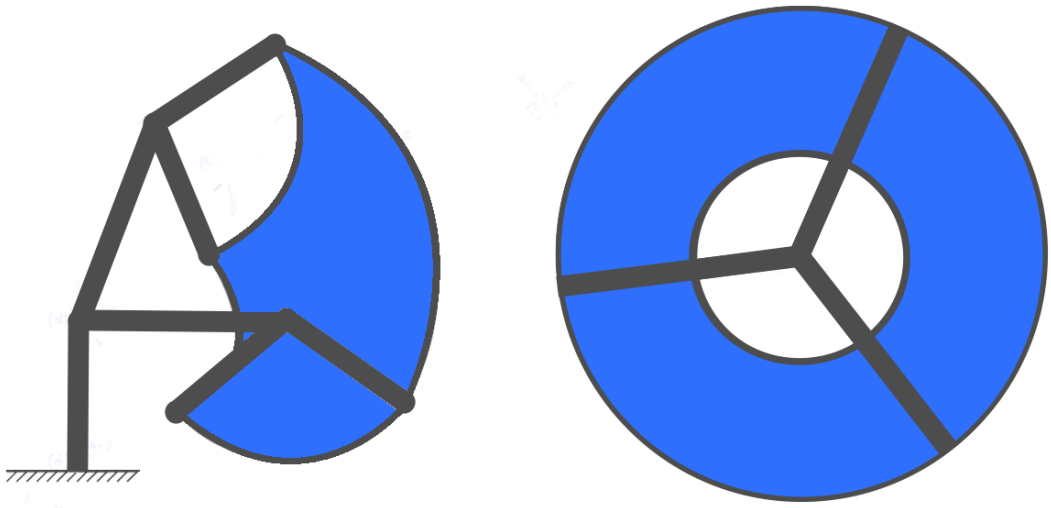

Figure 2.7: The crane's work space is marked with the color blue. The left Figure shows the crane's work space in profile and the right Figure shows it from above.

2.4 Rotation matrices

To be able to find the homogeneous transformation matrices the rotation matrices must be derived. This section gives first a short description of the fundamental rotation matrix theory before the rotation matrices for the crane are derived.

A rotation matrix is a matrix used to perform a rotation in Euclidean space. This rotation matrix is represented by three unit vectors (2.3)–(2.5) combined in the 3x3 rotation matrix:

$$\boldsymbol{R} = \begin{bmatrix} x' & y' & z' \end{bmatrix} = \begin{bmatrix} x'_x & y'_x & z'_x \\ x'_y & y'_y & z'_y \\ x'_z & y'_z & z'_z \end{bmatrix} = \begin{bmatrix} \boldsymbol{x}'^T\boldsymbol{x} & \boldsymbol{y}'^T\boldsymbol{x} & \boldsymbol{z}'^T\boldsymbol{x} \\ \boldsymbol{x}'^T\boldsymbol{y} & \boldsymbol{y}'^T\boldsymbol{y} & \boldsymbol{z}'^T\boldsymbol{y} \\ \boldsymbol{x}'^T\boldsymbol{z} & \boldsymbol{y}'^T\boldsymbol{z} & \boldsymbol{z}'^T\boldsymbol{z} \end{bmatrix} \tag{2.7}$$

The column vectors of $\boldsymbol{R}$ are mutually orthogonal since they represent the unit vectors of an orthonormal frame (2.8) and they have unit norm (2.9).

$$\boldsymbol{x}'^T\boldsymbol{y}' = 0 \qquad \boldsymbol{y}'^T\boldsymbol{z}' = 0 \qquad \boldsymbol{z}'^T\boldsymbol{x}' = 0 \tag{2.8}$$

$$\boldsymbol{x}'^T\boldsymbol{x}' = 1 \qquad \boldsymbol{y}'^T\boldsymbol{y}' = 1 \qquad \boldsymbol{z}'^T\boldsymbol{z}' = 1 \tag{2.9}$$

This results in $\boldsymbol{R}$ beeing an orthogonal matrix:

$$\boldsymbol{R}^T\boldsymbol{R} = \boldsymbol{I} \qquad\qquad \boldsymbol{R}^T = \boldsymbol{R}^{-1} \tag{2.10}$$

Now suppose that the reference frame $O - xyz$ is rotated α degrees about the x-axis. $O - x'y'z'$ is the new frame and this gives the unit vectors

$$\boldsymbol{x}' = \begin{bmatrix} 1 \\ 0 \\ 0 \end{bmatrix} \qquad \boldsymbol{y}' = \begin{bmatrix} 0 \\ \cos\alpha \\ \sin\alpha \end{bmatrix} \qquad \boldsymbol{z}' = \begin{bmatrix} 0 \\ -\sin\alpha \\ \cos\alpha \end{bmatrix} \tag{2.11}$$

which results in the rotation matrix of frame $O - x'y'z'$ with respect to $O - xyz$

$$\boldsymbol{R}_x(\alpha) = \begin{bmatrix} 1 & 0 & 0 \\ 0 & \cos\alpha & -\sin\alpha \\ 0 & \sin\alpha & \cos\alpha \end{bmatrix} \tag{2.12}$$

The same procedure can be done for rotations about the y-axis (angle β) and the z-axis (angle γ) which gives the rotation matrices:

$$\boldsymbol{R}_y(\beta) = \begin{bmatrix} \cos\beta & 0 & \sin\beta \\ 0 & 1 & 0 \\ -\sin\beta & 0 & \cos\beta \end{bmatrix} \qquad \boldsymbol{R}_z(\gamma) = \begin{bmatrix} \cos\gamma & -\sin\gamma & 0 \\ \sin\gamma & \cos\gamma & 0 \\ 0 & 0 & 1 \end{bmatrix} \tag{2.13}$$

If all of the basic rotations are done one total rotation matrix can be defined:

$$\begin{aligned} \boldsymbol{R} =& \boldsymbol{R}_z(\gamma)\boldsymbol{R}_y(\beta)\boldsymbol{R}_x(\alpha) \\ =& \begin{bmatrix} c_\gamma c_\beta & c_\gamma s_\beta s_\alpha - s_\gamma c_\alpha & c_\gamma s_\beta c_\alpha + s_\gamma s_\alpha \\ s_\gamma c_\beta & s_\gamma s_\beta s_\alpha + c_\gamma c_\alpha & s_\gamma s_\beta c_\alpha - c_\gamma s_\alpha \\ -s_\beta & c_\beta s_\alpha & c_\beta c_\alpha \end{bmatrix} \end{aligned} \tag{2.14}$$

where $c_\gamma = \cos(\gamma)$, $s_\beta = \sin(\beta)$ and so on. This rotation is expressed in Euler angles ZYX and is obtained by rotations with respect to the fixed frame $O - xyz$.

For the sake of explaining the rotation matrices the illustration of the position and the orientation of the crane is presented again in Figure 2.8. By investigating this Figure one can now, with the needed knowledge, derive the different rotation matrices in (2.15)–(2.17). The rotation matrix of frame $\{1\}$ with respect to $\{0\}$ is as following

$$\boldsymbol{R}_1^0 = \begin{bmatrix} c_1 & 0 & s_1 \\ s_1 & 0 & -c_1 \\ 0 & 1 & 0 \end{bmatrix} \tag{2.15}$$

and the rotation matrix of frame $\{2\}$ with respect to $\{0\}$ is

$$\boldsymbol{R}_2^0 = \boldsymbol{R}_1^0 \boldsymbol{R}_2^1 = \begin{bmatrix} c_1c_2 & -c_1s_2 & -s_1 \\ c_2s_1 & -s_1s_2 & c_1 \\ -s_2 & -c_2 & 0 \end{bmatrix} \tag{2.16}$$

and finally the rotation matrix of frame {3} with respect to {0} is

$$\boldsymbol{R}_3^0 = \boldsymbol{R}_1^0 \boldsymbol{R}_2^1 \boldsymbol{R}_3^2 = \begin{bmatrix} c_1c_2c_3 - c_1s_2s_3 & c_1c_2s_3 - c_1c_3s_2 & -s_1 \\ s_1c_2c_3 - s_1s_2s_3 & s_1s_3c_2 - s_1s_2c_3 & c_1 \\ -s_2c_3 - c_2s_3 & s_2s_3 - c_2c_3 & 0 \end{bmatrix} \tag{2.17}$$

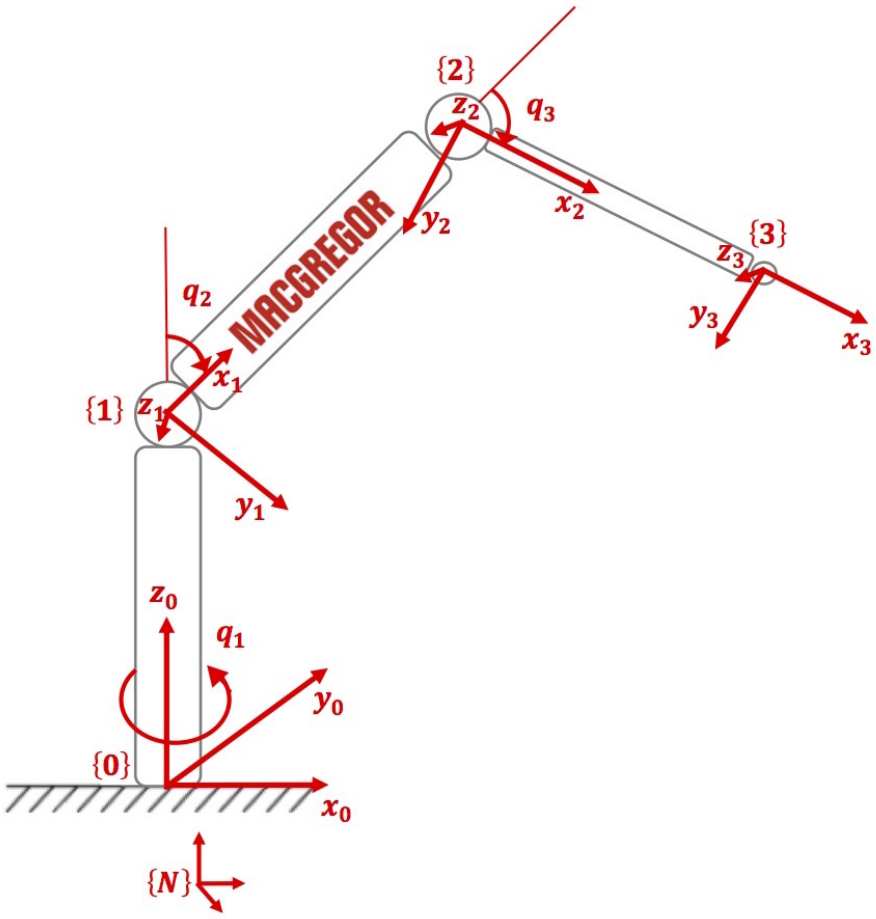

Figure 2.8: The crane with the different joints and frames. Frame {0} is called the base frame while frame {3} is the end effector frame.

2.5 Homogeneous transformations

The coordinate transformation is both the translation and the rotation put together and is defined in (2.18). Here the p^0 is the vector coordinates of P (which is an arbitrary point in space) with respect to frame 0. p^1 on the other hand is the vector coordinates of P with respect to frame 1. The origin of frame 1 with respect to frame 0 is described by o_1^0 and the rotation matrix of frame 1 with respect to frame 0 is R_1^0. Frame 0, frame 1, vector p^0 and vector p^1 can be seen in Figure 2.9. By simple mathematics the inverse transformation can be obtained as illustrated in (2.19) and (2.20).

$$\boldsymbol{p}^0 = \boldsymbol{o}_1^0 + \boldsymbol{R}_1^0 \boldsymbol{p}^1 \tag{2.18}$$

$$\boldsymbol{p}^1 = -\boldsymbol{R}_1^{0T} \boldsymbol{o}_1^0 + \boldsymbol{R}_1^{0T} \boldsymbol{p}^0 \tag{2.19}$$

$$\boldsymbol{p}^1 = -\boldsymbol{R}_0^1 \boldsymbol{o}_1^0 + \boldsymbol{R}_1^0 \boldsymbol{p}^0 \tag{2.20}$$

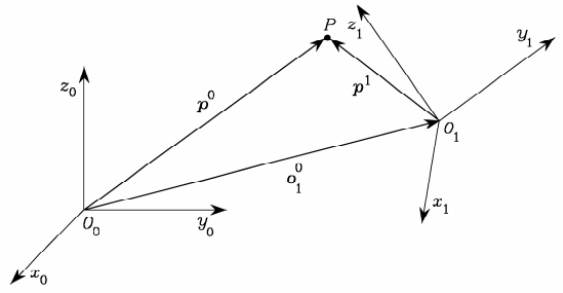

Figure 2.9: Representation of P in different coordinate systems.

$\tilde{\boldsymbol{p}}$ is **the homogeneous representation** of a generic vector $\boldsymbol{p}$ and is formed by adding a fourth unit component. This is done to achieve a compact representation of the relationship between the coordinates of one point in two different frames.

$$\tilde{\boldsymbol{p}} = \begin{bmatrix} \boldsymbol{p} \\ 1 \end{bmatrix} \tag{2.21}$$

The homogeneous transformation matrix is the coordinate transformation in form of a $4x4$ matrix and can be seen in (2.22).

$$\boldsymbol{A}_1^0 = \begin{bmatrix} \boldsymbol{R}_1^0 & \boldsymbol{o}_1^0 \\ \boldsymbol{0}^T & 1 \end{bmatrix} \tag{2.22}$$

By examine Figure 2.8 one can easily observe that the distance from the origin of frame $\{0\}$ to the origin of frame $\{1\}$ can be described by the vector $\boldsymbol{o}_1^0 = \begin{bmatrix} 0 & 0 & l_1 \end{bmatrix}^T$ where l_1 is the length of the crane king. $\boldsymbol{R}_1^0$ is the rotation matrix of frame $\{1\}$ with respect to frame $\{0\}$ presented in 2.15 and $\mathbf{0}^T$ is a $3x3$ vector containing only zero-elements. The homogeneous transformation matrices will be further derived in Section 2.7.1.

The homogeneous transformation matrix (2.22) gives the possibility to compactly rewrite (2.18):

$$\tilde{\boldsymbol{p}}^0 = \boldsymbol{A}_1^0 \tilde{\boldsymbol{p}}^1 \tag{2.23}$$

$\tilde{\boldsymbol{p}}^1$ and $\boldsymbol{A}_0^1$ are obtainend as shownn in (2.24) and (2.25).

$$\tilde{\boldsymbol{p}}^1 = \boldsymbol{A}_0^1 \tilde{\boldsymbol{p}}^0 = (\boldsymbol{A}_1^0)^{-1} \tilde{\boldsymbol{p}}^0 \tag{2.24}$$

$$\boldsymbol{A}_0^1 = \begin{bmatrix} \boldsymbol{R}_1^{0T} & -\boldsymbol{R}_1^{0T} \boldsymbol{o}_1^0 \\ \mathbf{0}^T & 1 \end{bmatrix} = \begin{bmatrix} \boldsymbol{R}_0^1 & -\boldsymbol{R}_0^1 \boldsymbol{o}_1^0 \\ \mathbf{0}^T & 1 \end{bmatrix} \tag{2.25}$$

Notice that in general for the homogeneous transformation matrix the orthogonality property doesn't hold:

$$\boldsymbol{A}^{-1} \neq \boldsymbol{A}^T \tag{2.26}$$

A sequence of coordinate transformations can be calculated easily (Sciavicco and Siciliano, 1996):

$$\tilde{\boldsymbol{p}}^0 = \boldsymbol{A}_1^0 \boldsymbol{A}_2^1 ... \boldsymbol{A}_n^{n-1} \tilde{\boldsymbol{p}}^n \tag{2.27}$$

The given information on homogeneous transformations will be used in the Denavit–Hartenberg Convention in Section 2.7.1. First the basics of kinematics will be presented.

2.6 Introduction kinematics

In order to derive the crane dynamics some kinematics theory of the system has to be investigated. Kinematics describes the motion of points, bodies and systems of bodies without considering the forces acting on the masses nor the masses it selves. It describes the geometry of the system and its initial conditions in terms of position, velocity and acceleration. From the geometrical description it can then determine any part of the system's position, velocity and acceleration(Beggs, 1983).

There are two main parts of kinematics, namely **direct kinematics** and **inverse kinematics**. The direct kinematics determines the position and orientation of the end effector with a given manipulator configuration illustrated in the left part of Figure 2.10. The inverse kinematics is the reverse process meaning that it determines the manipulator configuration with a given position and orientation, and this process is shown in the right part of Figure 2.10. These two parts of the kinematics will be explained and derived in the coming sections.

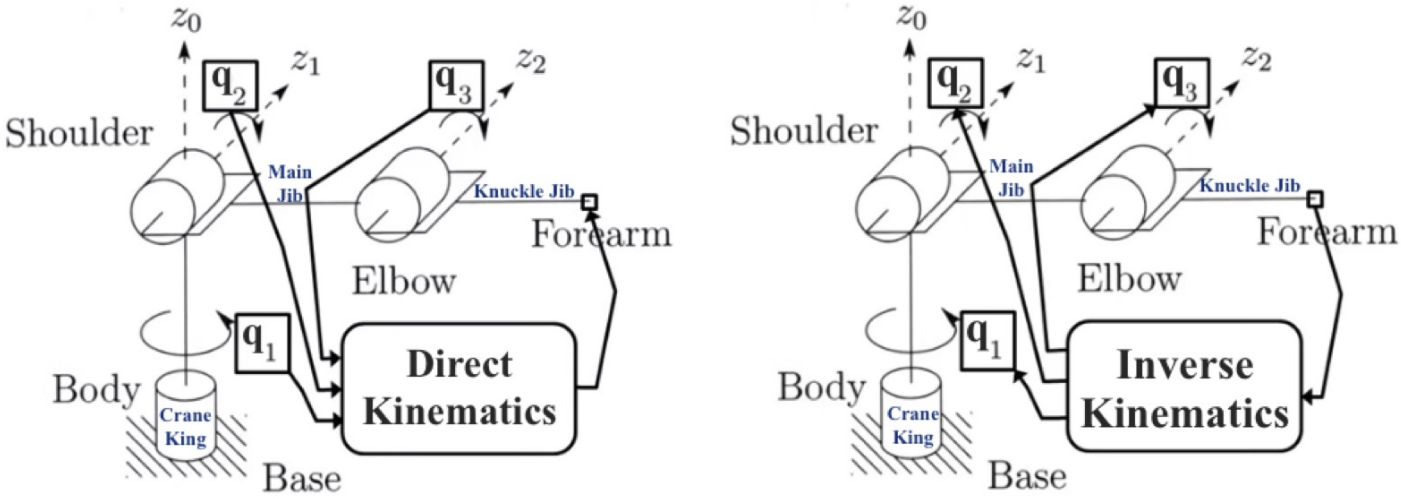

Figure 2.10: This figure illustrates the direct kinematics and the inverse kinematics of the crane investigated. The end effector for this system is the crane tip which can be seen at the end of the *forearm*.

2.7 Direct kinematics

The direct kinematics can more clearly be seen in Figure 2.11. Here one can observe that the position of the crane tip is derived by direct kinematics with the different joint angles as input. In this thesis the Denavit-Hartenberg Convention was chosen to deduce the direct kinematics.

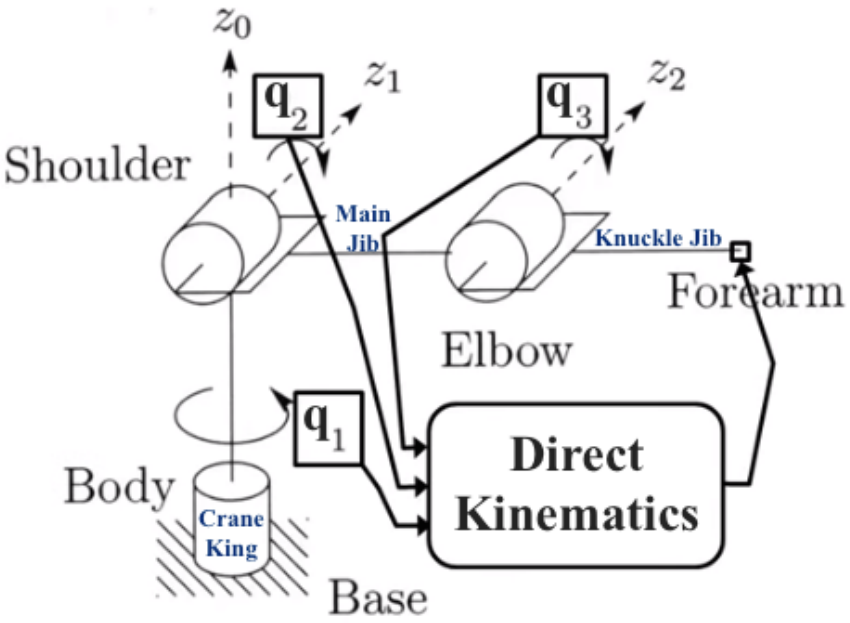

Figure 2.11: Figure illustrating that the direct kinematics derives the position of the crane tip with the different joint angles as input.

2.7.1 The Denavit-Hartenberg Convention – transformation matrices

The Denavit-Hartenberg convention provide an operating procedure for the computation of direct kinematics. In some cases the kinematics for a robot manipulator is complex and this convention helps simplifying this process. In this convention the homogeneous transformations are represented as a product of two rotations and two translations

$$\boldsymbol{A}_i = Rot_{z,\theta_i} Trans_{z,d_i} Trans_{x,a_i} Rot_{x,\alpha_i} \tag{2.28}$$

where the first element Rot_{z,θ_i} is a rotation with angle θ about the z-axis, $Trans_{z,d_i}$ is a

translation along the z-axis with distance d_i, $Trans_{x,a_i}$ is a translation along the x-axis with distance a_i and Rot_{x,α_i} is a rotation with angle α_i about the $x - axis$.

Then by performing these multiple homogeneous transformations the transformation matrix can be derived

$$\boldsymbol{T}_n^0 = \boldsymbol{A}_1^0(q_1)\boldsymbol{A}_2^1(q_2)...\boldsymbol{A}_n^{n-1}(q_n) \tag{2.29}$$

The four parameters presented in (2.28) represent

- a_i is **link length** of link i
  The distance between the axes z_{i-1} and z_i, measured along x_i.
- α_i is **link twist** of link i
  The angle between the axes z_{i-1} and z_i, measured in a plane normal to x_i. The positive sense for θ is determined from z_0 to z_1 by the right hand rule.
- d_i is **link offset** of link i
  The distance from the origin of $o_{i-1}x_{i-1}y_{i-1}z_{i-1}$ to the intersection of z_{i-1} and x_i, measured along z_{i-1}. d_i is the joint variable if the joint is prismatic.
- θ_i is **joint angle** of link i
  The angle of rotation from x_{i-1} to the x_i axis, measured in a plane normal to z_{i-1}. θ_i is the joint variable if the joint is revolute.

Here it is worth mentioning that a_i and α_i is fixed as long as the robot is not reconfigured. It is convenient to set some rules when assigning the coordinate axes

1. z_{i-1} is the axis of actuation of joint i
2. x_i is set so that it is perpendicular to and intersects z_{i-1}
3. Derive y_i axis based on x_i and z_i by using the right-hand rule

The coordinate axes for the crane system can now be defined and seen in Figure 2.12. By comparison of this figure and the figure of the coordinate frames of an anthropomorphic arm (Figure 2.13) one can easily observe the similarities. In both illustrations all of the

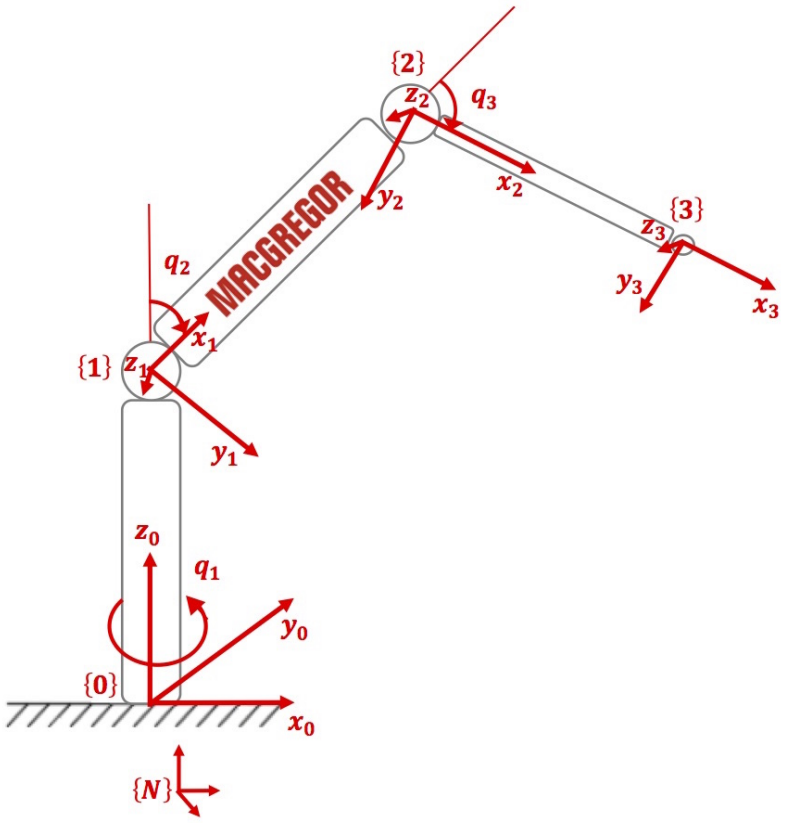

Figure 2.12: The different coordinate frames of the crane.

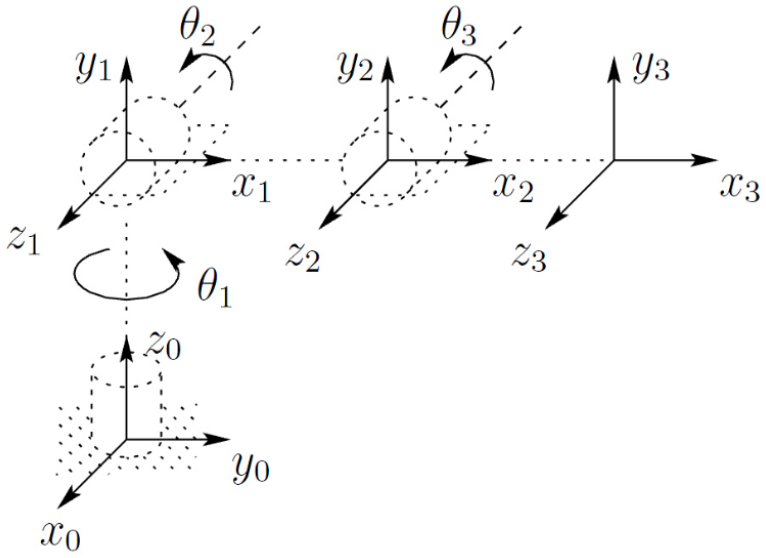

Figure 2.13: Coordinate frames, anthropomorphic arm (Sciavicco and Siciliano, 1996).

three joints are revolute. The first revolute joint is vertical while the two last joints are horizontal and in parallel. This leads to finding the Denavit-Hartenberg parameters.

Table 2.6 shows the Denavit-Hartenberg parameters for the crane system which is almost like the anthropomorphic arm presented in Sciavicco and Siciliano (1996). The only difference is that the base frame is moved so that d_1 differs between the two of them.

Table 2.6: The Denavit-Hartenberg parameters for the crane system.

Link	$\boldsymbol{a_i}$	$\boldsymbol{\alpha_i}$	$\boldsymbol{d_i}$	$\boldsymbol{\theta_i}$
1	0	90°	l_1	q_1
2	l_2	0°	0	q_2
3	l_3	0°	0	q_3

The distance between the axes z_0 and z_1 measured along x_1 is called the link length of link 1, a_1. By observing Figure 2.12 one can easily see that a_1 equals zero, a_2 equals to the length of the main jib, l_2, and a_3 equals to the length of the knuckle jib l_3.

α_1 is defined as the link twist of link 1, which means the angle between axes z_0 and z_1 measured in a plane normal to x_1. Since joint 1 is perpendicular to joint 2 this equals 90°. Since z_1, z_2 and z_3 are in parallel α_2 and α_3 equals zero degrees.

d_1 is as mentioned the distance between the origin of frame $\{0\}$ and the intersection of z_0 and x_1 measured along z_0 axis. By looking at Figure 2.12 one can observe that this is equal to the length of crane king, l_1. Due to the fact that z_1, z_2 and z_3 are in parallel d_2 and d_3 equals zero. Since all of the joints are revolute θ_1 is the joint angle of link 1, q_1, θ_2 is the joint angle of link 2, q_2, and θ_3 is the joint angle of link 3, q_3.

The homogeneous transformation between each link of the crane can now be deduced. The homogeneous transformation of frame $\{1\}$ with respect to $\{0\}$ is

$$\boldsymbol{A}_1^0 = \begin{bmatrix} c_1 & 0 & s_1 & 0 \\ s_1 & 0 & -c_1 & 0 \\ 0 & 1 & 0 & l_1 \\ 0 & 0 & 0 & 1 \end{bmatrix}, \tag{2.30}$$

the homogeneous transformation matrix of frame $\{2\}$ with respect to $\{1\}$ is

$$\boldsymbol{A}_2^1 = \begin{bmatrix} c_2 & -s_2 & 0 & l_2c_2 \\ s_2 & c_2 & 0 & l_2s_2 \\ 0 & 0 & 1 & 0 \\ 0 & 0 & 0 & 1 \end{bmatrix} \tag{2.31}$$

and at last the homogeneous transformation matrix of frame {3} with respect to {2} is as following

$$\boldsymbol{A}_3^2 = \begin{bmatrix} c_3 & -s_3 & 0 & l_3c_3 \\ s_3 & c_3 & 0 & l_3s_3 \\ 0 & 0 & 1 & 0 \\ 0 & 0 & 0 & 1 \end{bmatrix} \tag{2.32}$$

By using 2.29 the transformation matrices for the crane can now be derived. The transformation matrix of frame {1} with respect to {0} is

$$\boldsymbol{T}_1^0 = \boldsymbol{A}_1^0 = \begin{bmatrix} c_1 & 0 & s_1 & 0 \\ s_1 & 0 & -c_1 & 0 \\ 0 & 1 & 0 & l_1 \\ 0 & 0 & 0 & 1 \end{bmatrix}, \tag{2.33}$$

the transformation matrix of frame {2} with respect to {0} is

$$\boldsymbol{T}_2^0 = \boldsymbol{A}_1^0\boldsymbol{A}_2^1 = \begin{bmatrix} c_1c_2 & -c_1s_2 & -s_1 & l_2c_1c_2 \\ c_2s_1 & -s_1s_2 & c_1 & l_2c_2s_1 \\ -s_2 & -c_2 & 0 & l_2s_2 + l_1 \\ 0 & 0 & 0 & 1 \end{bmatrix} \tag{2.34}$$

and the transformation matrix of frame {3} with respect to {0} is

$$\boldsymbol{T}_3^0 = \boldsymbol{A}_1^0\boldsymbol{A}_2^1\boldsymbol{A}_3^2 = \begin{bmatrix} c_1c_2c_3 - c_1s_2s_3 & c_1c_2s_3 - c_1c_3s_2 & -s_1 & l_3c_1c_{23} + l_2c_1c_2 \\ s_1c_2c_3 - s_1s_2s_3 & s_1s_3c_2 - s_1s_2c_3 & c_1 & l_3s_1c_{23} + l_2s_1c_2 \\ -s_2c_3 - c_2s_3 & s_2s_3 - c_2c_3 & 0 & l_3s_{23} + l_2s_2 + l_1 \\ 0 & 0 & 0 & 1 \end{bmatrix} \tag{2.35}$$

where c_1, c_2, c_3, s_1, s_2, s_3, c_{23}, s_{23} and mathematical simplifications used are explained in Table 2.3.

2.7.2 Velocity - the Jacobian

In order to compute the kinetic energy as a function of the generalized coordinates later on it is necessary to derive the Jacobian matrices. This can be applied to the intermediate link other than the end effector, yielding

$$\dot{\boldsymbol{p}}_i = \boldsymbol{j}_{\dot{p}_1}^{(i)}\dot{q}_1 + ... + \boldsymbol{j}_{\dot{p}_i}^{(i)}\dot{q}_i = \boldsymbol{J}_{\dot{p}}^{(i)}\dot{\boldsymbol{q}} \tag{2.36}$$

$$\boldsymbol{\omega}_i = \boldsymbol{j}_{\omega_1}^{(i)}\dot{q}_1 + ... + \boldsymbol{j}_{\omega_i}^{(i)}\dot{q}_i = \boldsymbol{J}_{\omega}^{(i)}\dot{\boldsymbol{q}} \tag{2.37}$$

where $\dot{\boldsymbol{p}}_i$ is the linear velocity and $\boldsymbol{\omega}_i$ is the angular velocity, both expressed in $o_i x_i y_i z_i$. These two velocities gives the foundation to find the linear, $\boldsymbol{J}_{\dot{p}}^{(i)}$, and the angular, $\boldsymbol{J}_{\omega}^{(i)}$, Jacobian matrices.

$$\boldsymbol{J}_{\dot{p}}^{(i)} = \begin{bmatrix} \boldsymbol{j}_{\dot{p}_1}^{(i)} & ... & \boldsymbol{j}_{\dot{p}_i}^{(i)} & 0 & ... & 0 \end{bmatrix} \tag{2.38}$$

$$\boldsymbol{J}_{\omega}^{(i)} = \begin{bmatrix} \boldsymbol{j}_{\omega_1}^{(i)} & ... & \boldsymbol{j}_{\omega_i}^{(i)} & 0 & ... & 0 \end{bmatrix} \tag{2.39}$$

When the joint is revolute, as for this crane, the elements in the Jacobian matrices are defined like this

$$\begin{bmatrix} \boldsymbol{j}_{\dot{p}_j}^{(i)} \\ \boldsymbol{j}_{\omega_j}^{(i)} \end{bmatrix} = \begin{bmatrix} \boldsymbol{z}_{j-1} \times (\boldsymbol{p} - \boldsymbol{p}_{j-1}) \\ \boldsymbol{z}_{j-1} \end{bmatrix} \tag{2.40}$$

where $\boldsymbol{z}_{j-1}$ is the first three elements of the third column of $\boldsymbol{T}_{j-1}^{0}$ and $\boldsymbol{p}_{j-1}$ are the first three elements of the fourth column of $\boldsymbol{T}_{j-1}^{0}$. For the crane investigated the Jacobian is

$$\boldsymbol{J} = \begin{bmatrix} \boldsymbol{z}_0 \times (\boldsymbol{p} - \boldsymbol{p}_0) & \boldsymbol{z}_1 \times (\boldsymbol{p} - \boldsymbol{p}_1) & \boldsymbol{z}_2 \times (\boldsymbol{p} - \boldsymbol{p}_2) \\ \boldsymbol{z}_0 & \boldsymbol{z}_1 & \boldsymbol{z}_2 \end{bmatrix} = \begin{bmatrix} \boldsymbol{J}_{\dot{p}} \\ \boldsymbol{J}_{\omega} \end{bmatrix} \tag{2.41}$$

and computation of the position vectors of the various links gives

$$\boldsymbol{p}_0 = \begin{bmatrix} 0 \\ 0 \\ 0 \end{bmatrix} \qquad \boldsymbol{p}_1 = \begin{bmatrix} 0 \\ 0 \\ l_1 \end{bmatrix}$$
$$\boldsymbol{p}_2 = \begin{bmatrix} l_2 c_1 c_2 \\ l_2 c_2 s_1 \\ l_2 s_2 + l_1 \end{bmatrix} \qquad \boldsymbol{p} = \begin{bmatrix} l_3 c_1 c_{23} + l_2 c_1 c_2 \\ l_3 s_1 c_{23} + l_2 s_1 c_2 \\ l_3 s_{23} + l_2 s_2 + l_1 \end{bmatrix} \tag{2.42}$$

while computation of the unit vectors of revolute joint axes gives

$$\boldsymbol{z}_0 = \begin{bmatrix} 0 \\ 0 \\ 1 \end{bmatrix} \qquad \boldsymbol{z}_1 = \boldsymbol{z}_2 = \begin{bmatrix} s_1 \\ -c_1 \\ 0 \end{bmatrix} \tag{2.43}$$

The Jacobian matrices can now be found from 2.40 and 2.41

$$\boldsymbol{J}_{\dot{p}}^{(1)} = \begin{bmatrix} 0 & 0 & 0 \\ 0 & 0 & 0 \\ 0 & 0 & 0 \end{bmatrix} \qquad \boldsymbol{J}_{\omega}^{(1)} = \begin{bmatrix} 0 & 0 & 0 \\ 0 & 0 & 0 \\ 1 & 0 & 0 \end{bmatrix}$$
$$\boldsymbol{J}_{\dot{p}}^{(2)} = \begin{bmatrix} -l_2 c_2 s_1 & -l_2 c_1 s_2 & 0 \\ l_2 c_1 c_2 & -l_2 s_1 s_2 & 0 \\ 0 & l_2 c_2 & 0 \end{bmatrix} \qquad \boldsymbol{J}_{\omega}^{(2)} = \begin{bmatrix} 0 & s_1 & 0 \\ 0 & -c_1 & 0 \\ 1 & 0 & 0 \end{bmatrix}$$
$$\boldsymbol{J}_{\dot{p}}^{(3)} = \begin{bmatrix} -l_3 s_1 c_{23} - l_2 c_2 s_1 & -l_3 c_1 s_{23} - l_2 c_1 s_2 & -l_3 c_1 s_{23} \\ l_3 c_1 c_{23} + l_2 c_1 c_2 & -l_3 s_1 s_{23} - l_2 s_1 s_2 & -l_3 s_1 s_{23} \\ 0 & l_3 c_{23} + l_2 c_2 & l_3 c_{23} \end{bmatrix}$$
$$\boldsymbol{J}_{\omega}^{(3)} = \begin{bmatrix} 0 & s_1 & s_1 \\ 0 & -c_1 & -c_1 \\ 1 & 0 & 0 \end{bmatrix} \tag{2.44}$$

$$\boldsymbol{J} = \begin{bmatrix} -l_3 s_1 c_{23} - l_2 c_2 s_1 & -l_3 c_1 s_{23} - l_2 c_1 s_2 & -l_3 c_1 s_{23} \\ l_3 c_1 c_{23} + l_2 c_1 c_2 & -l_3 s_1 s_{23} - l_2 s_1 s_2 & -l_3 s_1 s_{23} \\ 0 & l_3 c_{23} + l_2 c_2 & l_3 c_{23} \\ 0 & s_1 & s_1 \\ 0 & -c_1 & -c_1 \\ 1 & 0 & 0 \end{bmatrix} \tag{2.45}$$

Only three of the six rows of the Jacobian (2.45) are linearly independent. Since the system has three degrees of mobility only the upper (3x3) block is used.

$$\boldsymbol{J} = \begin{bmatrix} -l_3 s_1 c_{23} - l_2 c_2 s_1 & -l_3 c_1 s_{23} - l_2 c_1 s_2 & -l_3 c_1 s_{23} \\ l_3 c_1 c_{23} + l_2 c_1 c_2 & -l_3 s_1 s_{23} - l_2 s_1 s_2 & -l_3 s_1 s_{23} \\ 0 & l_3 c_{23} + l_2 c_2 & l_3 c_{23} \end{bmatrix} \tag{2.46}$$

When the crane is fully stretched out, i.e. $\boldsymbol{q} = [0\ 0\ 0]^T$, the Jacobian matrix looses rank and it's determinant equals to zero. This means that there is no inverse Jacobian matrix and a kinematic singularity occurs. Intuitively this means that a kinematic singularity is a point where the crane loses it's ability to move the crane tip in some directions no matter how it moves it's joints.

This singularity is avoided by setting the initial joint values to $\boldsymbol{q}_{init} = [0\ \frac{\pi}{2}\ -\frac{\pi}{4}]$, which is the natural starting point for the crane shown in Figure 2.3. Due to the fact that the critical point, $\boldsymbol{q} = [0\ 0\ 0]^T$, is outside of the workspace, which means that the crane will never have this configuration later on, this is a possible approach. If the circumstances were different a damped least-square method would be preferable.

Damped Least Square Method

A damped least-square method, which is a local optimization method, would help prevent the infeasible joint velocities near the singular configuration by using a damping factor, λ, to control the norm of the joint velocity vector, $\dot{\boldsymbol{q}}$. In other words this prevents the joint velocity to become excessively high (Deo and Walker, 1995). Remembering the relationship between the end effector velocity, $\dot{\boldsymbol{p}}$, and the joint velocities $\dot{\boldsymbol{q}}$

$$\dot{\boldsymbol{p}} = J\dot{\boldsymbol{q}} \tag{2.47}$$

one get with a nonredundant manipulator 2.48. This system is redundant therefore 2.49 is presented

$$\dot{\boldsymbol{q}} = J^{-1}\dot{\boldsymbol{p}} \tag{2.48}$$

$$\dot{\boldsymbol{q}} = J^{*}\dot{\boldsymbol{p}} \tag{2.49}$$

$$J^{*} = (J^{T} + \lambda I)^{-1} J^{T} \tag{2.50}$$

where J^* has been found to be effective in tackling ill-conditioned Jacobians and preventing high joint velocities near singularities. The role of the damping factor, λ, is to determine the trade-off between the accuracy and feasibility of the inverse kinematic solution. There are several different methods to compute an appropriate damping factor. For this system the method presented in Nakamura and Hanafusa (1986) is appropriate. This paper suggests adjusting the damping factor according to the value of the manipulability measure $\omega = \sqrt{det(JJ^T)}$ using a threshold value ω_t. When a configuration is singular the nonnegative measure ω becomes zero. This gives the foundation of deriving the damping factor:

$$\begin{aligned} \lambda &= \lambda_0 \left(1 - \frac{\omega}{\omega_t}\right)^2, && \text{if} \quad \omega < \omega_t \\ \lambda &= 0, && \text{if} \quad \omega \geq \omega_t \end{aligned} \tag{2.51}$$

2.8 Inverse kinematics

Inverse kinematics is defined as the use of the kinematics equations of a robot to determine the joint parameters that provide a desired position of the end effector (Paul, 1981) as illustrated in Figure 2.14. Motion planning is the specification of the movement of a robot so that its end effector reaches a desired behavior. Inverse kinematics transforms the motion plan into joint actuator trajectories for the robot. As mentioned before the direct kinematics uses the joint angles to determine the end effector position, so the inverse kinematics reverses this calculation to determine the joint parameters which gives the desired configuration (McCarthy and Soh, 2010).

By using the inverse kinematics method one can use algorithms to keep a fixed end effector position. In this thesis this means that one can use algorithms to compensate for the ship's

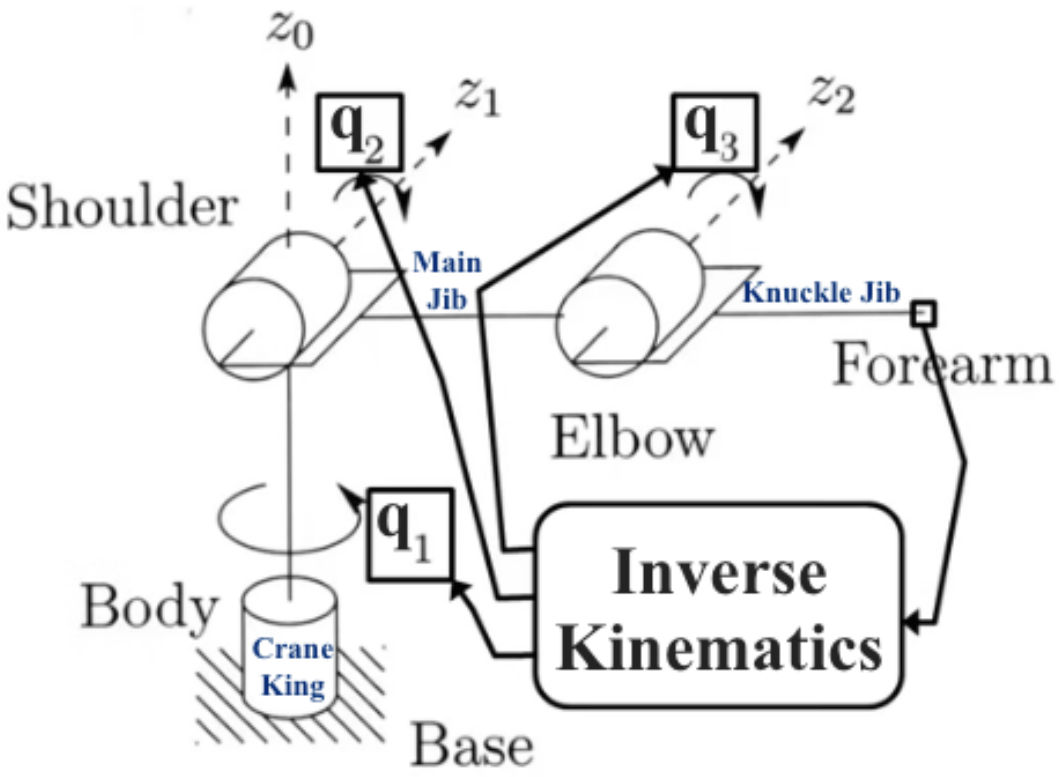

Figure 2.14: Joint angles are defined by end effector position using inverse kinematics.

orientation and position and keep a desired crane tip position. Inverse kinematics can also be used by the crane operator to control the crane tip in work space. Unfortunately there are no good universal algorithms for producing the inverse kinematics of a serial link manipulator.

The inverse kinematics problem is much more complex than the direct kinematics problem for the following reasons (Sciavicco and Siciliano, 1996):

- The equations to solve are in general nonlinear, and thus it is not always possible to find a closed-form solution. For the nonlinear crane system the overall complexity makes the closed-form solution difficult to find.
- Multiple solutions may exist which is the case in this thesis. There are, naturally, several joint angle combinations which gives the same end effector position.
- Infinite solutions may exist, e.g., in the case of a kinematically redundant manipulator. The model investigated has non singularities, so this will not be a problem.

- There might be no admissible solutions, in view of the manipulator kinematic structure. Figure 2.7 illustrates the cranes workspace, and every solution inside of this workspace are admissible solutions. Solutions outside of workspace are not admissible.

As a result of the above arguments it was decided to not include inverse kinematics in this system, explained further in Section 5.1.

3 Crane Dynamics

In order to simulate the crane system and examine different control designs the derivation of the crane dynamics is essential. This way one can avoid using the actual physical system, which makes the regulating and optimizing part easier. One also avoids damaging anything or spend needless amount of money. The method used in this thesis for deriving the Equations of Motion (EOM) is based on the Lagrange formulation and this method is both simple and systematic. After the finishing the crane dynamics it will be implemented in MATLAB (Appendix B).

3.1 Lagrange formulation

The dynamic model of the crane provides a description of the relationship between the joint actuator torques and the structure. The Lagrangian dynamic formulation is an energy based approach of the system, in other words it derives the dynamics by using kinetic ($\mathcal{T}$) and potential ($\mathcal{U}$) energy.

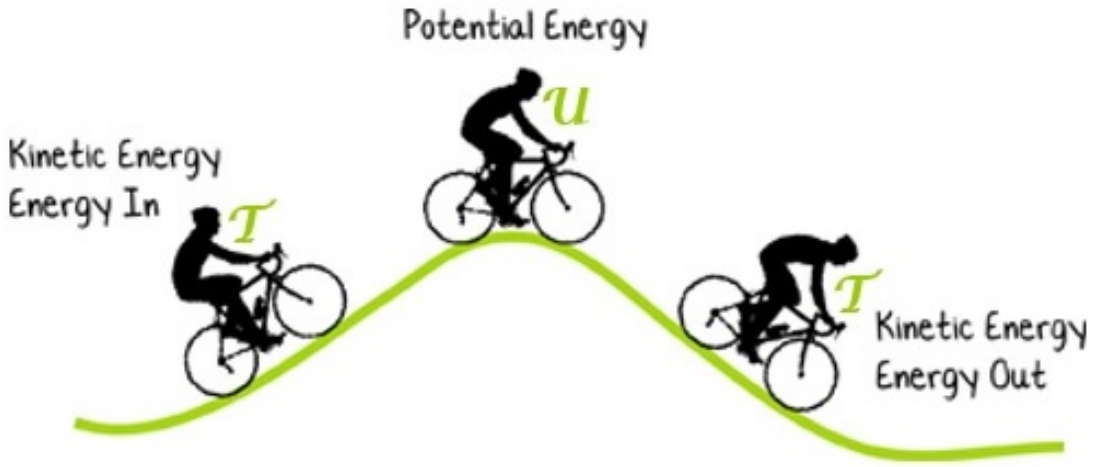

Figure 3.1: Simple illustration of the potential and kinematic energy which are the foundation of the Lagrangian dynamic formulation.

The difference between the kinetic and the potential energy is the Lagrangian ($\mathcal{L}$) of the system

$$\mathcal{L} = \mathcal{T} - \mathcal{U} \tag{3.1}$$

The Lagrangian equations are expressed by

$$\frac{d}{dt}\frac{\delta \mathcal{L}}{\delta \dot{\lambda}_i} - \frac{\delta \mathcal{L}}{\delta \lambda_i} = \xi_i \tag{3.2}$$

where ξ_i is the generalized force associated with generalized coordinate λ_i. This forms the relationship between the generalized forces applied to the crane and the joint positions, velocities and accelerations.

With Lagrange formulation the equations of motion can be derived without taking the reference coordinate frame into consideration. The generalized coordinates, $\lambda_i = 1, ..., n$, are chosen where n is the number of degree of mobility. Hence the generalized coordinates effectively describes the link position of the crane.

$$\begin{bmatrix} \lambda_1 \\ \vdots \\ \lambda_n \end{bmatrix} = \boldsymbol{q} \tag{3.3}$$

Briefly summarized the kinetic and the potential energy must be derived in order to to find the equations of motion.

3.2 Kinetic energy

Kinetic energy is defined as the energy that it possesses due to its motion. The total kinetic energy of a crane with n rigid links is therefore given by the sum of the contributions relative to the motion of each link and the contributions relative to the motion of each joint actuator

$$\mathcal{T} = \sum_{i=1}^{n} \mathcal{T}_i \tag{3.4}$$

where $\mathcal{T}_i$ is the kinetic energy of link i $\mathcal{T}_i$ is given by

$$\mathcal{T}_i = \frac{1}{2} \int_{V_i} \dot{\boldsymbol{p}}_i^{*T} \dot{\boldsymbol{p}}_i^{*} \rho dV \tag{3.5}$$

here $\dot{\boldsymbol{p}}_i^*$ is the linear velocity vector and ρ is the density of the elementary particle of volume dV. V_{l_i} is the volume of link i. $\boldsymbol{p}_i^*$ is the position vector of the element particle and $\boldsymbol{p}_{C_i}$ of the link center of mass. Both $\boldsymbol{p}_i^*$ and $\boldsymbol{p}_{C_i}$ are expressed in base frame.

$$\boldsymbol{r}_i = \begin{bmatrix} r_{ix} & r_{iy} & r_{iz} \end{bmatrix} = \boldsymbol{p}_i^* - \boldsymbol{p}_{l_i} \tag{3.6}$$

where, with m_i as the mass link

$$\boldsymbol{p}_i = \frac{1}{m_i} \int_{V_i} \boldsymbol{p}_i^* \rho dV \tag{3.7}$$

The link point velocity can be expressed as

$$\begin{aligned} \dot{\boldsymbol{p}}_i^* =& \dot{\boldsymbol{p}}_i + \boldsymbol{\omega}_i \times \boldsymbol{r}_i \\ =& \dot{\boldsymbol{p}}_i + \boldsymbol{S}(\boldsymbol{\omega}_i)\boldsymbol{r}_i \end{aligned} \tag{3.8}$$

here the linear velocity of the center of the mass is $\dot{\boldsymbol{p}}_i$ and the angular velocity of the link is $\boldsymbol{\omega_i}$.

The translational kinetic energy contribution is

$$\frac{1}{2} \int_{V_i} \dot{\boldsymbol{p}}_i^T \dot{\boldsymbol{p}}_i \rho dV = \frac{1}{2} m_i \dot{\boldsymbol{p}}_i^T \dot{\boldsymbol{p}}_i \tag{3.9}$$

The rotational kinetic energy contribution is

$$\begin{aligned} \frac{1}{2} \int_{V_i} =& \boldsymbol{r}_i^T \boldsymbol{S}^T(\boldsymbol{\omega}_i) \boldsymbol{S}(\boldsymbol{\omega}_i) \boldsymbol{r}_i \rho dV \\ =& \boldsymbol{\omega}_i^T \left(\int_{V_i} \boldsymbol{S}^T(\boldsymbol{r}_i) \boldsymbol{S}(\boldsymbol{r}_i) \rho dV \right) \end{aligned} \tag{3.10}$$

where $\boldsymbol{S}(\boldsymbol{\omega}_i)\boldsymbol{r}_i = -\boldsymbol{S}(\boldsymbol{r}_i)\boldsymbol{\omega}_i$

$$\boldsymbol{S}(\boldsymbol{r}_i) = \begin{bmatrix} 0 & -r_{iz} & r_{iy} \\ r_{iz} & 0 & -r_{ix} \\ -r_{iy} & r_{ix} & 0 \end{bmatrix} \tag{3.11}$$

$$\frac{1}{2}\int_{V_i} \boldsymbol{r}_i^T \boldsymbol{S}^T(\boldsymbol{\omega}_i)\boldsymbol{S}(\boldsymbol{\omega}_i)\boldsymbol{r}_i \rho dV = \frac{1}{2}\boldsymbol{\omega}_i^T \boldsymbol{I}_i \boldsymbol{\omega}_i \tag{3.12}$$

where the matrix $\boldsymbol{I}_i$ represents the symmetric inertia tensor relative to the center of mass of link i.

$$\begin{aligned} \boldsymbol{I}_i &= \begin{bmatrix} \int (r_{iy}^2 + r_{iz}^2)\rho dV & -\int r_{ix} r_{iy} \rho dV & -\int r_{ix} r_{iz} \rho dV \\ * & \int (r_{ix}^2 + r_{iz}^2)\rho dV & -\int r_{iy} r_{iz} \rho dV \\ * & * & \int (r_{ix}^2 + r_{iy}^2)\rho dV \end{bmatrix} \\ &= \begin{bmatrix} I_{ixx} & -I_{ixy} & -I_{ixz} \\ * & I_{iyy} & -I_{iyz} \\ * & * & I_{izz} \end{bmatrix} \end{aligned} \tag{3.13}$$

where the symbol $*$ represents the symmetrical elements of the matrix. For the crane investigated there are three links, i, and a inertia tensor matrix for each of these links. The inertia tensor matrix of link i will be expressed in local frame and defined as I_i.

$$\boldsymbol{I}_i = \begin{bmatrix} I_{ix} & 0 & 0 \\ 0 & I_{iy} & 0 \\ 0 & 0 & I_{iz} \end{bmatrix} \tag{3.14}$$

Since matrix (3.13) is symmetric the off diagonal elements equals to zero. Below the inertia tensor matrix for the king (link 1), main jib (link 2) and the knuckle jib (link 3) are defined.

Inertia tensor matrix, king

$$\boldsymbol{I}_{1x} = \frac{m_1(3r_1^2 + l_1^2)}{12} \tag{3.15}$$

$$\boldsymbol{I}_{1y} = m_1 r_1^2 \tag{3.16}$$

$$\boldsymbol{I}_{1z} = \frac{m_1(3r_1^2 + l_1^2)}{12} \tag{3.17}$$

where m_1 represents the mass, r_1 represents the radius and l_1 represents the length of the king.

Inertia tensor matrix, main jib

$$\boldsymbol{I}_{2x} = \frac{m_2(d_2^2 + h_2^2)}{12} \tag{3.18}$$

$$\boldsymbol{I}_{2y} = \frac{m_2(d_2^2 + l_2^2)}{12} \tag{3.19}$$

$$\boldsymbol{I}_{2z} = \frac{m_2(h_2^2 + l_2^2)}{12} \tag{3.20}$$

where m_2 represents the mass, d_2 represents the depth, h_2 represents the height and l_1 the length of the main jib.

Inertia tensor matrix, knuckle jib

$$\boldsymbol{I}_{3x} = \frac{m_3(d_3^2 + h_3^2)}{12} \tag{3.21}$$

$$\boldsymbol{I}_{3y} = \frac{m_3(d_3^2 + l_3^2)}{12} \tag{3.22}$$

$$\boldsymbol{I}_{3z} = \frac{m_3(h_3^2 + l_3^2)}{12} \tag{3.23}$$

where m_3 represents the mass, d_3 represents the depth, h_3 represents the height and l_3 the length of the main jib.

$$\boldsymbol{\omega}_i^i = \boldsymbol{R}_i^T \boldsymbol{\omega}_i \tag{3.24}$$

where $\boldsymbol{R}_i$ is the rotation matrix from link i frame to base frame. The inertia tensor is constant when referred to the link frame, then

$$\boldsymbol{I}_i = \boldsymbol{R}_i \boldsymbol{I}_i^i \boldsymbol{R}_i^T \tag{3.25}$$

$$\mathcal{T} = \frac{1}{2}\sum_{i=1}^{n}\sum_{j=1}^{n} m_{ij}(\boldsymbol{q})\dot{q}_i\dot{q}_j = \frac{1}{2}\dot{\boldsymbol{q}}^T\boldsymbol{M}(\boldsymbol{q})\dot{\boldsymbol{q}} \tag{3.26}$$

where

$$\boldsymbol{M}(\boldsymbol{q}) = \sum_{i=1}^{n}(m_i\boldsymbol{J}_{\dot{p}_i}^T\boldsymbol{J}_{\dot{p}_i} + \boldsymbol{J}_{\omega_i}^T\boldsymbol{R}_i\boldsymbol{I}_i^i\boldsymbol{R}_i^T\boldsymbol{J}_{\omega_i}) \tag{3.27}$$

where $\boldsymbol{M}(\boldsymbol{q})$ is a symmetric and positive definite nxn mass matrix. To find $\boldsymbol{M}(\boldsymbol{q})$ it is divided into three parts, one for each joint i. The first part, $\boldsymbol{M}_1(\boldsymbol{q})$, is for the king, the second part, $\boldsymbol{M}_2(\boldsymbol{q})$, is for the main jib and the third part, $\boldsymbol{M}_3(\boldsymbol{q})$, is for the knuckle jib. The sum of these three parts gives $\boldsymbol{M}(\boldsymbol{q})$. The Jacobian matrices were found in (2.44) and the rotation matrices from link i to the base frame in (2.15) – (2.17).

$\boldsymbol{M}_1(\boldsymbol{q})$:

$$\begin{aligned}\boldsymbol{M}_1(\boldsymbol{q}) = m_1 &\begin{bmatrix}0&0&0\\0&0&0\\0&0&0\end{bmatrix}\begin{bmatrix}0&0&0\\0&0&0\\0&0&0\end{bmatrix} + \\ &\begin{bmatrix}0&0&1\\0&0&0\\0&0&0\end{bmatrix}\begin{bmatrix}c_1&0&s_1\\s_1&0&-c_1\\0&1&0\end{bmatrix}\begin{bmatrix}I_{1x}&0&0\\0&I_{1y}&0\\0&0&I_{1z}\end{bmatrix}\begin{bmatrix}c_1&s_1&0\\0&0&1\\s_1&-c_1&0\end{bmatrix}\begin{bmatrix}0&0&0\\0&0&0\\1&0&0\end{bmatrix} \\ &= \begin{bmatrix}I_{1y}&0&0\\0&0&0\\0&0&0\end{bmatrix}\end{aligned} \tag{3.28}$$

$\boldsymbol{M}_2(\boldsymbol{q})$:

$$\begin{aligned}\boldsymbol{M}_2(\boldsymbol{q}) = m_2 &\begin{bmatrix}-l_2c_2s_1&l_2c_1c_2&0\\-l_2c_1s_2&-l_2s_1s_2&l_2c_2\\0&0&0\end{bmatrix}\begin{bmatrix}-l_2c_2s_1&-l_2c_1s_2&0\\l_2c_1c_2&-l_2s_1s_2&0\\0&l_2c_2&0\end{bmatrix} + \\ &\begin{bmatrix}0&0&1\\s_1&-c_1&0\\0&0&0\end{bmatrix}\begin{bmatrix}c_1c_2&-c_1s_2&-s_1\\c_2s_1&-s_1s_2&c_1\\-s_2&-c_2&0\end{bmatrix}\begin{bmatrix}I_{2x}&0&0\\0&I_{2y}&0\\0&0&I_{2z}\end{bmatrix}\begin{bmatrix}c_1c_2&c_2s_1&-s_2\\-c_1s_2&-s_1s_2&-c_2\\-s_1&c_1&0\end{bmatrix}\begin{bmatrix}0&s_1&0\\0&-c_1&0\\1&0&0\end{bmatrix}\end{aligned}$$

$$= \begin{bmatrix} m_2 l_2^2 c_2^2 + s_2^2 I_{2x} + c_2^2 I_{2y} & 0 & 0 \\ 0 & m_2 l_2^2 + I_{2z} & 0 \\ 0 & 0 & 0 \end{bmatrix} \tag{3.29}$$

$\boldsymbol{M}_{3\dot{p}}(\boldsymbol{q})$**:**

$$\boldsymbol{M}_{3\dot{p}}(\boldsymbol{q}) = m_3 \begin{bmatrix} -l_3 s_1 c_{23} - l_2 c_2 s_1 & l_3 c_1 c_{23} + l_2 c_1 c_2 & 0 \\ -l_3 c_1 s_{23} - l_2 c_1 s_2 & -l_3 s_1 s_{23} - l_2 s_1 s_2 & l_3 c_{23} + l_2 c_2 \\ -l_3 c_1 s_{23} & -l_3 s_1 s_{23} & l_3 c_{23} \end{bmatrix}$$
$$\begin{bmatrix} -l_3 s_1 c_{23} - l_2 c_2 s_1 & -l_3 c_1 s_{23} - l_2 c_1 s_2 & -l_3 c_1 s_{23} \\ l_3 c_1 c_{23} + l_2 c_1 c_2 & -l_3 s_1 s_{23} - l_2 s_1 s_2 & -l_3 s_1 s_{23} \\ 0 & l_3 c_{23} + l_2 c_2 & l_3 c_{23} \end{bmatrix}$$
$$= \begin{bmatrix} m_3((l_2 c_2 + l_3 c_{23})^2 & 0 & 0 \\ 0 & m_3(2 l_2 l_3 (s_2 s_{23} + c_2 c_{23}) + l_2^2 + l_3^2) & m_3 l_3 (s_{23}(l_2 s_2 + l_3 s_{23}) + c_{23}(l_2 c_2 + l_3 c_{23})) \\ 0 & m_3 l_3 (s_{23}(l_2 s_2 + l_3 s_{23}) + c_{23}(l_2 c_2 + l_3 c_{23})) & m_3 l_3^2 \end{bmatrix} \tag{3.30}$$

$\boldsymbol{M}_{3\omega}(\boldsymbol{q})$**:**

$$\boldsymbol{M}_{3\omega}(\boldsymbol{q}) = \begin{bmatrix} 0 & 0 & 1 \\ s_2 & -c_1 & 0 \\ s_1 & -c_1 & 0 \end{bmatrix} \begin{bmatrix} c_1 c_2 c_3 - c_1 s_2 s_3 & c_1 c_2 s_3 - c_1 c_3 s_2 & -s_1 \\ s_1 c_2 c_3 - s_1 s_2 s_3 & s_1 s_3 c_2 - s_1 s_2 c_3 & c_1 \\ -s_2 c_3 - c_2 s_3 & s_2 s_3 - c_2 c_3 & 0 \end{bmatrix} \begin{bmatrix} I_{3x} & 0 & 0 \\ 0 & I_{3y} & 0 \\ 0 & 0 & I_{3z} \end{bmatrix}$$
$$\begin{bmatrix} c_1 c_2 c_3 - c_1 s_2 s_3 & s_1 c_2 c_3 - s_1 s_2 s_3 & -s_2 c_3 - c_2 s_3 \\ c_1 c_2 s_3 - c_1 c_3 s_2 & s_1 s_3 c_2 - s_1 s_2 c_3 & s_2 s_3 - c_2 c_3 \\ -s_1 & c_1 & 0 \end{bmatrix} \begin{bmatrix} 0 & s_1 & s_1 \\ 0 & -c_1 & -c_1 \\ 1 & 0 & 0 \end{bmatrix}$$
$$= \begin{bmatrix} I_{3x}(c_2 s_3 + c_3 s_2)^2 + I_{3y}(s_2 s_3 - c_2 c_3)^2 & 0 & 0 \\ 0 & I_{3z}(s_1^2 - c_1^2) & I_{3z}(s_1^2 - c_1^2) \\ 0 & I_{3z}(s_1^2 - c_1^2) & I_{3z}(s_1^2 - c_1^2) \end{bmatrix} \tag{3.31}$$

The mass matrix for the crane, $\boldsymbol{M}(\boldsymbol{q})$, can then be written as

$$\boldsymbol{M}(\boldsymbol{q}) = \boldsymbol{M}_1(\boldsymbol{q}) + \boldsymbol{M}_2(\boldsymbol{q}) + \boldsymbol{M}_{3\dot{p}}(\boldsymbol{q}) + \boldsymbol{M}_{3\omega}(\boldsymbol{q}) = \begin{bmatrix} m_{11} & m_{12} & m_{13} \\ m_{21} & m_{22} & m_{23} \\ m_{31} & m_{32} & m_{33} \end{bmatrix} \tag{3.32}$$

where

$$
\begin{aligned}
m_{11} =& I_{1y} + s_2^2 I_{2x} + c_2^2 I_{2y} + s_{23}^2 I_{3x} - c_{23}^2 I_{3y} + m_2 l_2^2 c_2^2 + m_3 (l_2 c_2 + l_3 c_{23})^2 \\
m_{12} =& m_{21} = 0 \\
m_{13} =& m_{31} = 0 \\
m_{22} =& (s_1^2 - c_1^2)(I_{2z} + I_{3z}) + m_2 l_2^2 + m_3 ((l_2 s_2 + l_3 s_{23})^2 + (l_2 c_2 + l_3 c_{23})^2) \\
m_{23} =& m_{32} = (s_1^2 - c_1^2) I_{3z} + m_3 l_3 (s_{23}(l_2 s_2 + l_3 s_{23}) + c_{23}(l_2 c_2 + l_3 c_{23})) \\
m_{33} =& (s_1^2 - c_1^2) I_{3z} + m_3 l_3^2
\end{aligned} \tag{3.33}
$$

The Coriolis and centripetal matrix were derived by using $M(q)$:

$$
c_{ij} = \sum_{i=1}^{n} c_{ijk} \dot{q_k} \tag{3.34}
$$

$$
c_{ijk} = \frac{1}{2} \left(\frac{\partial m_{ij}}{\partial q_k} + \frac{\partial m_{ik}}{\partial q_j} - \frac{\partial m_{jk}}{\partial q_i} \right) \tag{3.35}
$$

$$
\boldsymbol{C}(\boldsymbol{q}, \dot{\boldsymbol{q}}) = \begin{bmatrix} c_{11} & c_{12} & c_{13} \\ c_{21} & c_{22} & c_{23} \\ c_{31} & c_{32} & c_{33} \end{bmatrix} \tag{3.36}
$$

where

$$
\begin{aligned}
c_{11} =& (s_2 c_2 (I_{2x} - I_{2y}) + I_{3x} s_{23}(c_2 c_3 - s_2 s_3) + I_{3y} s_{23}(s_2 s_3 - c_2 c_3) \\
& - m_2 l_2^2 c_2 s_2 + m_3 (l_2 c_2 +_3 c_{23})(-l_2 s_2 - l_3 s_{23})) \dot{q_2} \\
& + (I_{3x} s_{23}(c_2 c_3 - s_2 s_3) + I_{3y} s_{23}(s_2 s_3 - c_2 c_3) - m_3 l_3 s_{23}(l_2 c_2 + l_3 c_{23})) \dot{q_3} \\
c_{12} =& (c_2 s_2 (I_{2x} - I_{2y}) + s_{23} c_{23} (I_{3x} - I_{3y}) \\
& + m_2 l_2^2 c_2 s_2 + m_3 (l_2 c_2 + l_3 c_{23})(-l_2 s_2 - l_3 s_{23})) \dot{q_1} \\
& - 2 c_1 s_1 (I_{2z} + I_{3z}) \dot{q_2} \\
& - 2 c_1 s_1 I_{3z} \dot{q_3} \\
c_{13} =& (c_{23} s_{23} (I_{3x} - I_{3y}) - m_3 l_3 s_{23}(l_2 c_2 + l_3 c_{23})) \dot{q_1} \\
& - 2 I_{3z} c_1 s_1 \dot{q_2}
\end{aligned}
$$

$$
\begin{aligned}
&\quad - 2I_{3z}c_1s_1\dot{q_3} \\
c_{21} =&(c_2s_2(-I_{2x}+I_{2y}) - s_{23}c_{23}(I_{3x}-I_{3y}) + m_2l_2^2c_2s_2 \\
&\quad - m_3(l_2c_2+l_3c_{23})(l_2s_2-l_3s_{23}))\dot{q_1} \\
&\quad + 2c_1s_1(I_{2z}+I_{3z})\dot{q_2} \\
&\quad + 2c_1s_1I_{3z}\dot{q_3} \\
c_{22} =&((I_{2z}+I_{3z})c_1s_12)\dot{q_1} \\
&\quad + ((l_2s_2+l_3s_{23})(l_2c_2+l_3c_{23}) + m_3(l_2c_2+l_3c_{23})(-l_2s_2-l_3s_{23}))\dot{q_2} \\
&\quad + ((l_2s_2+l_3s_{23})l_3c_{23} - m_3l_3s_{23}(l_2c_2+l_3c_{23}))\dot{q_3} \\
c_{23} =&2I_{3z}c_1s_1\dot{q_1} \\
&\quad + ((l_2s_2+l_3s_{23})l_3c_{23} - (l_2c_2+l_3c_{23})l_3s_{23})m_3\dot{q_2} \\
&\quad + ((l_2s_2+l_3s_{23})c_{23} - (l_2c_2+l_3c_{23})s_{23})l_3m_3\dot{q_3} \\
c_{31} =&- c_{13} \\
c_{32} =&2I_{3z}c_1s_1\dot{q_1} \\
&\quad - ((l_2s_2+l_3s_{23})l_3c_{23} - (l_2c_2+l_3c_{23})l_3s_{23})m_3\dot{q_2} \\
c_{33} =&0
\end{aligned}
\tag{3.37}
$$

3.3 Potential energy

The potential energy is energy possessed by the crane by virtue of its position relative to the ship, stresses within itself and other factors. As done for the kinetic energy, the potential energy stored in the manipulator is the sum of the contribution relative to each link i, $\mathcal{U}_i$. When assuming only rigid links the only source of potential energy is the gravity.

$$
\begin{aligned}
\mathcal{U} =& \sum_{i=1}^{n} \mathcal{U}_{l_i} \\
\mathcal{U}_i =& - \int_{V_{l_i}} \boldsymbol{q}_0^T \boldsymbol{p}_i^* \rho dV = -m_{l_i} \boldsymbol{q}_0^T \boldsymbol{p}_{\boldsymbol{l_i}}
\end{aligned}
\tag{3.38}
$$

which gives

$$
\mathcal{U} = - \sum_{i=1}^{n} m_i \boldsymbol{q}_0^T \boldsymbol{p_i} \tag{3.39}
$$

where $\boldsymbol{q}_0$ is the $3x1$ gravity acceleration vector in the base frame and $\boldsymbol{p_i}$ is the distance from $o_0x_0y_0z_0$ to center of gravity of link i. When z is the vertical axis then $\boldsymbol{q}_0 = \begin{bmatrix} 0 & 0 & -g \end{bmatrix}$. For the crane investigated, with three links i, the potential energy can be written as

$$\mathcal{U} = m_1 \frac{l_1}{2} g + m_2 g(\frac{l_2}{2} s_2 + l_1) + m_3 g(\frac{l_3}{2} s_{23} + l_2 s_2 + l_1) \tag{3.40}$$

where the potential energy contribution to the Euler-Lagrange (3.2) is

$$\frac{\partial \mathcal{U}}{\partial q_i} = -\sum_{j=1}^{n} m_j \boldsymbol{g}_0^T \boldsymbol{j}_{\dot{p}_i}^j = g_i(\boldsymbol{q}) \tag{3.41}$$

$\boldsymbol{g}(\boldsymbol{q})$ is derived by using following equation:

$$\boldsymbol{g}(\boldsymbol{q}) = \begin{bmatrix} 0 \\ m_2 g l_{2c} c_2 + m_3 g l_{3c} c_{23} + l_2 c_2 \\ m_3 g l_{3c} c_{23} \end{bmatrix} \tag{3.42}$$

3.4 Equations of motion

When the kinetic and the potential energy is derived the Lagrangian for the crane can be written

$$\begin{aligned} \mathcal{L}(\boldsymbol{q}, \dot{\boldsymbol{q}}) =& \mathcal{T}(\boldsymbol{q}, \dot{\boldsymbol{q}}) - \mathcal{U}(\boldsymbol{q}) \\ =& \frac{1}{2} \sum_{i=1}^{n} \sum_{j=1}^{n} m_{ij}(\boldsymbol{q}) \dot{q}_i \dot{q}_j + \sum_{i=1}^{n} m_i \boldsymbol{g}_0^T \boldsymbol{p}_i(\boldsymbol{q}) \end{aligned} \tag{3.43}$$

$\mathcal{U}$ does not depend on $\dot{\boldsymbol{q}}$, therefore inserting in (3.2)

$$\frac{d}{dt}\left(\frac{\delta \mathcal{L}}{\delta \dot{q}_i}\right) = \frac{d}{dt}\left(\frac{\delta \mathcal{T}}{\delta \dot{q}_i}\right) = \sum_{j=1}^{n} m_{ij}(\boldsymbol{q}) \ddot{q}_j + \sum_{j=1}^{n} \frac{d m_{ij}(\boldsymbol{q})}{dt} \dot{q}_j$$

$$= \sum_{j=1}^{n} m_{ij}(\boldsymbol{q})\ddot{q}_j + \sum_{j=1}^{n}\sum_{k=1}^{n} \frac{\delta m_{ij}(\boldsymbol{q})}{\delta q_k}\dot{q}_k\dot{q}_j \tag{3.44}$$

Switching the indices of summation one get

$$\frac{\delta \mathcal{T}}{\delta q_i} = \frac{1}{2}\sum_{j=1}^{n}\sum_{k=1}^{n} \frac{\delta m_{jk}(\boldsymbol{q})}{\delta q_k}\dot{q}_k\dot{q}_j \tag{3.45}$$

$$\begin{aligned}\frac{\delta \mathcal{U}}{\delta q_i} &= -\sum_{j=1}^{n} m_j \boldsymbol{g}_0^T \frac{\delta \boldsymbol{p}_j}{\delta q_i} \\ &= -\sum_{j=1}^{n} m_j \boldsymbol{g}_0^T \boldsymbol{j}_{p_i}^{(j)}(\boldsymbol{q})\end{aligned} \tag{3.46}$$

$$\begin{aligned}\frac{d}{dt}\frac{\delta \mathcal{L}}{\delta \dot{\lambda}_i} - \frac{\delta \mathcal{L}}{\delta \lambda_i} &= \xi_i \\ \sum_{j=1}^{n} m_{ij}(\boldsymbol{q})\ddot{q}_j + \sum_{j=1}^{n}\sum_{k=1}^{n} h_{ijk}(\boldsymbol{q})\dot{q}_k\dot{q}_j + g_i(\boldsymbol{q}) &= \xi_i\end{aligned} \tag{3.47}$$

which gives

$$h_{ijk} = \frac{\delta m_{ij}}{\delta q_k} - \frac{1}{2}\frac{\delta m_{jk}}{\delta q_i} \tag{3.48}$$

Summed up the joint space dynamical model no becomes

$$\boldsymbol{M}(\boldsymbol{q})\ddot{\boldsymbol{q}} + \boldsymbol{C}(\boldsymbol{q}, \dot{\boldsymbol{q}})\dot{\boldsymbol{q}} + \boldsymbol{g}(\boldsymbol{q}) = \boldsymbol{\tau} \tag{3.49}$$

$$\begin{bmatrix} m_{11} & m_{12} & m_{13} \\ m_{21} & m_{22} & m_{23} \\ m_{31} & m_{32} & m_{33} \end{bmatrix} \ddot{\boldsymbol{q}} + \begin{bmatrix} c_{11} & c_{12} & c_{13} \\ c_{21} & c_{22} & c_{23} \\ c_{31} & c_{32} & c_{33} \end{bmatrix} \dot{\boldsymbol{q}} + \begin{bmatrix} 0 \\ m_2 g l_{2c} c_2 + m_3 g l_{3c} c_{23} + l_2 c_2 \\ m_3 g l_{3c} c_{23} \end{bmatrix} = \boldsymbol{\tau} \tag{3.50}$$

The formulas used in Chapter 2 and 3 were inspired by Sciavicco and Siciliano (1996). The dynamic model of the crane (3.50) was implemented in MATLAB/Simulink (Appendix B).

4 Compensator Dynamics

This chapter will go through the chosen strategy for the heave compensating system. As mentioned before the wave influence on surge and sway will be taken care of by the controller system. At the end of this chapter the trajectory of the wave influence upon all of the DOF is created with the intention of behave as similar to a real life wave as possible. First an introduction is included to present the chosen strategy for compensating for the wave influence upon the whole system.

4.1 Introduction

MacGregor's crane is an advanced offshore crane which sometimes operates under rough weather conditions. In this regard the crane must be able to compensate for the wave influence whenever it has to carry out difficult tasks with the right precision. At present time the crane investigated compensates for the wave disturbances with the wire only, i.e. it compensates for the movements in the z-axis. One could question this decision considering that the end effector's x and y positions also changes continuously as a consequence of the waves as one can imagine by looking at Figure 4.1. There are mainly two reasons

Figure 4.1: Picture illustrating the rough conditions affecting all of the DOF. Reproduced with kind permission from MacGregor.

why they do not compensate for the xy-plane movement. Firstly the MacGregor's engineers believe that hydraulic system is to slow to be precise enough to achieve the wanted accuracy. Secondly the active heave compensation is a function the crane driver primarily uses when the payload is deep in the water. When this is the case the slowness of the water will delay and damp the unwanted movement of the crane tip in the xy-plane. The

conclusion of the engineers in MacGregor is therefore that the best solution is to compensate for the heave changes only. Nevertheless this thesis will investigate the effect of compensating for the xy–plane as well as the z movement. As a result of some intense brainstorming it was decided to only compensate for the heave movement with the wire and compensate for the xy-plane movement with the manipulator as illustrated in Figure 4.2. This figure gives an overall overview of the system

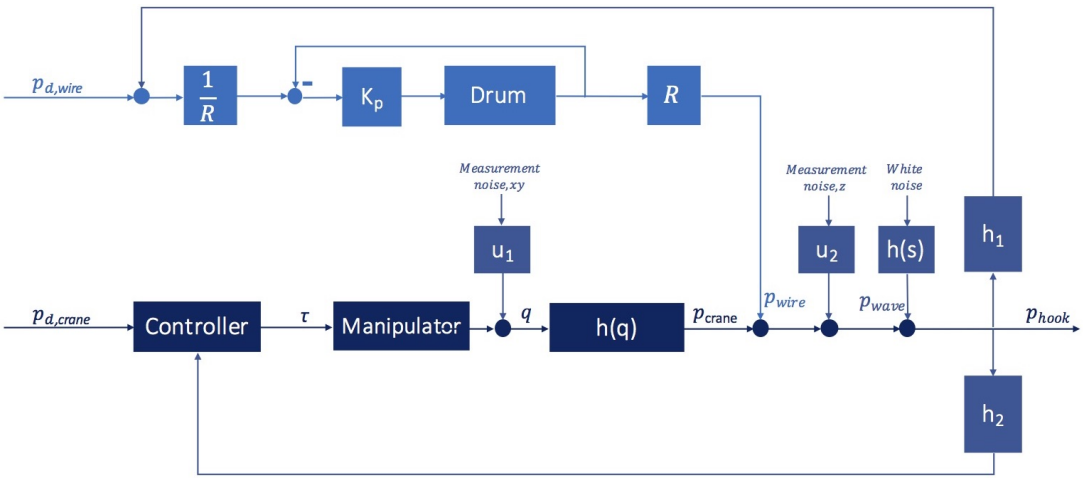

Figure 4.2: The entire system implemented in Simulink (Appendix B). As displayed the hook position has a z–feedback back to the wire part of the system and a xy–feedback to the controller part.

where

$$p_z = H_1 p, \qquad H_1 = \begin{bmatrix} 0 & 0 & 0 \\ 0 & 0 & 0 \\ 0 & 0 & 1 \end{bmatrix} \qquad \text{and} \qquad p_{xy} = H_2 p, \qquad H_2 = \begin{bmatrix} 1 & 0 & 0 \\ 0 & 1 & 0 \\ 0 & 0 & 0 \end{bmatrix} \tag{4.1}$$

which confirms that the z movement is regulated by the wire (**??**) and the xy movement is regulated by the manipulator (4.1).

The next section will derive the heave compensating system ($\boldsymbol{p}_{wire}$) while Section 4.3 derives the irregular wave influencing the crane ($\boldsymbol{p}_{wave}$). The crane part of the overall overview consists of a controller, the manipulator and the kinematics. The latter is derived in Chapter 2, the manipulator in Chapter 3 and different controllers are derived and compared in Chapter 5.

4.2 Heave compensation system

The way MacGregor controls the z position is to compensate the ships vertical movement by changing the wire length. This section derives the wire model and the PI regulator suggested for this system.

Figure 4.3: Illustrating the dynamics of the wire compensating with a constant radius of 1.75 m. The drum will initiate the opposite movement of the influence of the waves upon heave.

Figure 4.3 illustrates the Δz compensating part of the crane control system. When the wire drum moves with an angle θ the wire hook changes the z value. When sensitive tasks are to be done one can use this active heave compensation by changing the wire length opposite of the ships vertical movement, Δz (written as $p_{d,wire}$ in the block diagram illustrated in Figure 4.5). In MacGregor's case the Δz is given by Kongsberg Maritime's MRU H, seen in appendix C, and it is a result of the ships movements in heave, yaw, pitch and roll. Section 4.3 derives a realistic replacement of the MRU's signal which basically is the wave influence upon the crane.

The angle change needed to achieve a desired wire length change can be derived by basic

geometry illustrated in Figure 4.4, where θ is the drum angle change measured in radians, Δz is the change of wire length and R is the drum radius. For the sake of simplicity the radius of the drum is set to be constant.

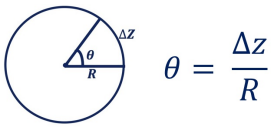

Figure 4.4: Simple drawing of the drum with radius R, angle change θ and wire length change Δz and the relation between these parameters.

The angular velocity is defined as $\omega = \dot{\theta}$

and the transfer function is $$H(s) = \frac{\omega}{\omega_d} = \frac{K_p}{Ts+1} \quad (4.2)$$

Newton's second law of motion gives the transfer function from the desired angular velocity, ω_d, to the real angular velocity, ω. K_p is the proportional gain. Figure 4.5 illustrates the block diagram for this system. K_p and T had to be tuned to give a sensible result. To achieve this the behavior of the real wire drum was studied and the values were tuned to such a degree that the outcome matched the real life drum behavior. The different values used for this part of the system is shown in the equations below (4.5).

$$R = 1.75 \text{ m} \quad (4.3)$$

$$K_p = 10 \quad (4.4)$$

$$T = 9 \text{ sec} \quad (4.5)$$

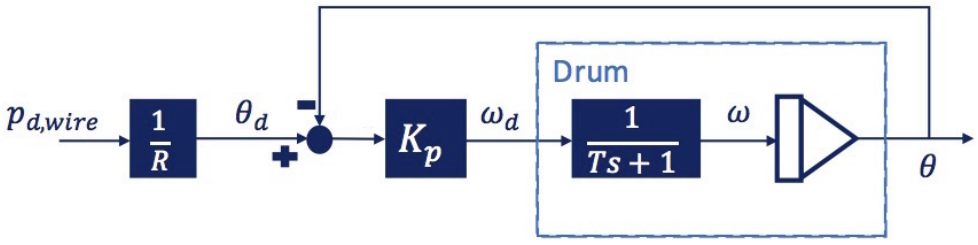

Figure 4.5: Wire compensating system implemented in Simulink (Appendix B).

This block diagram (Figure 4.5) with the given constants was implemented into the whole system as illustrated in Figure 4.2 and in Appendix B.

4.3 Irregular wave influence

The objective in this section is to create a signal in which behaves as similar to the MRU signal, when the waves are irregular, as possible. In order to do this a Band–Limited White Noise Simulink Block was set to be input of a band–pass filter as shown in Figure 4.6. This input generates normally distributed random numbers, in other words white noise.

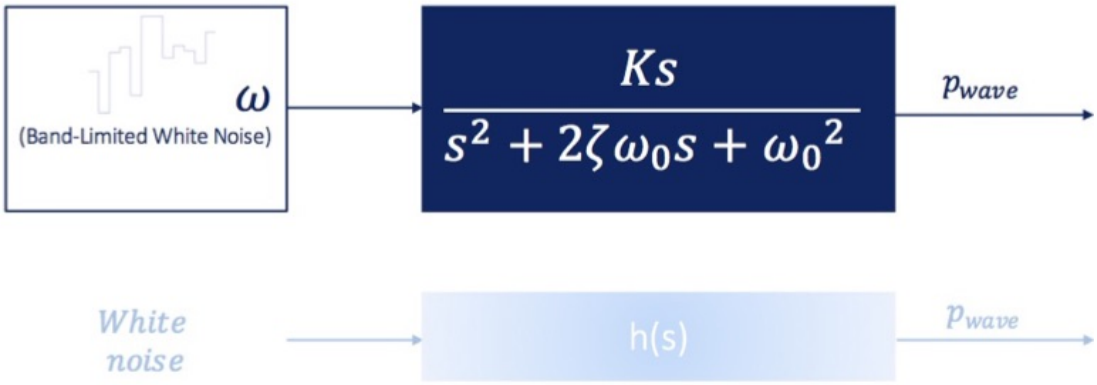

Figure 4.6: Making a realistic p_{wave}, which is the wave influence on the crane tip position. The light blue colored lower illustration illustrates how this part is marked in the overall overview in Figure 4.2.

The different parameters in the band–pass filter had to be tuned aiming for a realistic wave impact. The wave impact on x, y and z are not the same, hence different K-values had to be chosen to get different amplitudes. For simplicity's sake the damping factor, ζ, and the frequency, ω_0, were chosen to be the same for all of signals.

The value of ζ was chosen to be equal to 0.1 as a result of reading example 8.1 in Fossen (2011) and engineering intuition. According to MacGregor a period length of 8 minutes should be appropriate which lead to the deriving of ω_0

$$\omega_0 = \frac{2\pi}{T} = \frac{2\pi[\text{rad}]}{8[\text{min}] * 60[\text{sec/min}]} = \quad 0.013 \text{ [rad/sec]} \tag{4.6}$$

4.3.1 Influence on heave

For the influence on heave the value of K was chosen with the goal of reaching the significant wave height, H_s. The significant wave height is defined as the mean wave height of the highest third of the waves. According to MacGregor a proper approximation of the significant wave height is in between 2 and 4 mH_s. Several simulations gave the knowledge that a K value of 0.25 resulted in a 3.0 mH_s. This K value was chosen since it gave a significant wave height inside of the recommended interval.

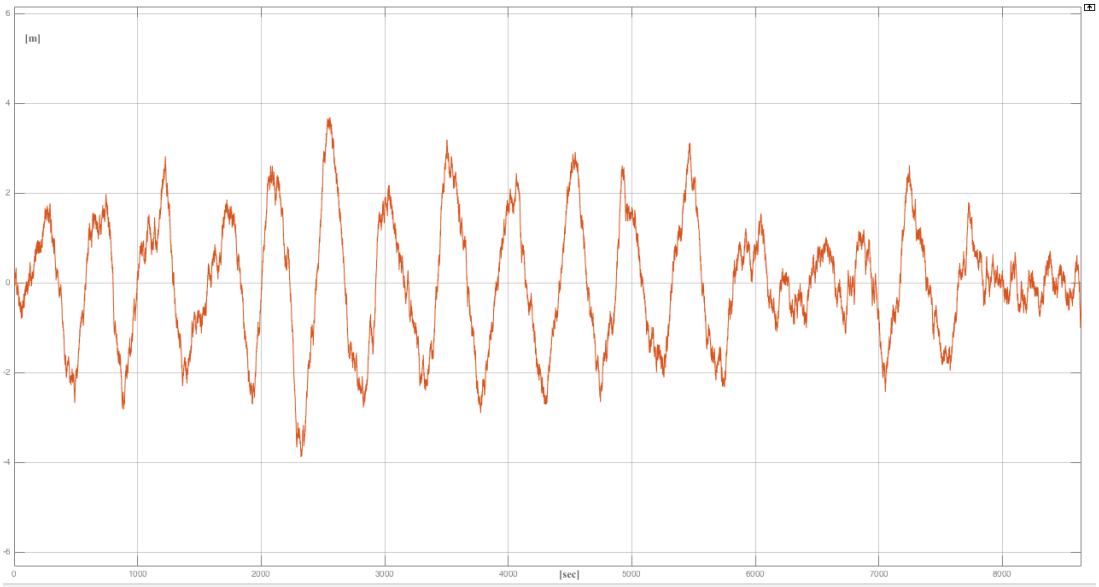

Figure 4.7: The chosen irregular wave movement upon the crane king in z–direction.

As a result of the above arguments the parameters in the band–pass filter for the influence on heave were set to be

$$\zeta = 0.1 \tag{4.7}$$

$$\omega_0 = 0.013 \text{ [rad/sec]} \tag{4.8}$$

$$K = 0.25 \tag{4.9}$$

which result in the chosen irregular wave influence on the crane king given in Figure 4.7.

4.3.2 Influence on the xy-plane

As previously stated the K value were chosen differently for the wave influence on the surge, x, and the sway, y, position compared to the z position. The maximum amplitude should intuitively be 1 m which lead to the tuning of the K value. Simulations resulted in choosing K equal to 0.07 illustrated in Figure 4.8. Hence the parameters in the band–pass filter for the influence on both x and y were set to be

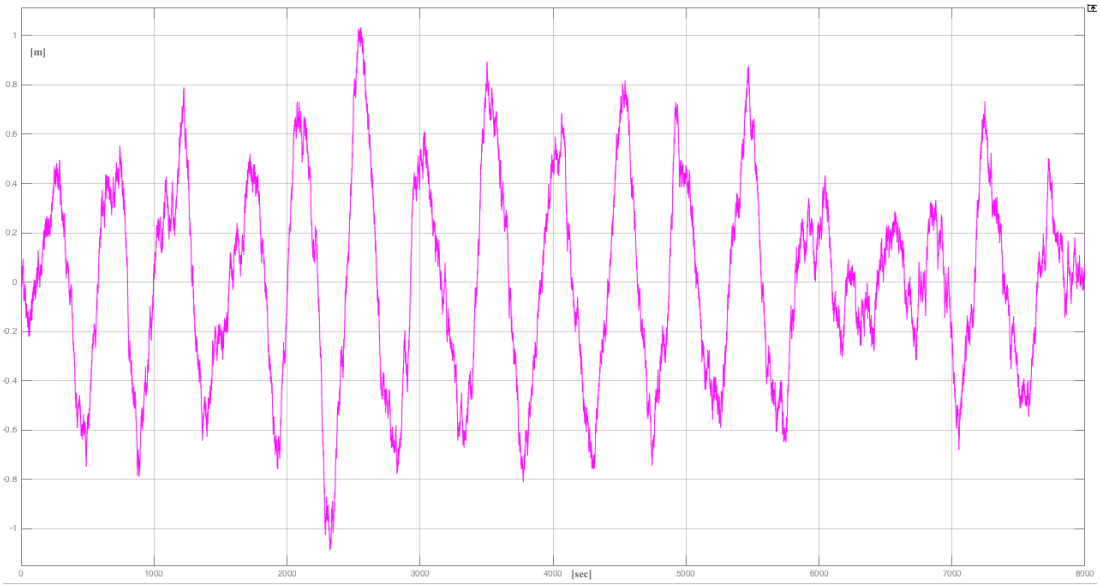

Figure 4.8: The chosen wave influence upon the crane king in both x– and y–direction.

$$\zeta = 0.1 \tag{4.10}$$

$$\omega_0 = 0.013 \text{ [rad/sec]} \tag{4.11}$$

$$K = 0.07 \tag{4.12}$$

In addition the seed numbers inside of the Band–Limited White Noise Simulink Block were chosen differently for the x and the y disturbance signal in order to create two individual signals.

After the process of creating wave influences upon heave, surge and sway the blocks illustrated in Figure 4.6 were implemented in the whole system (Figure 4.2).

5 Control System Design

In the following sections four different control system designs will be presented and explained. These are the foundation of the results in Chapter 6 and all of the controllers are operational space controllers. An short description of what operational space controllers are and the reason why they were chosen in this system is included in the first section of this chapter. The second chapter goes through the controllers common factors.

5.1 Operational space control

Often the motion specifications are assigned in operational space, which is the case for this crane system. Due to this an inverse kinematics algorithm has to be utilized to transform the operational space references into the corresponding joint space references. The process

Figure 5.1: Considering the fact that MacGregor's AHC offshore crane is placed on board a ship the environment is of concern. Reproduced with kind permission from MacGregor.

of kinematic inversion includes both the inversion of direct kinematics and the inversion of first-order and second-order differential kinematics to transform the desired time history of the end effectors position, velocity and acceleration into the corresponding quantities at joint level. This gives the process an increasing computational load. For this reason it is preferable to compute the joint positions through kinematics inversion and then perform a numerical differentiation to compute velocities and acceleration.

An alternative to this approach is to consider control schemes developed directly in the operational space. When the motion is specified in terms of operational space variables the measured joint space variables must be transformed into the corresponding operational space variables thorough direct kinematics. By comparing the desired input with the reconstructed variables one allows the design of feedback control loops where trajectory inversion is replaced with a suitable coordinate transformation embedded in the feedback loop.

Operational space controllers are presented in face of the above limitation. These controllers becomes especially relevant if the problem of controlling interaction between the manipulator and the environment is of concern (Siciliano, 2009). Seeing that the crane is placed on a ship, illustrated in Figure 5.1, these controllers can be suited for this system. Therefore four different operational space control controllers are presented below.

The first two controllers are intuitive, hence they have their weaknesses. There is no guarantee that they are effective in terms of stability and trajectory tracking. In this regard the mathematical solution controllers 3 and 4 are included since these controllers are able to improve these factors. These two controllers will be shown to be substantially equivalent to the first two controllers.

5.2 Common factors

The controllers investigated has some common factors and in the following sections these are described. Figure 5.2 illustrates the structure of the Simulink file used for all of the controllers, which is further explained in Chapter 6 and can be found in Appendix B.

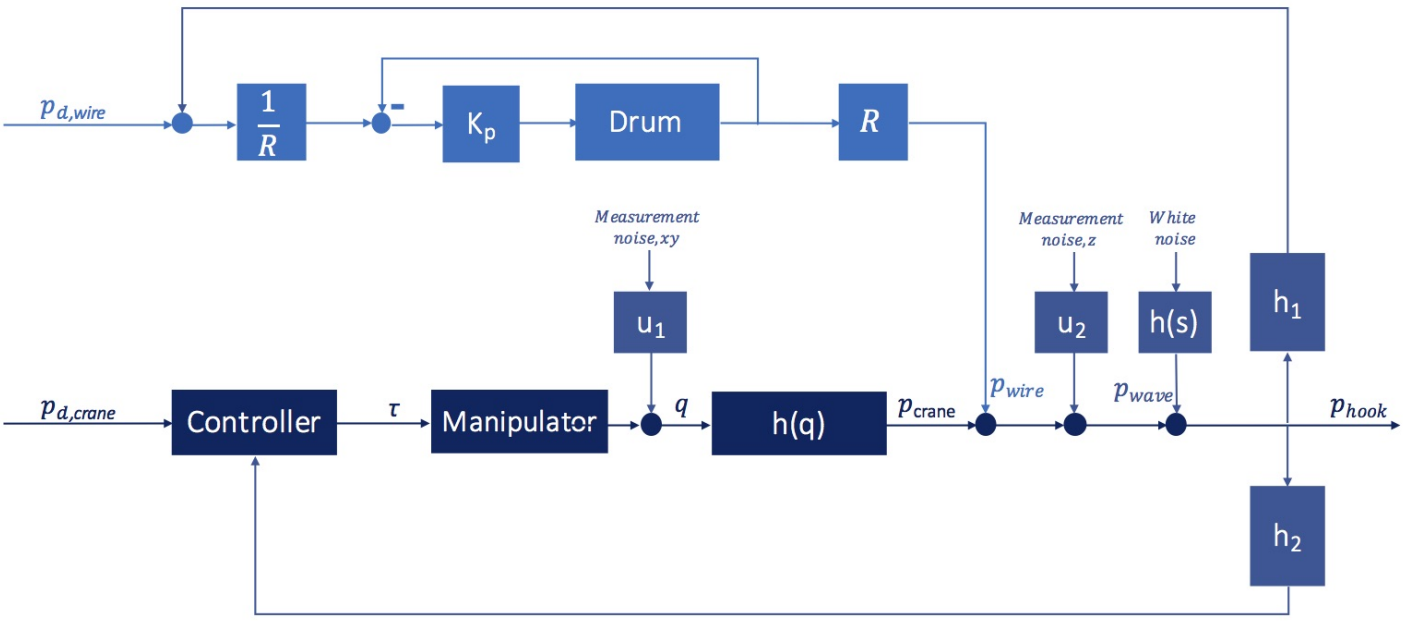

Figure 5.2: The overall system derived in this thesis used for all the controllers, which is further explained in Chapter 6.

5.2.1 Initial joint values

At first the initial joint position is set to be $\boldsymbol{q}_{init} = [0\ \frac{\pi}{2}\ -\frac{\pi}{4}]$, which is the typical starting position for the crane shown in Figure 2.3.

5.2.2 Desired input value

The desired input value for the testing of the system was set to be $p_d = [2\ 3\ 4]'$. Several other input values were tested which lead to the conclusion that this input value represented the relationship between the different controllers.

All of the inputs are filtered to avoid steps and obtain a smooth signal. These are labeled as reference filter in Figure 5.3, 5.4, 5.5 and 5.6. In the three first controllers a low–pass filter were used with $T_{lp} = 0.5$. The fourth controller used a second order filter described in Section 5.6.1. The reason why a different filter were used for controller four is that this controller uses the input speed and acceleration as well as the position in the design. This reason is further explained in Section 5.6.

5.2.3 Measurement noise

The datasheet for Kongsberg Maritime's MRU H, which is the MRU MacGregor uses, is included in appendix C. In order to create a realistic measurement noise the accuracy of this MRU is needed. In the Technical Specifications section one can find that

- Roll and pitch output accuracy $\Rightarrow 0.05°$ RMS
- Heave output accuracy $\Rightarrow$ 5 cm

This is the foundation of creating the measurement noise for the system. The measurement noise was created by adding a Band-Limited White Noise block on the $\boldsymbol{q}$ signal for x and y and on the $\boldsymbol{p}$ signal for z in Simulink. In order to match the signal with the MRU's accuracy for roll, pitch and heave the noise power was tuned to be

$$\text{Noise power} = 2 \times 10^{-5} \tag{5.1}$$

which gave a white noise output with a maximum of 5 cm for heave and a maximum of 0.05 ° RMS for roll and pitch.

5.2.4 Torque saturation

As explained in Section 2.2.2 there were set a saturation block in the controller blocks to make sure that the torque value does not exceed the specification of the electric motors used. The value in the saturation block were set to be $\tau \leq 5$ kNm in all of the controllers. Section 6.1.1, 6.1.2 and 6.1.3 describe the tuning process, as a result of the torque saturation, of the tuning constants T and K for controller 1, 2, 3 and 4 respectively.

5.2.5 h($\boldsymbol{q}$) and manipulator

The block h($\boldsymbol{q}$) is included in all of the controllers to transform the joint angle values into position values. Equation 2.42 is used in this transformation. The manipulator is derived in Section 3.4.

5.3 Controller 1 – Jacobian inverse control

The first controller examined is called Jacobian inverse control and is illustrated in Figure 5.3. Firstly the position reference goes through a reference model explained in Section 5.2.2. In this controller the end effector position, p, pose in the operational space is compared with the desired position, p_d. This comparison gives the operational space deviation Δp. Assuming that the deviation Δp is sufficiently small it can be transformed into a corresponding joint space deviation Δq by the inverse manipulator Jacobian (explained in Section 2.7.2). Furthermore the control input generalized forces (τ) can be derived on the basis of this deviation through a suitable feedback matrix gain (see Section 6.1).

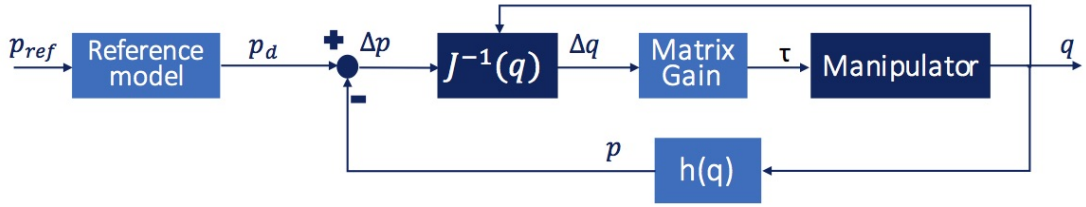

Figure 5.3: Block scheme of controller 1 – Jacobian inverse control.

In other words the Jacobian inverse control leads to an overall system which intuitively behaves like a mechanical system with generalized n-dimensional spring in the joint space, whose constant stiffness is determined by the feedback matrix gain. The role of such system is to take the deviation delta q to zero. If the matrix gain is diagonal the generalized spring corresponds to n independent elastic elements, one for each joint.

5.4 Controller 2 – Jacobian transpose control

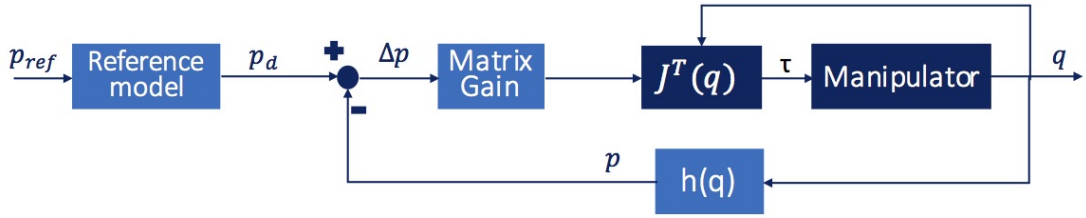

Figure 5.4: Block scheme of controller 2 – Jacobian transpose control

Controller 2 is a conceptually analogous controller called Jacobian transpose control and can be seen in Figure 5.4. This controller differs from the first controller in that the operational space error is treated first through a matrix gain (see Section 6.1) where the output of this box can be considered as the elastic force generated by a generalized spring whose function in the operational space is to reduce or cancel the position deviation Δp. This output is then transformed into joint space generalized forces through the transpose of the Jacobian.

5.5 Controller 3 – PD control with gravity compensation

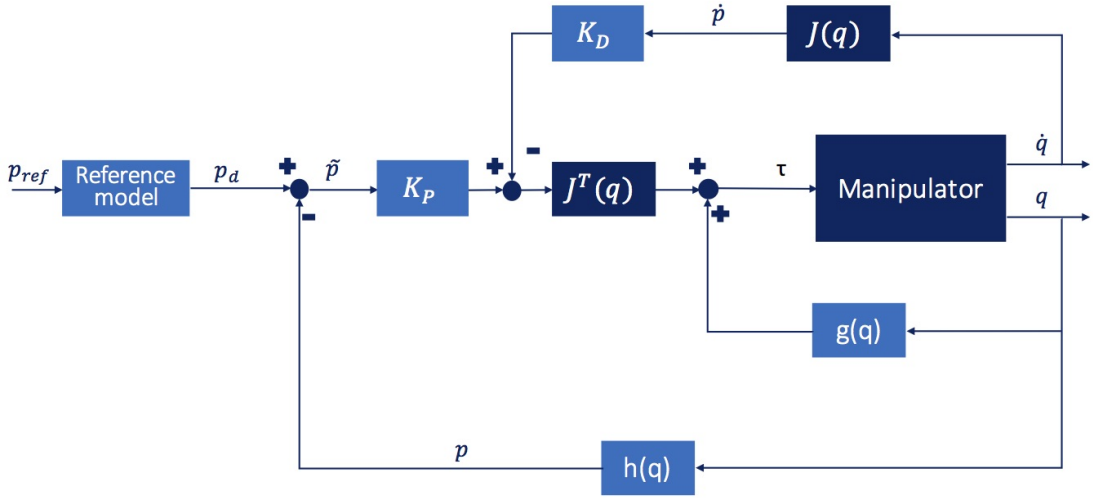

Figure 5.5: Block scheme of controller 3 – operational space PD control with gravity compensation.

Given a constant desired end effector position $\boldsymbol{p}_d$ the control structure should be chosen so that the operational space error

$$\tilde{\boldsymbol{p}} = \boldsymbol{p}_d - \boldsymbol{p} \tag{5.2}$$

tends asymptotically to zero. Choosing the following positive definite quadratic form as a Lyapunov function candidate

$$V(\dot{\boldsymbol{q}}, \tilde{\boldsymbol{p}}) = \frac{1}{2}\dot{\boldsymbol{q}}^T \boldsymbol{B}(\boldsymbol{q})\dot{\boldsymbol{q}} + \frac{1}{2}\tilde{\boldsymbol{p}}^T \boldsymbol{K}_P \tilde{\boldsymbol{p}} > 0 \qquad \forall \dot{\boldsymbol{q}}, \tilde{\boldsymbol{p}} \neq 0 \tag{5.3}$$

where $\boldsymbol{K}_P$ (derived in Section 6.1) should be a symmetric positive definite matrix. When differentiating (5.3) with respect to time one gets

$$\dot{V} = \dot{\boldsymbol{q}}^T \boldsymbol{B}(\boldsymbol{q})\ddot{\boldsymbol{q}} + \frac{1}{2}\dot{\boldsymbol{q}}^T \dot{\boldsymbol{B}}(\boldsymbol{q})\dot{\boldsymbol{q}} + \dot{\tilde{\boldsymbol{p}}}^T \boldsymbol{K}_P \tilde{\boldsymbol{p}} \tag{5.4}$$

$\dot{\boldsymbol{p}} = \boldsymbol{0}$ gives

$$\dot{\tilde{p}} = -\boldsymbol{J}(\boldsymbol{q})\dot{\boldsymbol{q}} \tag{5.5}$$

which leads to

$$\dot{V} = \dot{\boldsymbol{q}}^T \boldsymbol{B}(\boldsymbol{q})\ddot{\boldsymbol{q}} + \frac{1}{2}\dot{\boldsymbol{q}}^T \dot{\boldsymbol{B}}(\boldsymbol{q})\dot{\boldsymbol{q}} - \dot{\boldsymbol{q}}^T \boldsymbol{J}^T(\boldsymbol{q})\boldsymbol{K}_P \tilde{\boldsymbol{p}}. \tag{5.6}$$

Recalling the expression of the joint space manipulator dynamic model the expression is no given by

$$\dot{V} = -\dot{\boldsymbol{q}}^T \boldsymbol{F}\dot{\boldsymbol{q}} + \dot{\boldsymbol{q}}^T(\boldsymbol{u} - \boldsymbol{g}(\boldsymbol{q}) - \boldsymbol{J}^T(\boldsymbol{q})\boldsymbol{K}_P \tilde{\boldsymbol{p}}) \tag{5.7}$$

where $\boldsymbol{g}(\boldsymbol{q})$ can be seen Section 3.3. The structure of the controller is suggested by this expression (5.7) so by choosing the control law

$$\boldsymbol{u} = \boldsymbol{g}(\boldsymbol{q}) + \boldsymbol{J}^T(\boldsymbol{q})\boldsymbol{K}_P \tilde{\boldsymbol{p}} - \boldsymbol{J}^T(\boldsymbol{q})\boldsymbol{K}_D \boldsymbol{J}(\boldsymbol{q})\dot{\boldsymbol{q}} \tag{5.8}$$

where $\boldsymbol{K}_D$ (derived in Section 6.1) should be positive definite (5.7) becomes

$$\dot{V} = -\dot{\boldsymbol{q}}^T \boldsymbol{F}\dot{\boldsymbol{q}} - \dot{\boldsymbol{q}}^T \boldsymbol{J}^T(\boldsymbol{q})\boldsymbol{K}_D \boldsymbol{J}(\boldsymbol{q})\dot{\boldsymbol{q}}. \tag{5.9}$$

When comparing Figure 5.5 and Figure 5.4 one can easily see the similarities. The main difference is that the control law (5.8) performs a nonlinear compensation action of joint

space gravitational forces and an operational space linear PD control action. The PD control action is included to enhance the system damping.

By looking at (5.9) one can see that for any system trajectory the Lyapunov function decreases as long as $\dot{\boldsymbol{q}} \neq \boldsymbol{0}$ in which the system reaches equilibrium posture. This posture is determined by a stability argument:

$$\boldsymbol{J}^T(\boldsymbol{q})\boldsymbol{K}_P\tilde{\boldsymbol{q}} = 0. \tag{5.10}$$

Under the assumption of full rank Jacobian (derived in Section 2.7.2) it can be recognized from (5.10) that

$$\tilde{\boldsymbol{p}} = \boldsymbol{p}_d - \boldsymbol{p} = 0 \tag{5.11}$$

which is as desired in first place.

5.6 Controller 4 – Inverse dynamics control

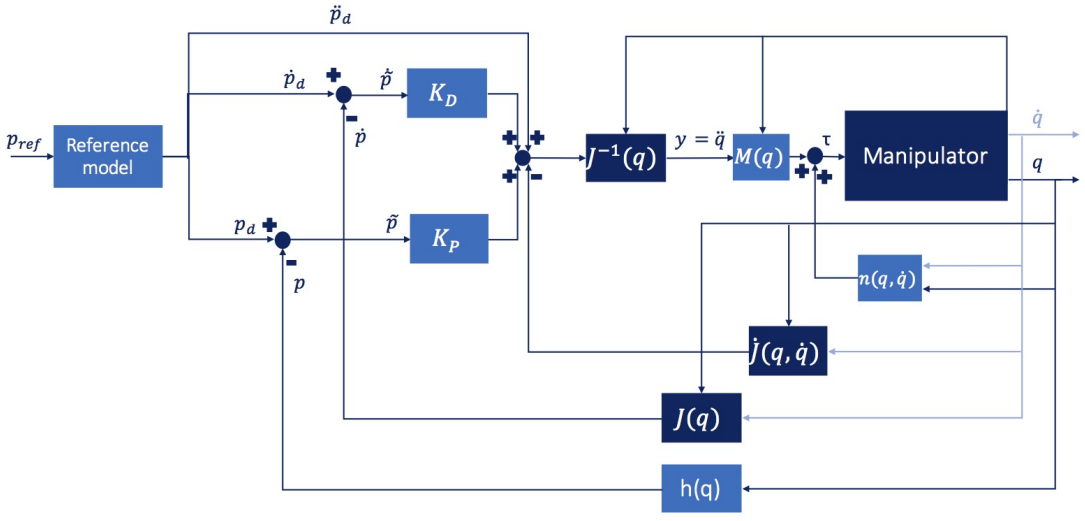

Figure 5.6: Block scheme of operational space inverse dynamics control

Considering the problem of tracking an operational space trajectory the manipulator dynamic model must be included:

$$\boldsymbol{M}(\boldsymbol{q})\ddot{\boldsymbol{q}} + \boldsymbol{n}(\boldsymbol{q}, \dot{\boldsymbol{q}}) = \boldsymbol{\tau} \tag{5.12}$$

where $\boldsymbol{M}(\boldsymbol{q})$ can be found in Section 3.2 and $\boldsymbol{n}(\boldsymbol{q}, \dot{\boldsymbol{q}})$ is given by (6.48) in Sciavicco and Siciliano (1996).

$$\boldsymbol{n}(\boldsymbol{q}, \dot{\boldsymbol{q}}) = \boldsymbol{C}(\boldsymbol{q}, \dot{\boldsymbol{q}})\dot{\boldsymbol{q}} + \boldsymbol{g}(\boldsymbol{q}) \tag{5.13}$$

when friction is neglected. $\boldsymbol{C}(\boldsymbol{q}, \dot{\boldsymbol{q}})$ is given in Section 3.2 and $\boldsymbol{g}(\boldsymbol{q})$ in Section 3.3.

The choice of the inverse dynamics linearizing control

$$\boldsymbol{\tau} = \boldsymbol{M}(\boldsymbol{q})\boldsymbol{y} + \boldsymbol{n}(\boldsymbol{q}, \dot{\boldsymbol{q}}) \tag{5.14}$$

leads to the system of double integrators

$$\ddot{\boldsymbol{q}} = \boldsymbol{y} \tag{5.15}$$

$\boldsymbol{y}$ is to be designed so as to be yield tracking of a trajectory specified by $\boldsymbol{p}_d$. This gives the second-order differential equation on the form

$$\ddot{\boldsymbol{p}} = \boldsymbol{J}(\boldsymbol{q})\ddot{\boldsymbol{q}} + \dot{\boldsymbol{J}}(\boldsymbol{q}, \dot{\boldsymbol{q}})\dot{\boldsymbol{q}} \tag{5.16}$$

which means that for a nonredundant manipulator the choice of control law is

$$\boldsymbol{y} = \boldsymbol{J}^{-1}(\boldsymbol{q})(\ddot{\boldsymbol{p}} + \boldsymbol{K}_D\dot{\tilde{\boldsymbol{p}}} + \boldsymbol{K}_P\tilde{\boldsymbol{p}} - \dot{\boldsymbol{J}}(\boldsymbol{q}, \dot{\boldsymbol{q}})\dot{\boldsymbol{q}}) \tag{5.17}$$

where $\boldsymbol{K}_P$ and $\boldsymbol{K}_D$ are positive definite diagonal matrices defined in Section 6.1. The Jacobian matrix is derived in Section 2.7.2. By substitution one gets

$$\ddot{\tilde{\boldsymbol{p}}} + \boldsymbol{K}_D\dot{\tilde{\boldsymbol{p}}} + \boldsymbol{K}_P\tilde{\boldsymbol{p}} = 0 \tag{5.18}$$

The derivative of the Jacobian is defined

$$\dot{\boldsymbol{J}}(\boldsymbol{q}, \dot{\boldsymbol{q}}) = \frac{d}{dt}\boldsymbol{J}(\boldsymbol{q}, \dot{\boldsymbol{q}}) = \frac{d}{dq}\boldsymbol{J}(\boldsymbol{q})\dot{\boldsymbol{q}} \tag{5.19}$$

and set to be equal to zero in this thesis. This approximation is done due to the slowness of the system.

$$\dot{\boldsymbol{J}}(\boldsymbol{q}, \dot{\boldsymbol{q}}) = 0 \tag{5.20}$$

5.6.1 Reference model controller 4

An reference model was implemented in Simulink to avoid steps and to obtain smooth position, velocity and acceleration signals into the controllers. The reference model described in this section is used for controller 4 only.

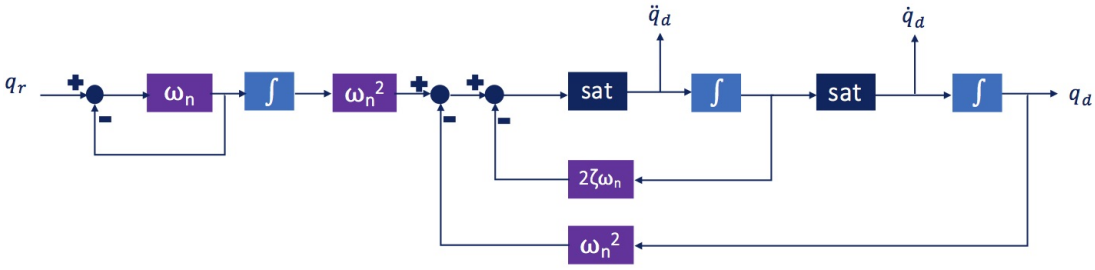

Figure 5.7: The reference model implemented in Simulink.

Figure 5.7 illustrates the implemented reference block diagram in Simulink. The reference joint angle $\boldsymbol{q}_r$, which is found by inverse kinematics of the joystick reference $\boldsymbol{p}_r$, is the input of this model. The outputs of the model are $\ddot{\boldsymbol{q}}_d$, $\dot{\boldsymbol{q}}_d$ and $\boldsymbol{q}_d$, which are the desired joint angle, angular velocity and angular acceleration.

ζ is the relative damping ratio and ω_n is the natural frequency. Both these parameters have to be chosen in in regard to the desired performance.

With $\zeta = 0$ the system is undamped, which means that no energy is removed from the system. By choosing $0 > \zeta < 1$ the system is under damped and $\zeta = 0$ gives a critically damped system. $\zeta > 1$ gives an over damped system.

For this thesis, where the crane is in normal mode, ω_n and ζ were chosen to be:

$$\omega_n = \begin{bmatrix} 0.1 \\ 0.1 \\ 0.1 \end{bmatrix}$$
$$\zeta = \begin{bmatrix} 1.0 \\ 1.0 \\ 1.0 \end{bmatrix} \tag{5.21}$$

This gives a critically damped system and with these parameters the reference model gives a quit realistic q_r.

5.7 Brief Summary

All of the four controllers were implemented in Simulink/MATLAB as described in the previous sections. This implementation can be seen in Appendix B and the tuning constants used are included in Section 6.1.

6 Results

This chapter will present the final result of this thesis. The entire system given in the previous chapters was implemented as illustrated in Figure 6.1 and the Simulink diagram is included in Appendix B.

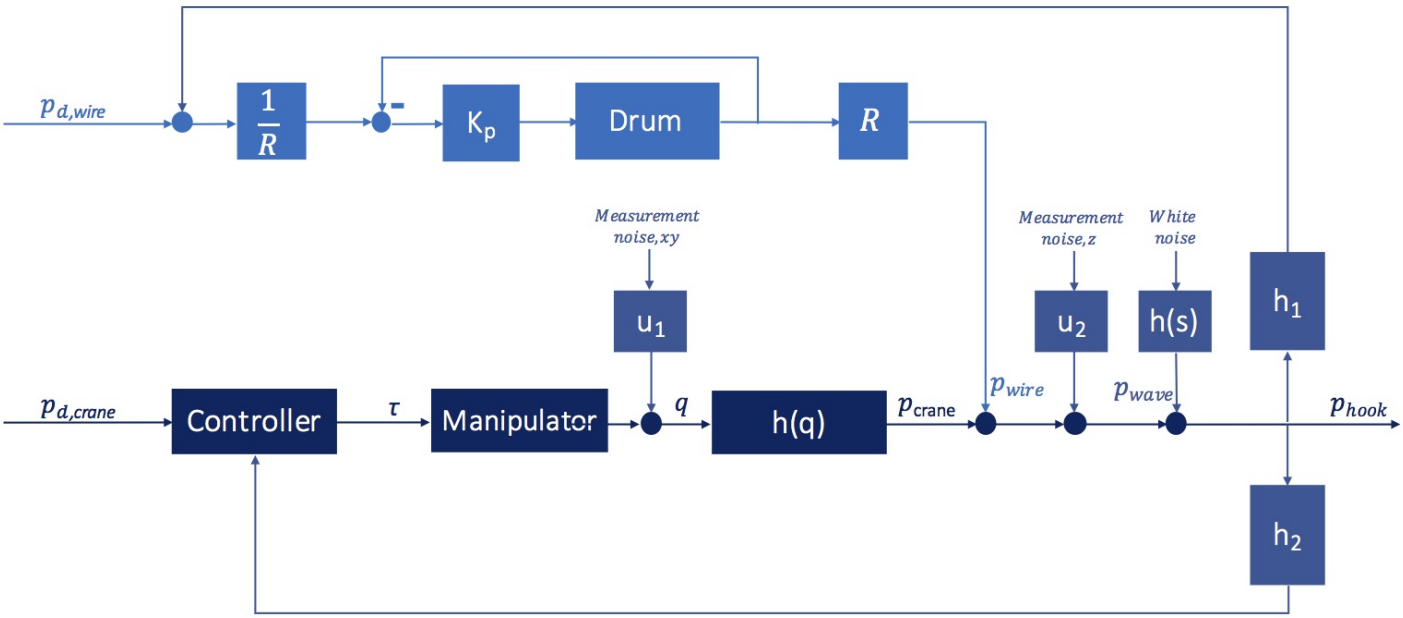

Figure 6.1: An illustration of the overall system implemented in Simulink (Appendix B), which is further explained in Chapter 6.

As can be seen in Figure 6.1 the heave movement is regulated by the wire and the surge and sway movement by the control system in the manipulator. In Section 4.2 the heave regulating part is described, while the surge and sway regulating part is described in Chapter 5. The white noise block gives the wave influence described in Section 4.3 and the measurement noise blocks gives the measurements realistic disturbances. These disturbances are expressed in Section 5.2.3. The input values are defined in Section 5.2.2. Heave, surge and sway each have their own desired movement and error subsections where the simulation plots are included. At the end a robustness analysis is included to help determine the credibility of the results. The joint angle and torque values in the simulations are included in Appendix E and F respectively. Firstly the tuning constants for the different controllers are includes as a part of the results.

6.1 Tuning constants

In this section these tuning constants, which are used inside the controllers, are presented:

T Time constant reference filter [s]
K_P Proportional gain
K_D Derivative gain

where one can find the time constant for reference filter in the reference model block in Figure 5.3, 5.4, 5.5 and 5.6. For controller 1 and 2 one can find the proportional gain in the matrix gain block in Figure 5.3 and 5.4. Controller 3 and 4 illustrates the proportional gain and derivative gain with their K_P and K_D blocks respectively in Figure 5.5 and 5.6.

The objective in the tuning process is to give a result as desirable as possible. Oscillations, time reaching desired value and overshoot were factors considered in this process. All of the tuning constants presented below are included in Appendix B.

6.1.1 Tuning constants controller 1

The tuning process for controller 1 was hard due to the fact that this control system did not work satisfactory. The tuning constants were chosen to be

$$T_{lp} = \begin{bmatrix} 0.1 \\ 0.1 \\ 0.1 \end{bmatrix} \tag{6.1}$$

$$K_P = \begin{bmatrix} 10 & 0 & 0 \\ 0 & 1 & 0 \\ 0 & 0 & 1 \end{bmatrix} \tag{6.2}$$

because this gave the least least bad outcome. If the controller had performed in a better way more time would be spend in the tuning process.

6.1.2 Tuning constants controller 2

Controller did, like controller 1, not give the desired behavior. Therefore the tuning process was quite difficult. The following tuning constants were chosen aiming a result as well as possible without spending too much time.

$$T_{lp} = \begin{bmatrix} 0.6 \\ 0.1 \\ 0.1 \end{bmatrix} \tag{6.3}$$

$$K_P = \begin{bmatrix} 10 & 0 & 0 \\ 0 & 1 & 0 \\ 0 & 0 & 1 \end{bmatrix} \tag{6.4}$$

6.1.3 Tuning constants controller 3 and 4

The tuning constants for controller 3 and 4 happened to be equal during the tuning process. This was because these values gave the most desirable result for both of the controllers. They were chosen to be:

$$T_{lp} = \begin{bmatrix} 0.1 \\ 0.1 \\ 0.1 \end{bmatrix} \tag{6.5}$$

$$K_P = \begin{bmatrix} 10 & 0 & 0 \\ 0 & 1 & 0 \\ 0 & 0 & 1 \end{bmatrix} \tag{6.6}$$

$$K_D = \begin{bmatrix} 10 & 0 & 0 \\ 0 & 10 & 0 \\ 0 & 0 & 10 \end{bmatrix} \tag{6.7}$$

Considering there may be errors, like dimensions deviations, both controller 3 and 4 should be tuned when implemented in the crane. In this regard a limited amount of time only was spent tuning these controllers.

6.2 Desired heave movement and error

At first the desired heave movement and the error are presented. This is an external system, which means that the different controllers give the same heave error. The desired heave movement is a step input, with a reference filter, where the y value should move four meters down (Section 5.2.2). This is illustrated in Figure 6.2. Figure 6.3 illustrates the heave error of the system. As one can see there are quite small deviations considering the powerful wave influence. The overshoot in the beginning indicates a slowness of the system which can be tuned more perfectly, or removed by adjusting the reference filter in future work.

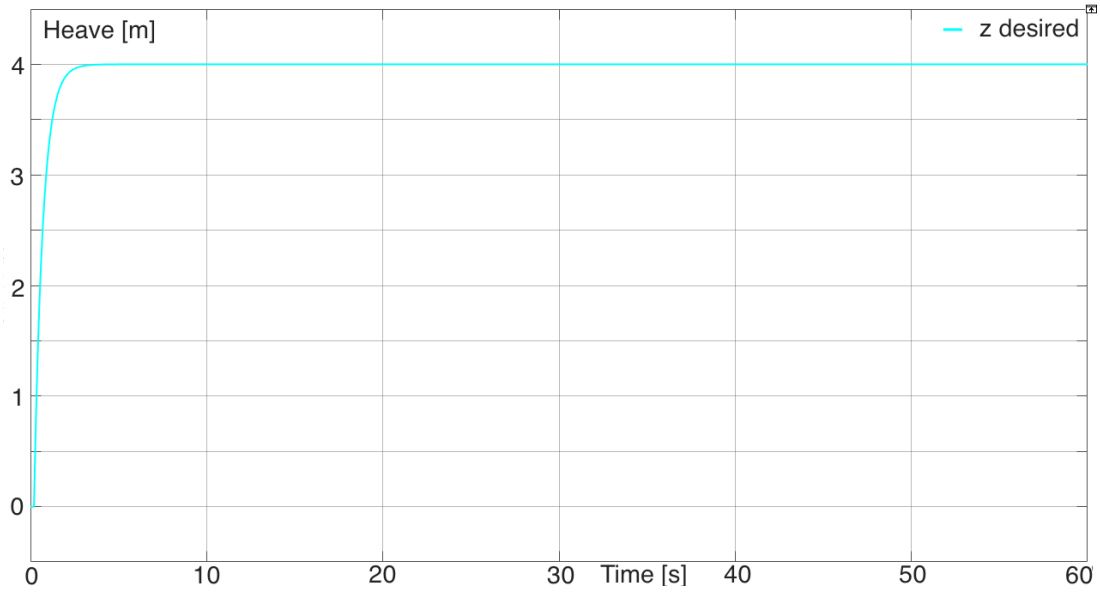

Figure 6.2: Desired heave movement. The desired final value is four meters down for all of the controller systems.

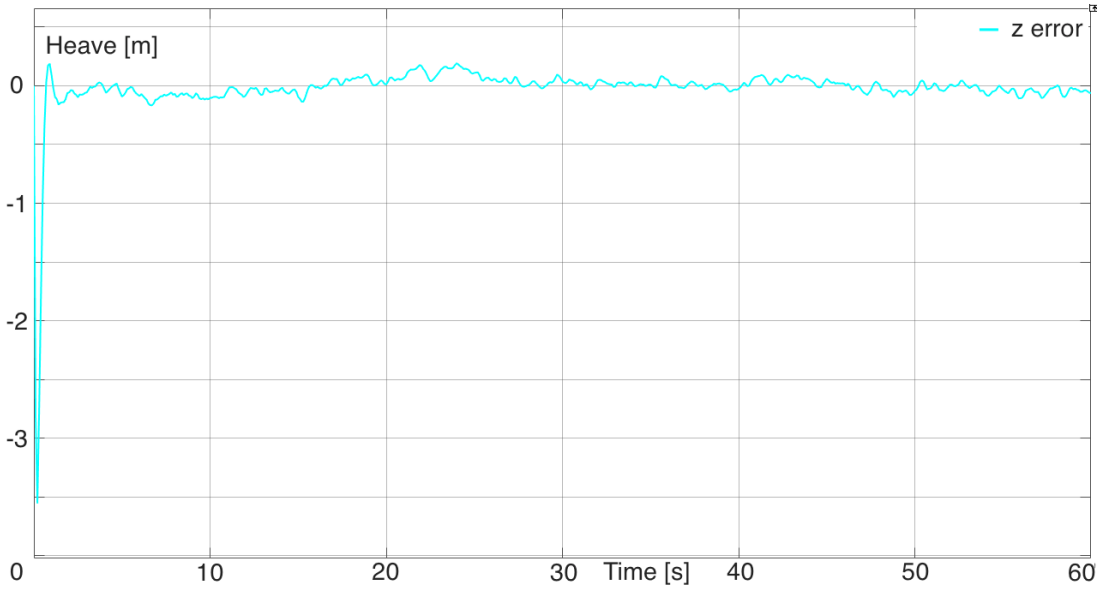

Figure 6.3: Heave error. This error is the same for all of the controllers by reason of winch-controlled heave movement. As the graph displays the deviations are small.

6.3 Desired surge movement and error

Secondly the desired surge movement and error is presented. Here the desired movement is two meters in positive x–direction as illustrated in Figure 6.4. A step input, with a low–pass filter, is set as input as described in Section 5.2.2. The result from the four different controllers will be given in the next sections.

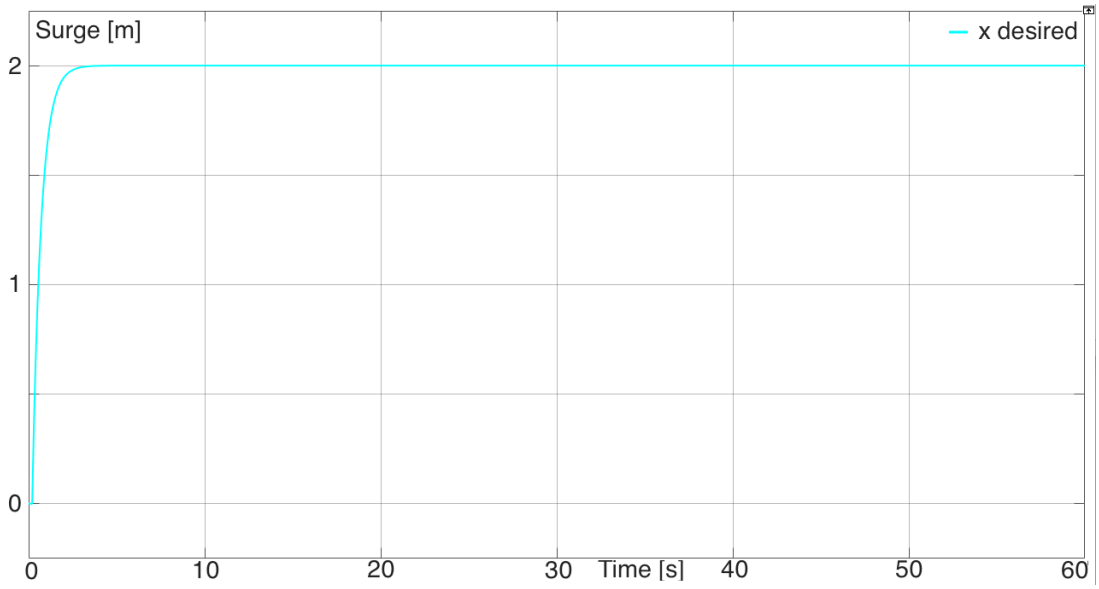

Figure 6.4: Desired surge movement for all of the controllers. The desired value is two meters in positive x–direction.

As Figure 6.5 and 6.6 shows that controller 1 and 2 are not able to compensate for the wave impact on the surge axis. This is no surprise due to the simple nonmodel–based design of these controllers. The systems behaves so badly with these controllers that the crane would not handle it, and it would terrible idea implementing them into MacGregor's system.

On the other hand controller 3 and 4 are in some way able to compensate for the powerful wave movements affecting the surge axis. As illustrated in Figure 6.7 and 6.8 controller 3 has some more oscillations but a smaller overshoot than controller 4. These deviations could be handled with an even more thorough tuning process, but due to time limitations and knowing there may be dimensions errors, this was not accomplished in this thesis. Anyhow these results indicates that there certainly are potential for surge compensations in the control design for MacGregor.

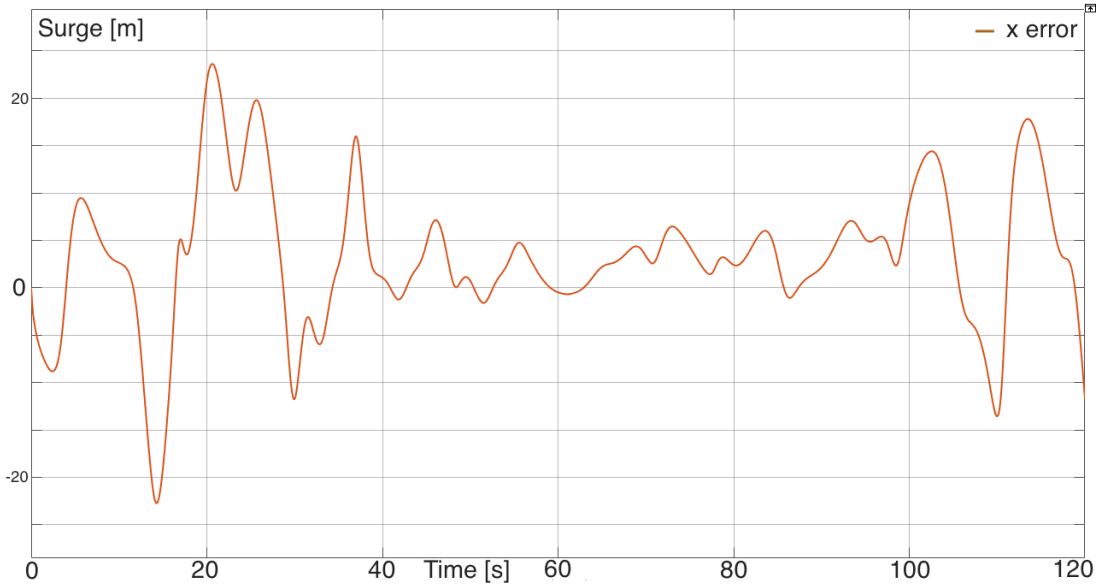

Figure 6.5: **Surge error in controller 1 – Jacobian inverse control**. It is not able to compensate for the wave movements upon the crane, in fact it behaves worse than without the control system.

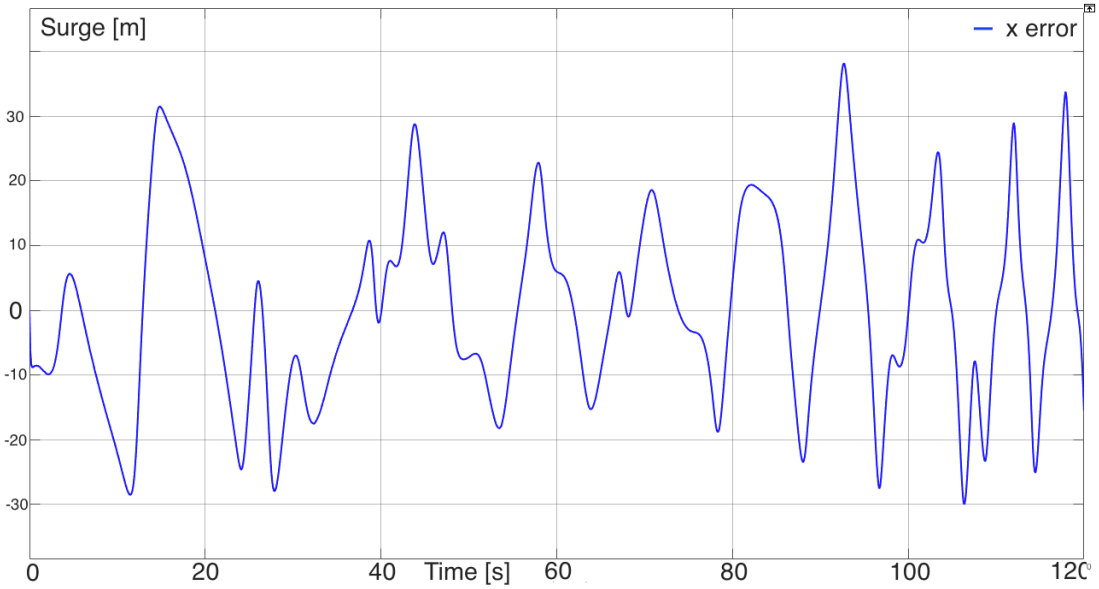

Figure 6.6: **Surge error in controller 2 – Jacobian transpose control**. This controller is not either able to control for the wave influence upon the crane.

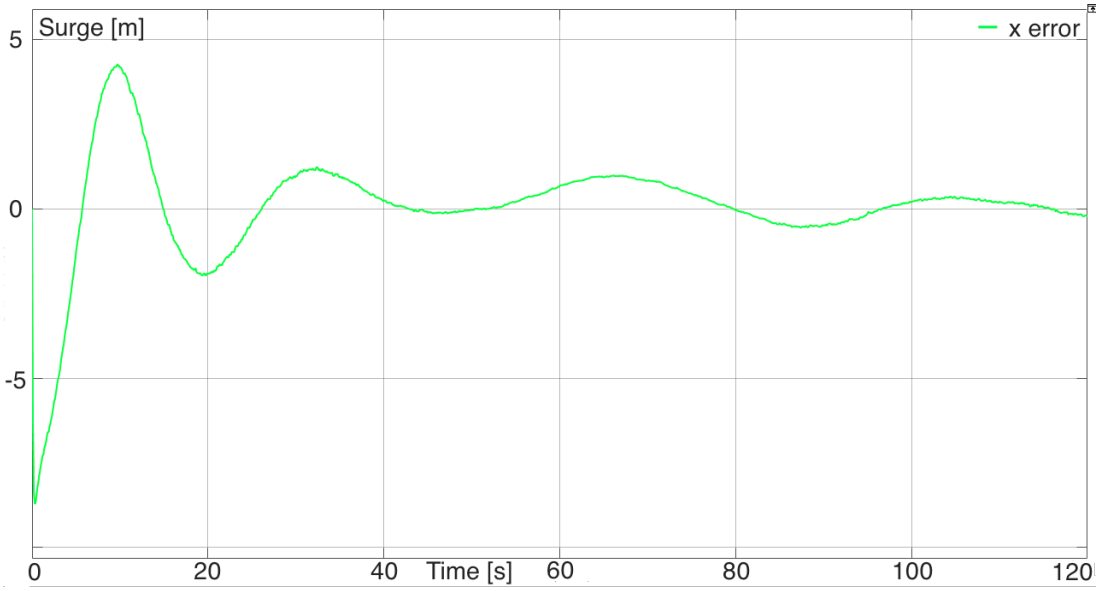

Figure 6.7: **Surge error in controller 3 – PD control with gravity compensation**. This controller is in some level able to compensate for the wave movements, even though it should be tuned some more before it can be applied.

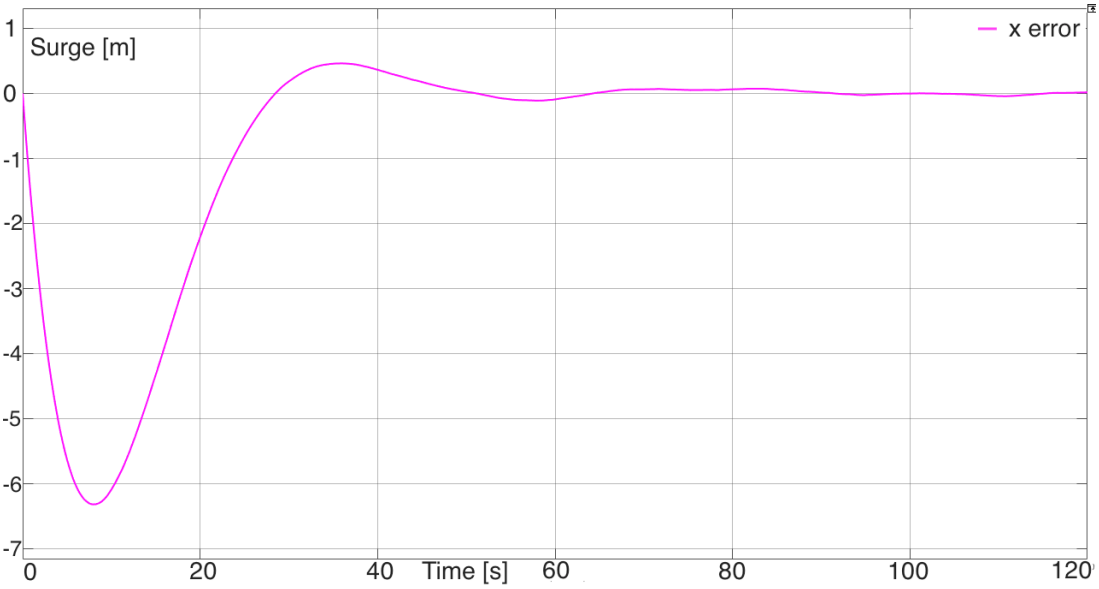

Figure 6.8: **Surge error in controller 4 – Inverse dynamics control**. After about 30 seconds this controllers compensate excellent for the wave influence. This also needs some more perfection before it can be applied.

6.4 Desired sway movement and error

Finally the desired sway movement and error is presented. Like the heave and the surge input the sway input is a step input with a reference filter presented in Section 5.2.2. The desired movement is three meters in positive y–direction. In the following sections one can see the results for the four different controllers.

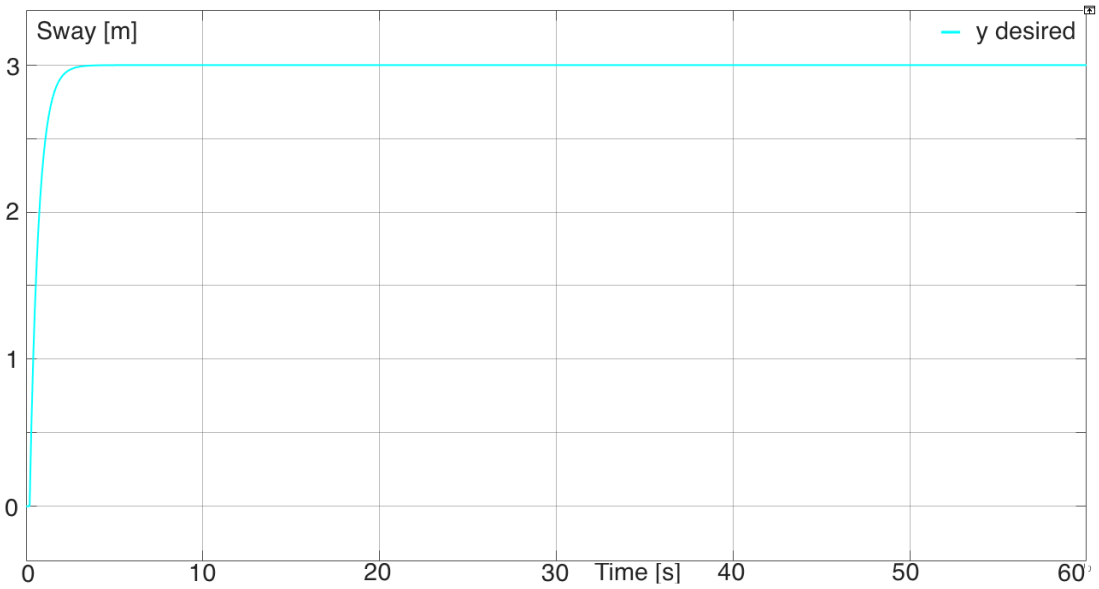

Figure 6.9: Desired sway movement for all of the controllers. The desired value is three meters in positive y–direction.

The errors on the sway movements indicates the same as for the surge movements, controller 1 and 2 do not behave satisfactory but controller 3 and 4 do. One can see that also here the output errors of controller 1 and 2 are too much for the crane system to handle. Controller 3 and 4 has smaller deviations than in surge axis, but the still need to be handled with more thorough tuning. In summation controller 1 and 2 can be ruled out, while controller 3 and 4 gives a proper foundation for further work.

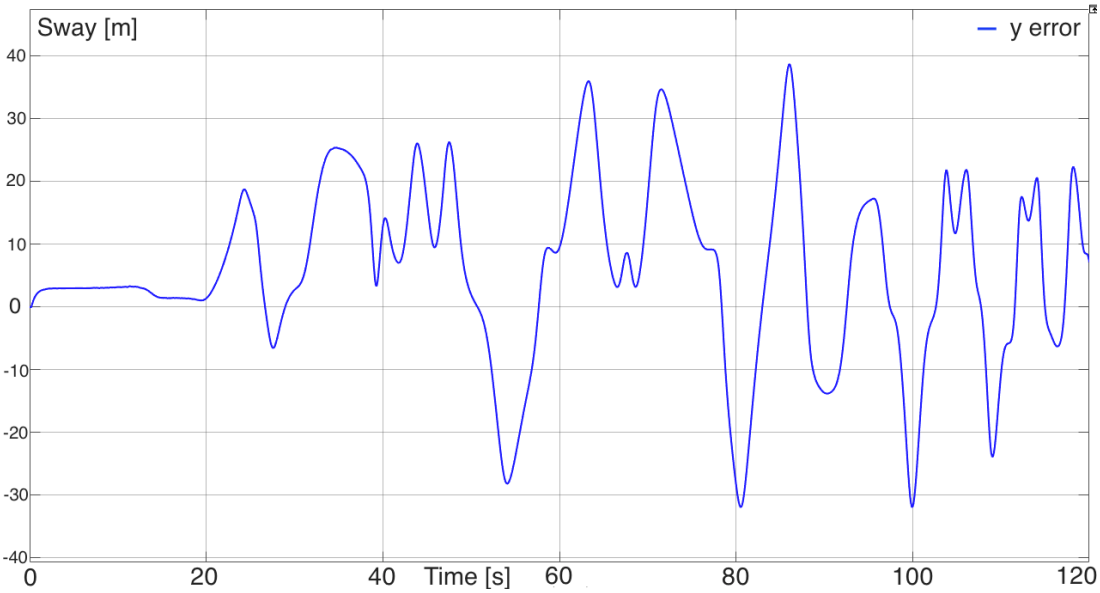

Figure 6.10: **Sway error in controller 1 – Jacobian inverse control**. This controller should not be applied due to its bad performance.

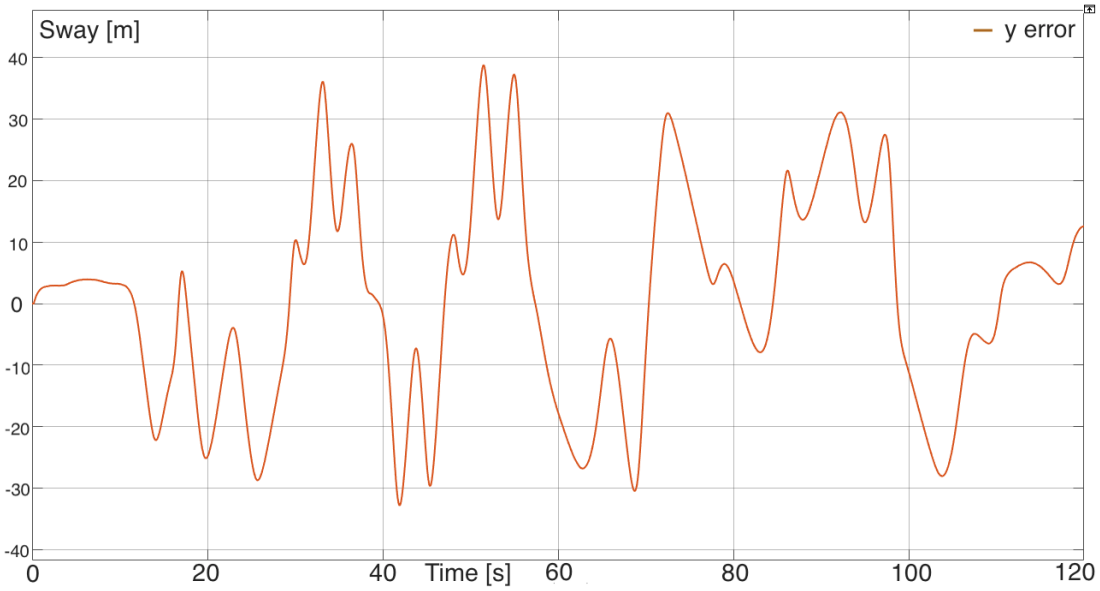

Figure 6.11: **Sway error in controller 2 – Jacobian transpose control**. Like in surge direction controller 2 is not able to compensate for the wave influence upon the crane sway direction.

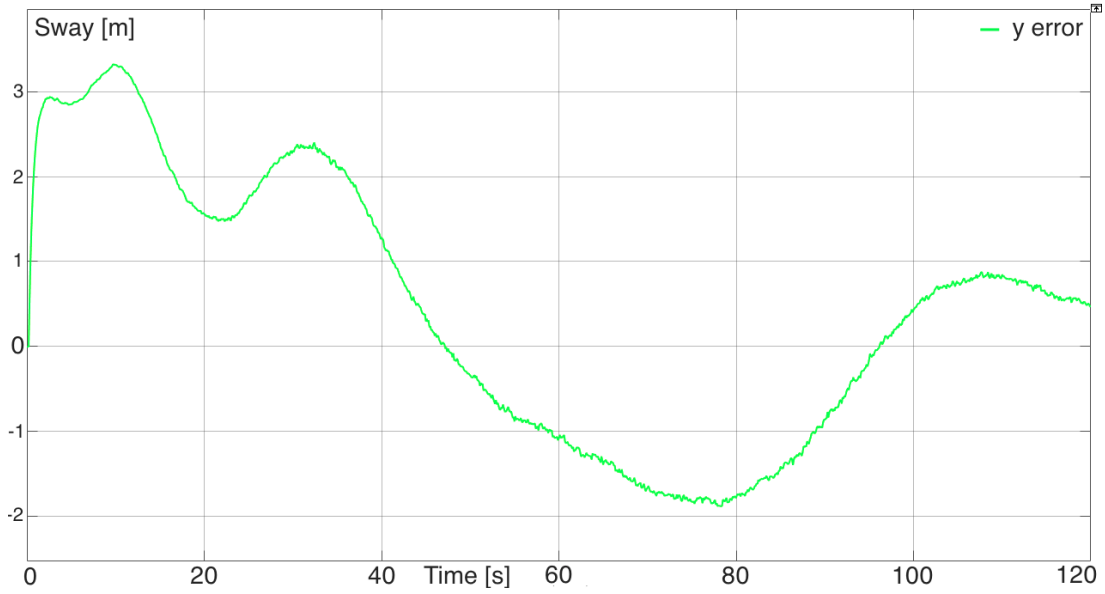

Figure 6.12: **Sway error in controller 3 – PD control with gravity compensation**. Some more perfecting of the tuning controllers needs to be done before applying, but this simulation gives a satisfying foundation.

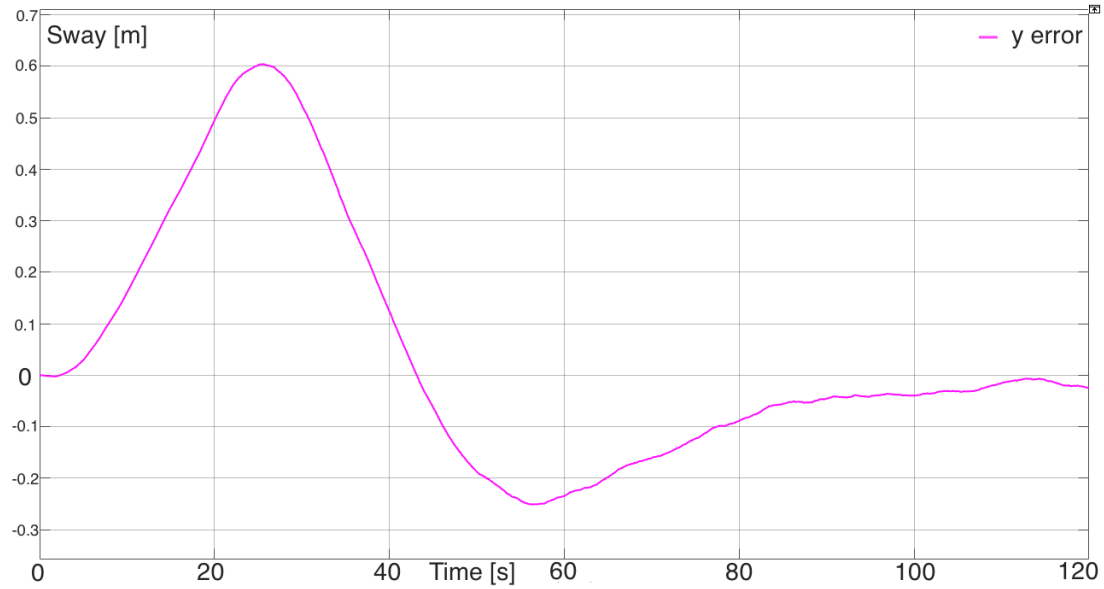

Figure 6.13: **Sway error in controller 4 – Inverse dynamics control**. It compensates exceptional for the wave influence upon the crane in sway direction.

6.5 Robustness analysis

Sections 6.2 – 6.4 gives the results for the different controllers given a perfect modeled crane. The different dimensions used in this thesis are given by appendix A and are shown in Table 2.4. With the objective of giving a result as realistic as possible questioning these dimensions is necessary. One way of doing that is to perform a robustness analysis. This analysis is, in this thesis, done by adding a random error on each of the dimension constants. The error will vary in the range between -10% and 10%. For instance the length of the king with an added error is calculated like this

$$l_{1e} = l_1 + \Delta l_1 \qquad \text{where} \qquad \Delta l_1 = 0.1\, l_1 \tag{6.8}$$

When using the same procedure for all of the dimensions, with Δ chosen randomly satisfying $-0.1 \leq \Delta \leq 0.1$, one get:

Table 6.1: Crane dimensions with error.

Length, king	l_1	9.3 m	$\Delta =$ 0.06	l_{1e}	9.86 m
Length, main jib	l_2	24.0 m	$\Delta =$ -0.07	l_{2e}	22.32 m
Length, knuckle jib	l_3	13.3 m	$\Delta =$ -0.09	l_{3e}	12.10 m
Radius, king	r_1	1.8 m	$\Delta =$ 0.03	r_{1e}	1.85 m
Height, main jib	h_2	2.0 m	$\Delta =$ -0.10	h_{2e}	1.80 m
Height, knuckle jib	h_3	1.5 m	$\Delta =$ 0.04	h_{3e}	1.56 m
Depth, main jib	d_2	1.9 m	$\Delta =$ 0.02	d_{2e}	1.94 m
Depth, main jib	d_3	1.0 m	$\Delta =$ 0.07	d_{3e}	1.07 m
Mass, king	m_1	168.5 kg	$\Delta =$ 0.05	m_{1e}	175.93 kg
Mass, main jib	m_2	130.0 kg	$\Delta =$ -0.01	m_{2e}	128.70 kg
Mass, knuckle jib	m_3	69.5 kg	$\Delta =$ -0.03	m_{3e}	67.42 kg

The purpose of this robustness analysis is to see how the different controllers behaves differently when this error is included. Due to the fact that the heave compensation part of this thesis is not directly affected by the dimensions of the crane the robustness analysis does not include heave error. Controller 1 and 2 were also neglected in this section considering their poor behavior. This leaves the surge and sway error for controller 3 and

4. The following sections provides the results from this robustness analysis, which can be seen in Appendix B.

When comparing the results with added errors with the original results one can easily observe that even small dimension errors gives a significantly different outcome. Having that said the tuning constants were not changed in the simulation in the robustness analysis. In a big picture the controllers behaves in a desirable way. In conclusion the model with added errors behaves quite the same as for the original system, but it has to be tuned slightly differently. This emphasises the importance of conduct a thorough tuning process even after the crane system is implemented in the crane, due to the risk of errors in the theoretical description of the crane.

6.5.1 Surge error with added dimension errors

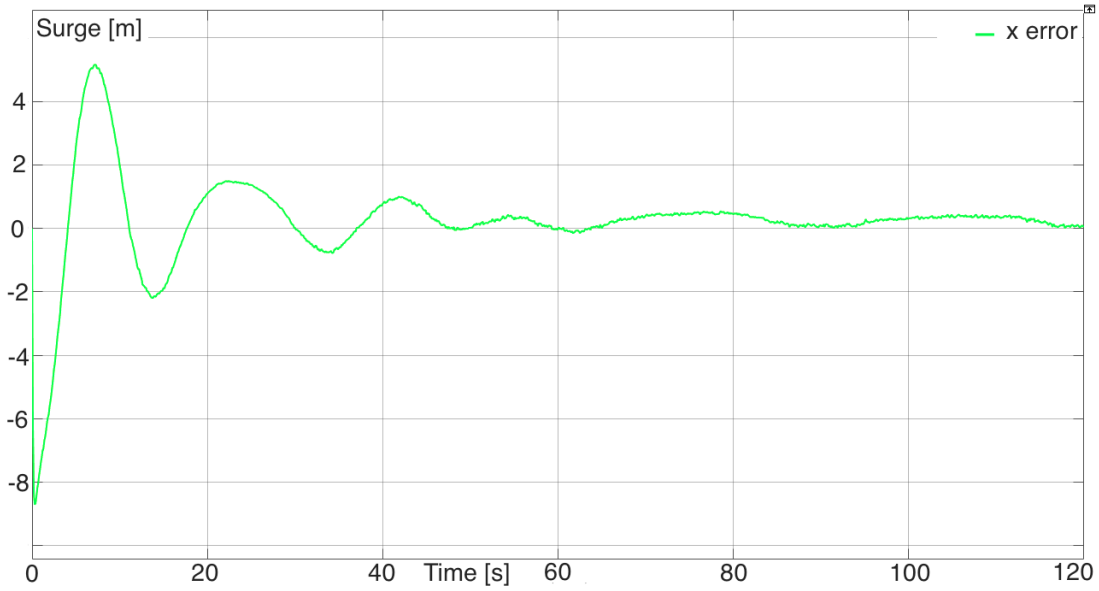

Figure 6.14: Surge error for controller 3 – PD control with gravity compensation with added dimension errors.

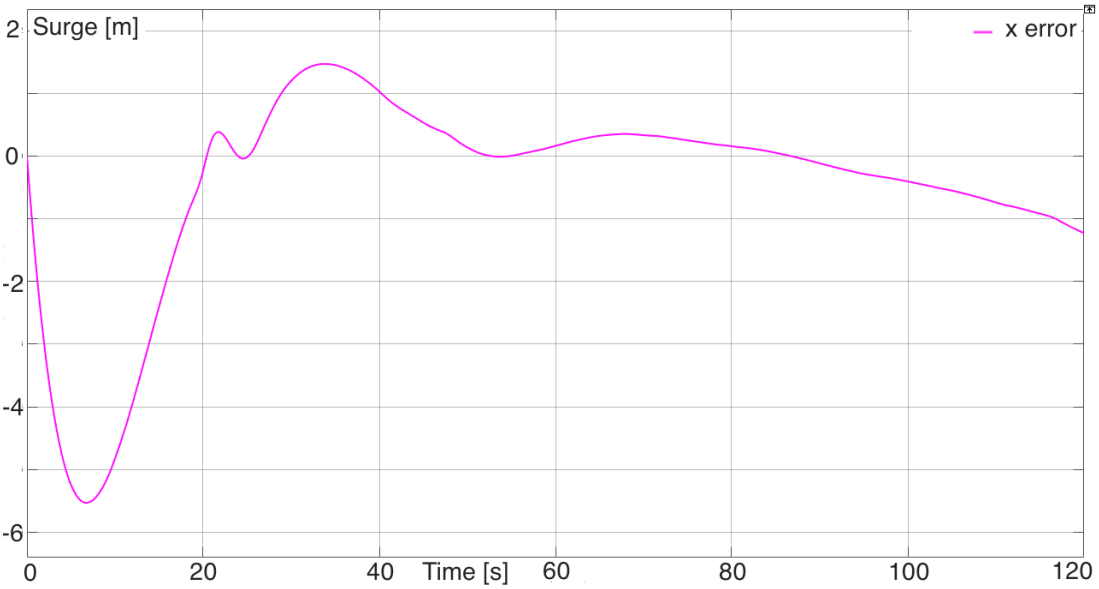

Figure 6.15: Surge error for controller 4 – Inverse dynamics control with added dimension errors.

6.5.2 Sway error with added dimension errors

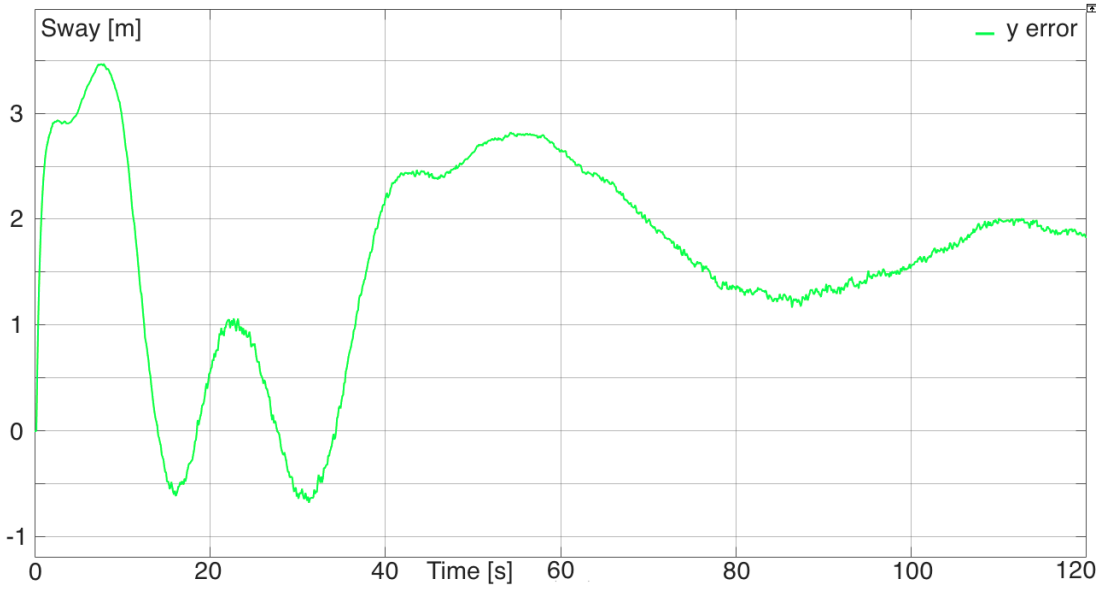

Figure 6.16: Sway error for controller 3 – PD control with gravity compensation with added dimension errors.

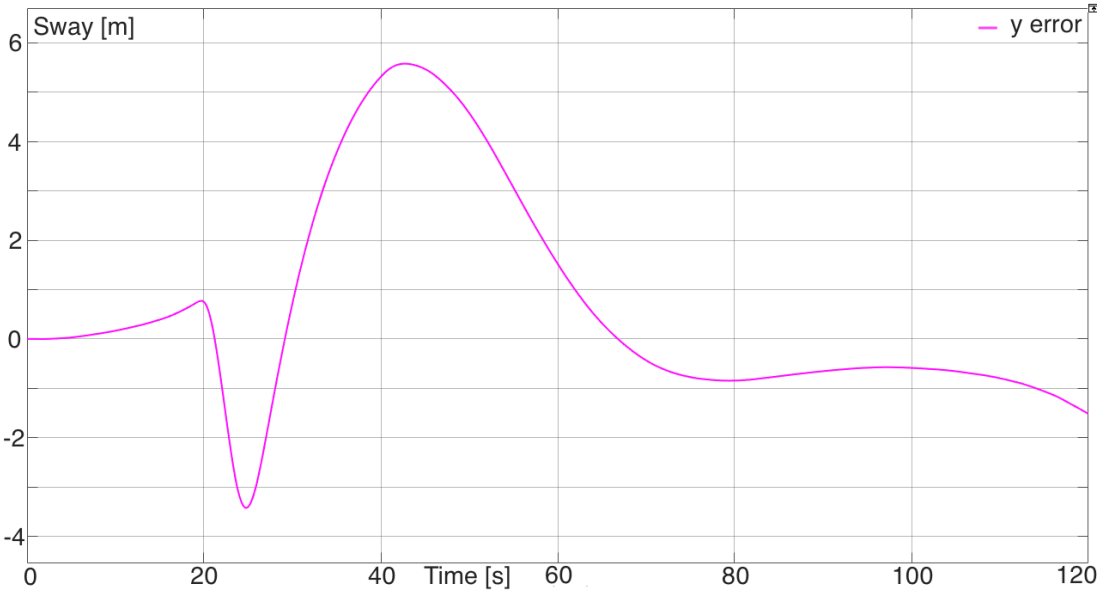

Figure 6.17: Sway error for controller 4 – Inverse dynamics control with added dimension errors.

7 Conclusion

In this thesis MacGregor's active heave compensated crane has been introduced mathematically and implemented in MATLAB. After this different controller strategies were presented, implemented in Simulink/MATLAB, simulated and compared. It is now time to discuss and conclude the results, give some advice for further studies and recommendations for MacGregor.

7.1 Conclusion

Today MacGregor compensate for wave influence using the wire only. In other words they compensate in heave direction only. One could question this decision considering the the impact the wave has on the xy-plane, especially when the crane carries out difficult tasks that require high precision. In their defence they stress the fact that the crane system is slow which makes it hard to control the fast wave movements. Additionally they argue with the natural slowness of the water. In the situations, in which need the highest precision, the payload are placed at the bottom of the ocean. This means that the water in itself dampens out the oscillations in the xy-plane. This is of course true, but after my two summers in MacGregor I was inspired to investigate the possibility to compensate for the movements in the xy-plane. If they could compensate for all directions they would be able to handle these difficult tasks at sea bottom with greater precision, resulting in less damage and fewer accidents. In addition it would result in a lower weather sensibility leading to more operating hours for the crane. It would also give the possibility to handle high precision tasks when the payload is above water, for instance during ship–to–ship tasks. As these issues were of interest to MacGregor, they asked me to investigate them further in my master's thesis.

In the interest of keeping their existing wire compensating system the heave movements are only compensated for by the wire. The xy-plane compensating part on the other hand had to be placed in the control system of the crane. With the huge, nonlinear hydraulic crane system in mind the choice of controller strategy became crucial. Since the desired task is specified in the operational space and requires precise control of the crane tip (end effector) motion it was decided to use operational space control methods. The alternative would have been joint space control methods, but they would not have been suitable for this system.

Four different operational space controller methods were chosen and compared. The first two controllers, Jacobian inverse control and Jacobian transpose control, are intuitive and nonmodel–based, hence they have their weaknesses. The main difference between these controllers is that the Jacobian inverse control uses the Jacobian inverse matrix to convert from Δp to Δq, while the Jacobian transpose uses the Jacobian transpose in addition to change the position of the matrix gain to achieve the same. This is explained in more detail in Section 5.3 and 5.4 respectively.

The last two controllers, PD control with gravity compensation and Inverse dynamics control, were model–based controllers which meant that the mathematical models were included in the control system. These two controllers were substantially equivalent to the first two controllers, except for the model part, as demonstrated in Section 5.5 and 5.6.

Considering the mentioned challenges of the system it was no surprise that the two simple controllers behaved strangely. As the results suggest they are not able to compensate for the wave movement at all in the surge and sway direction. In fact, for these controllers, it would be better to use the heave compensating only and ignore the surge and sway compensating part, which is exactly what MacGregor is doing at the moment. However it was useful to acquire this information in order to ignore these kinds of controller methods in the future.

Figure 7.1: The picture illustrates an amazed Solveig after realising that the xy-compensating part of the wave movements may actually work for MacGregor.

The main advantage of the two model–based controllers is that occurring model errors are cancelled out by the model inside of the control structure. This makes the system more solid and reliable. The results chapter (6) illustrate clearly the differences in the behavior of the nonmodel–based and the model–based controllers. For both the PD controller with gravity compensation and the Inverse dynamics controller one can observe that they compensate for the powerful wave movements. The errors in the surge and sway output are small enough to make sense of building further on this work. As can be seen in Figure 6.7, 6.8, 6.12 and 6.13 the Inverse dynamics controller behaved in total slightly better than the PD controller with gravity compensation.To be able to take advantage of this, additional studies would be required. This was addressed in Section 7.2, but I'm quite surprised and excited by these results (Figure 7.1).

Because there has been no prior investigation of this, a critical approach to the result is appropriate. There are several factors that can question the outcome of this thesis. Here are some of the assumptions, simplifications and sources of error that are directly or indirectly affecting the result:

- The cable is modeled as stiff when it actually is flexible. If the system had been modeled with a flexible cable the result would have been worse.
- The crane is modeled as a rigid-body system even though the crane is softer than a rigid body. It is hard to tell how this would have affected the outcome.
- The drum is simplified. This only affects the heave compensating part, where MacGregor already have a suitable system.
- Friction is neglected. If included the result had most likely been worse.
- Joint angle limitations are not included in the simulations. This affected controller 1 and 2 only.
- Dimensions may have some deviations from the actual crane. The robustness test gives an indication of how this affects the results.
- The tuning process need to be more thorough before it can provide more certain answers.
- This is a theoretical thesis. One can never know for sure how a physical system will behave in real life.

The dimensions used in this thesis are collected from the AutoCAD drawing included in Appendix A. Unknown errors may have occurred while extracting this information. In addition one can always assume some deviations in the actual physical dimensions compared to the planned drawing, caused by various reasons. The robustness analysis in Section 6.5 was therefore done to illustrate the importance of the tuning process. Differences discovered when adding the errors mentioned above to the simulations can be cancelled out by changing the tuning parameters. Hence one must stress the importance of tuning the controllers when the crane is on site and ready for delivery.

Though the factors above brings about uncertainty concerning the results, I am sure they will provide MacGregor with ideas and inspiration on how to improve their system.

7.2 Further study and recommendations

Before any of the work done in this thesis are set in motion one has to go through all of the mathematics, the programming and implementing parts to make sure that there are no significant errors. In other words one has to perfect the system, the tuning process included. Even though much time was spent tuning the controllers, there may be room for improvements.

When the system is theoretically perfected one of the software engineers at MacGregor should investigate the controller systems and look at possible ways of implementing it into their system. As Section 7.1 emphasizes the first two controllers will not behave satisfactory for this system, so the engineer should not even consider these. Both of the two model–based controllers should on the other hand be studied. Although the last one behaves most desirable in theory one can never know how it will in reality. Besides it is really important for MacGregor that the chosen controller design fits into their existing system.

While the software engineer investigates the controllers there are several factors to consider. As mentioned above it should be possible to implement the control system in a preferable way in their existing system. It is also important that the program implemented is fast enough and worth the time and resources spent. Additionally the engineer should do some research on how this new control system could affect the crane negatively and if necessary study.

Finally, when these questions are answered they can program the chosen controller in

Figure 7.2: The final step in concluding if MacGregor should compensate for the wave influence upon the xy–plane is to tune the system inside the crane. This picture presents my self testing the crane last summer.

Simatic Step 7. After this new implementation they will have to perfect the tuning parameters even more on site as illustrated in Figure 7.2. I would also recommend, in light of the robustness analysis, creating a tuning manual for the test engineers. This way the test engineer can easily compensate for possible real life dimension errors.

Bibliography

Beggs, J. S. (1983). *Kinematics*. Hemisphere Publishing Corporation.

Crowder, R. M. (2016). Automation and robotics. *http://www.southampton.ac.uk/ rmc1/robotics/artactile.htm*. [Online; accessed February 21, 2016].

Deo, A. S. and Walker, I. D. (1995). Overview of Damped Least-Squares Methods for Inverse Kinematics of Robot manipulators. *Department of Electrical and Computer Engineering, Rice University, Houston TX 77251, U.S.A. Journal of Intelligent and Robotic Systems* ***14****: 43-68*.

Fossen, T. I. (2011). *Handbook of Marine Craft Hydrodynamics and Motion Control*. Wiley.

Kongsberg (2016). Motion reference unit. *http://www.km.kongsberg.com/*. [Online; accessed March 15, 2016].

McCarthy, J. M. and Soh, G. S. (2010). *Geometric Design of Linkages*. Springer, New York.

Nakamura, Y. and Hanafusa, H. (1986). Inverse kinematic solutions with singularity robustness for robot manipulator control. ASME J. D*ynamic* S*ystems,* M*easurement and* C*ontrol* ***108****: 163-171*.

Paul, R. (1981). *Robot manipulators: mathematics, programming, and control : the computer control of robot manipulators*. MIT Press, Cambridge, MA. ISBN 978-0-262-16082-7.

Scantrol (2015). Ahc technology. *http://www.scantrol.com/scantrol-ahc-4*. [Online; accessed January 27, 2016].

Sciavicco, L. and Siciliano, B. (1996). *Modeling and Control of Robot Manipulators*. McGraw-Hill International Editions, Electrical Engineering Series.

Siciliano, B., S. L. V. L. O. G. (2009). *Robotics - Modelling, Planning and Control*. Springer-Verlag London Limited 2010.

A Crane AutoCAD drawing

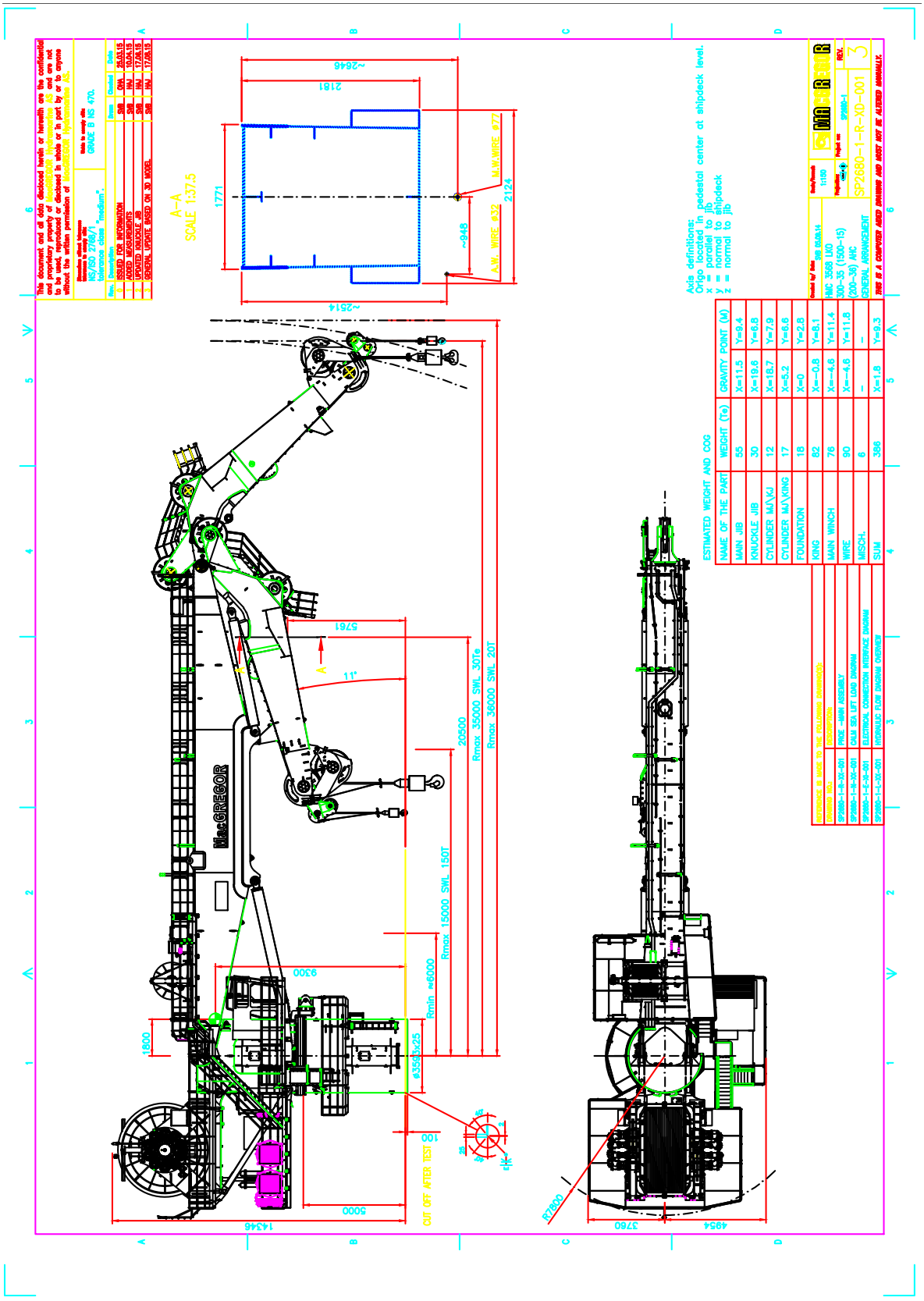

Figure A.1: AutoCAD drawing of the crane's dimensions given by MacGregor Norway AS. The numerical data used in the MATLAB file in Appendix B was found by examine this AutoCAD drawing.

B MATLAB/Simulink

B.1 Simulink

In the electronic appendix B one can find the Different Simulink and MATLAB files used in this thesis. The initial values used in these files are also included.

C Datasheet MRU H

MRU H

KONGSBERG

March 2014

THE VERSATILE HEAVE COMPENSATOR

This fifth generation MRU is specially designed for heave compensation applications.

Typical applications
The MRU H is specially designed for motion measurements in marine applications requiring highly accurate heave measurements in environments with extreme horizontal accelerations. This MRU is an ideal sensor for roll, pitch and heave compensation of offshore cranes and echo sounders. The MRU H can also be used on typical ship motion monitoring applications such as helideck motion monitoring, hydroacoustic positioning systems, as well as hull stress monitoring.

Function
The MRU H incorporates three highly accurate accelerometers and three Micro-Electro-Mechanical-Structures (MEMS) angular rate gyros. This unit achieves high reliability by using solid state sensors with no rotational or mechanical wear-out parts.

The unit is delivered with Windows based configuration and data presentation software. In this software vector arms from where the MRU is mounted to center of gravity (CG) and two individually configurable monitoring points (MPs), can be defined. The heave measurements can be output in four different locations (the MRU itself, CG, MP1 and MP2) simultaneously on serial lines or Ethernet port. Typical monitoring point is the transducer head or the crane tip.

Output variables
The MRU H outputs roll, pitch and heave together with linear acceleration in 3-axes. The MRU H outputs heave position, velocity and accelerations in adjustable frames. In addition roll and pitch angles and corresponding angular rate vectors are output.

External inputs
The MRU H accepts input of external speed and heading information on separate serial lines or Ethernet for improved accuracy in heave, roll and pitch during turns and accelerations. For time synchronization the MRU accepts 1-second time pulse (1PPS) input on a TTL line (XIN) or as RS-232/422 signal.

Digital I/O protocols
For this fifth generation MRU data is available through both Ethernet interface and serial lines enabling easy distribution of MRU data to multiple users on board the vessel. Output protocols for commonly used survey equipment are available on two individually configurable serial lines and Ethernet/UDP.

Figure C.1: (1/2) Datasheet of Kongsberg Maritime's MRU H(Kongsberg, 2016).

FEATURES MRU H

- High accuracy heave measurements even in dynamic environments
- Outputs on RS-232, RS-422 and Ethernet
- High output data rate (200 Hz)
- Precise heave at long wave periods by use of PFreeHeave® algorithms
- Lever arm compensation to two individually configurable monitoring points
- Meets IHO special order requirements
- Small size, light weight and low power consumption
- No limitation to mounting orientation
- Each MRU delivered with Calibration Certificate
- Selectable communication protocols in the Windows based MRU configuration software
- 2-year warranty

TECHNICAL SPECIFICATIONS

ROLL AND PITCH OUTPUT

Angular orientation range	±180°
Angular rate range	±100 °/s
Resolution roll, pitch	0.001°
Angular rate noise	0.1 °/s RMS
Static[2] accuracy	0.04° RMS
Dynamic[1] accuracy (for a ±5° amplitude)	0.05° RMS
Scale factor error	0.2 % RMS

HEAVE OUTPUT

Output range	±50 m
Periods (real-time)	0 to 25 s
Periods (delayed)	0 to 50 s
Heave accuracy (real-time)	5 cm or 5 %, whichever is highest
Heave accuracy (delayed)	3 cm or 3 %, whichever is highest

ACCELERATION OUTPUT

Acceleration range	±30 m/s2
Acceleration noise[2]	0.002 m/s2 RMS
Acceleration accuracy	0.01 m/s2 RMS

ELECTRICAL

Power requirements	10 to 36 V DC, max. 12 W
Serial ports:	
Com1	Bidirectional RS-422
Com2	Bidirectional RS-422 from junction box, user configurable RS-232, RS-422
Com3 & Com4	Input only, user configurable RS-232, RS-422
Analog channels (junction box)	# 4, ±10 V, 14 bit resolution

Specifications subject to change without any further notice.

Ethernet ports	Three output and one input
Ethernet UDP/IP	10/100 Mbps
Digital output variables	24 (max), serial or Ethernet
Output data rate (max)	200 Hz
Timing	<1 ms

ENVIRONMENTAL SPECIFICATIONS

Temperature range	-5 °C to +55 °C
Humidity range, electronics	Sealed, no limit
Enclosure protection	IP-66
Vibration	IEC 60945/EN 60945

ELECTROMAGNETIC COMPATIBILITY

Compliance to EMCD, immunity/emission	IEC 60945/EN 60945

OTHER DATA

MTBF (computed)	50000 h
Housing dimensions	Ø 105 x 140 mm (4.134" x 5.525")
Material	Anodised aluminium
Weight	2.4 kg
Connector	Souriau 851-36RG 16-26S50

DATA OUTPUT PROTOCOLS

- MRU normal	- Atlas Fansweep
- NMEA proprietary	- TSS1
- Sounder	- Seapath binary 23
- EM3000	- PFreeHeave®

1) When the MRU is exposed to a combined two-axes sinusoidal angular motion with 10 minutes duration.

2) When the MRU is stationary over a 30-minute period.

www.km.kongsberg.com/seatex
E-mail: km.seatex@kongsberg.com
Telephone: +47 73 54 55 00
KONGSBERG

Figure C.2: (2/2) Datasheet of Kongsberg Maritime's MRU H(Kongsberg, 2016).

D Datasheet Elctrical Motor

ABB Oy Motors & Generators	Classifying code or document type PERFORMANCE DATA OF MOTOR	

Department/Author	Date of issue	Lang.	Rev. date	Our ref.
	3/24/2014	En		WLU190314A04-1-A_Peter2

Customer ref.	Saving Ident	Rev./Changed by	Pages
WLU190314A04/1/A	WLU190314A04-1-A_Peter2	A	1/2

Driven Motor:

Motor type code		M3BP 355LKB 4G		
Motor type		Squirrel cage Motor		
Mounting designation		IM V3		
Protected by enclosure		IP 56		
Method of cooling		IC 411		
Insulation		Class F		
Standards		IEC		
Classification		ABS		
Ambient temperature, max.		50 °C		
Altitude, max.		1000 m.a.s.l.		
Duty type		S1		
Temp. rise		Class F		
Connection of stator winding		Delta		
Rated output		550 kW		
Voltage		690 V		
Frequency		60 Hz		
Speed		1789 rpm		
Current		549 A		
Relat. starting current		7.0		
Relat. starting torque		2.2		
Relat. maximum torque		2.4		
No load current		145 A		
Rated torque		2935 Nm		
Load characteristics	Load %	Current A	Efficiency %	Power Factor
	100	549	96.4	0.87
	75	419	96.4	0.86
	50	301	95.9	0.80

All Motor data is subject to tolerances in accordance with IEC.
Efficiency based on typical additional load losses acc. measurements based on IEC 60034-2-1: 2007.

Figure D.1: (1/2) Datasheet of electrical motor.

ABB Oy Motors & Generators	Classifying code or document type PERFORMANCE DATA OF MOTOR			
Department/Author	Date of issue 3/24/2014	Lang. En	Rev. date	Our ref. WLU190314A04-1-A_Peter2
Customer ref. WLU190314A04/1/A		Saving Ident WLU190314A04-1-A_Peter2	Rev./Changed by A	Pages 2/2

Motor type code: M3BP 355LKB 4G

Rated output	550 kW	Power Factor	0.87
Voltage	690 V	Rated torque	2935 Nm
Frequency	60 Hz	Relat. starting current	7.0
Speed	1789 rpm	Relat. starting torque	2.2
Current	549 A	Relat. maximum torque	2.4

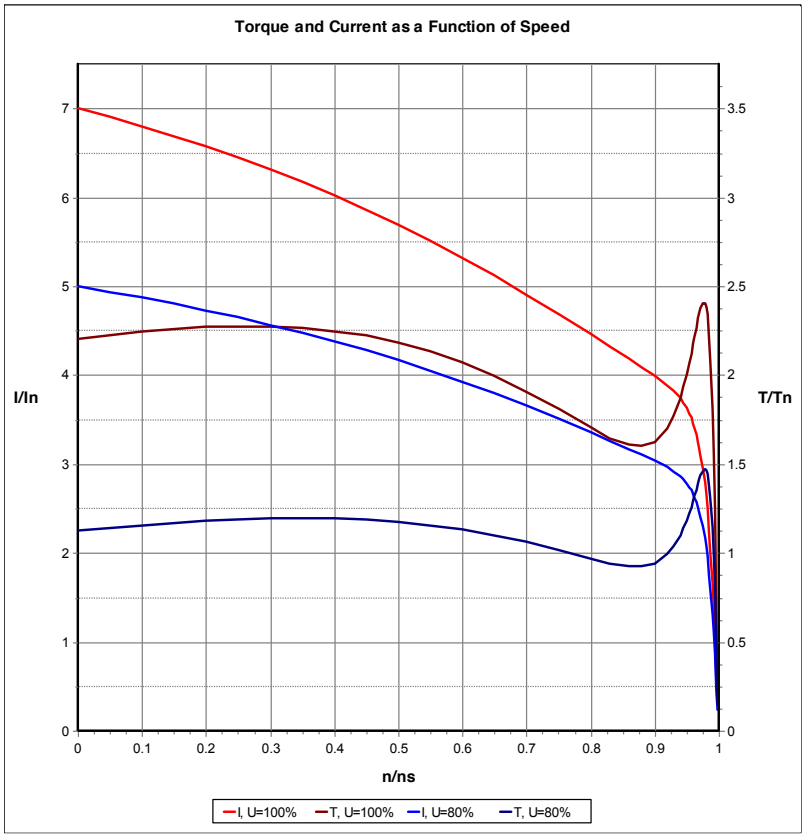

Figure D.2: (2/2) Datasheet of electrical motor.

E Joint Angles

The joint angles of the first two controllers exceeds the cranes limitations, illustrated in Figure E.1 and E.2. If these controllers had behaved better the crane's limitations would have to be included. Due to the fact that the joint angles of two last and best controllers were inside of the crane's limitations and time limitations this was not prioritized.

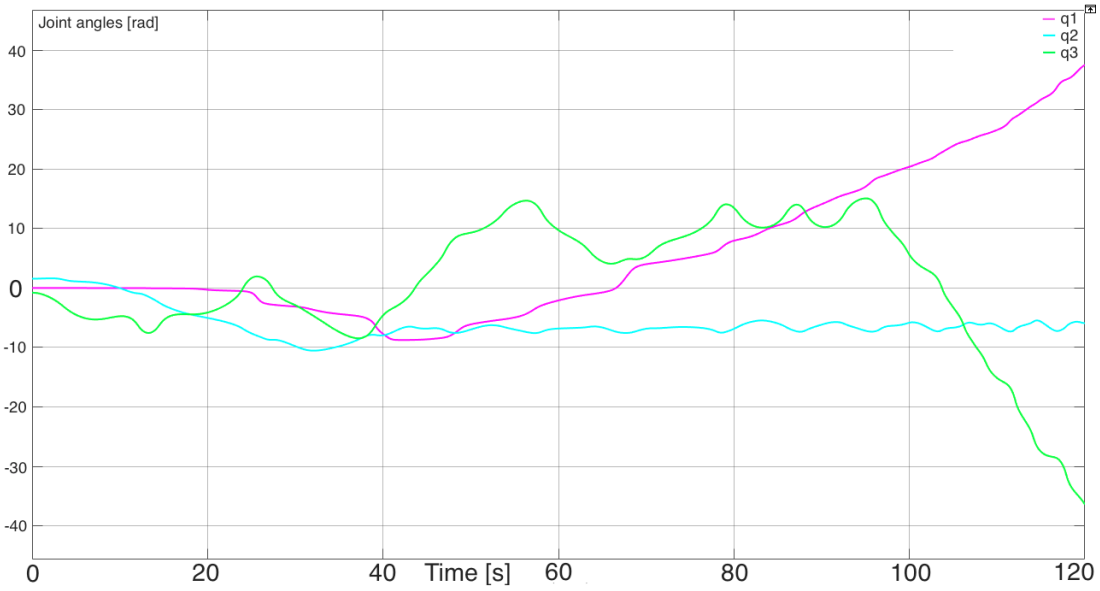

Figure E.1: Joint angles for controller 1 - Jacobian inverse control.

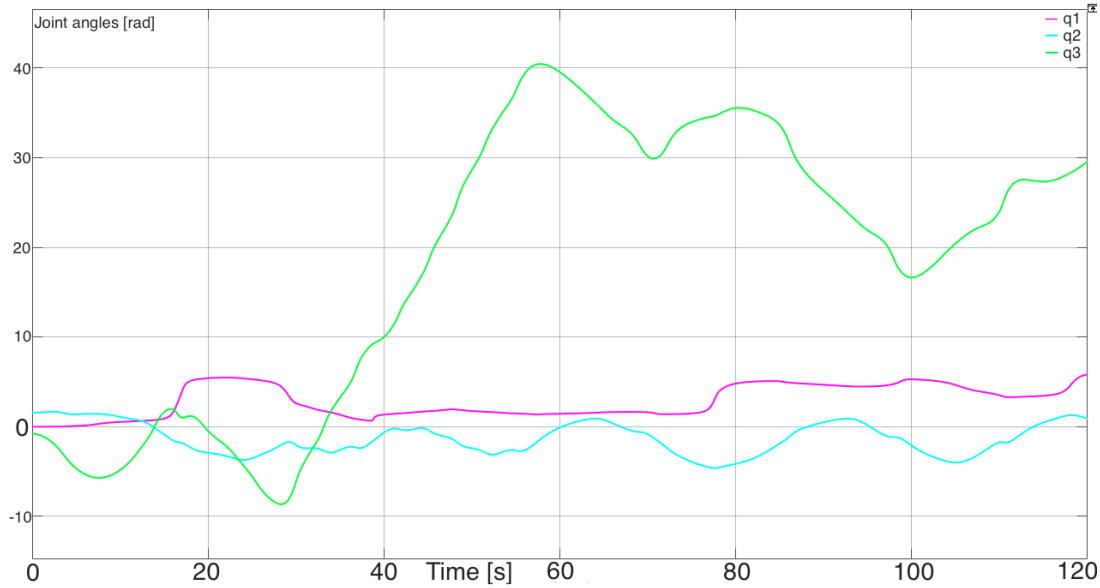

Figure E.2: Joint angles for controller 2 - Jacobian transpose control.

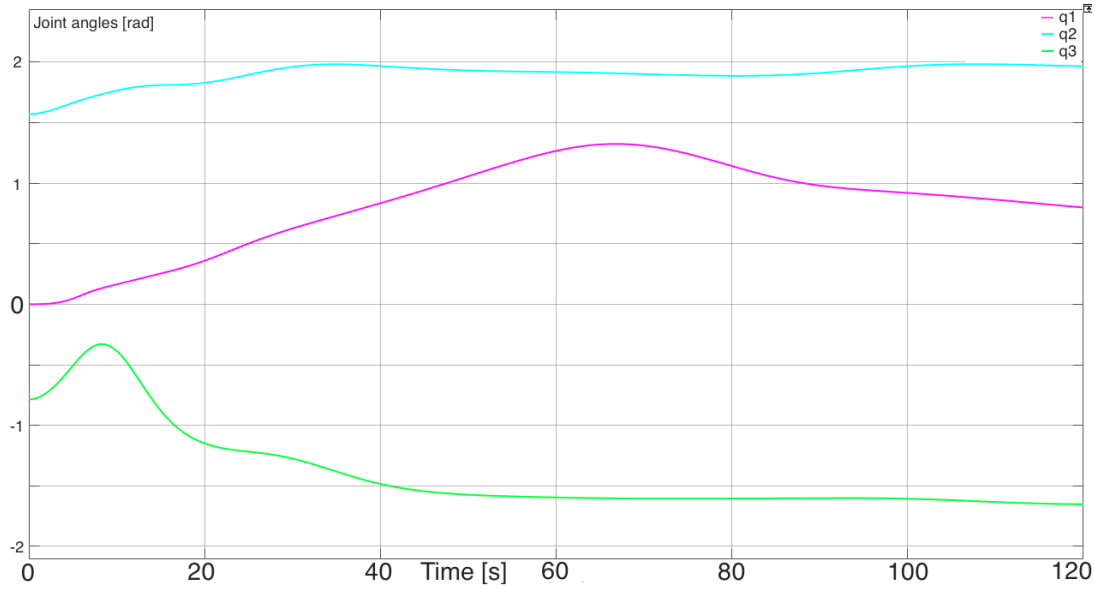

Figure E.3: Joint angles for controller 3 – PD control with gravity compensation.

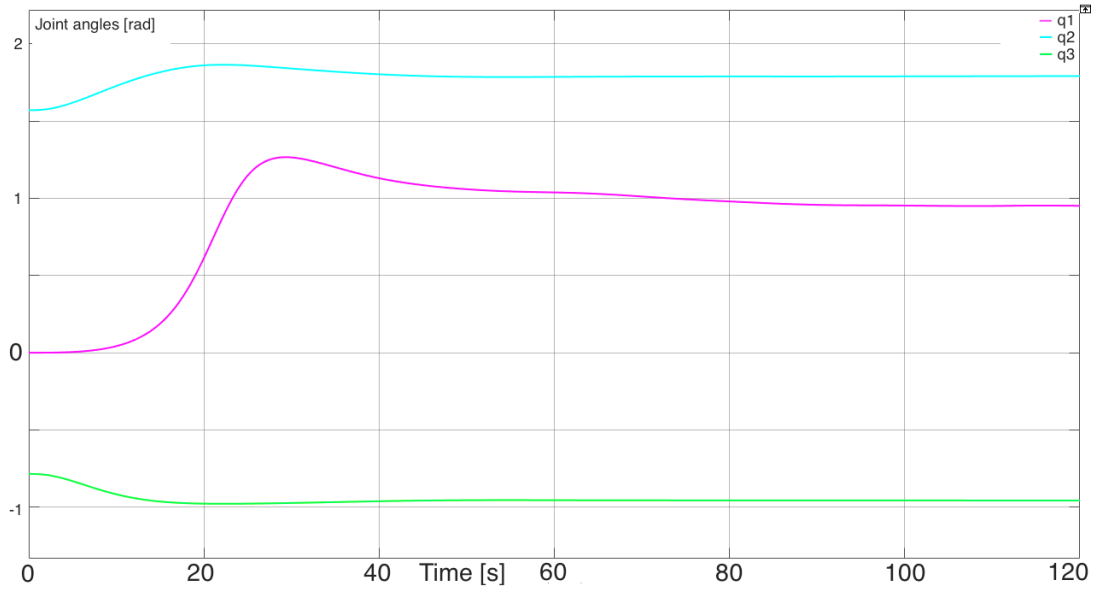

Figure E.4: Joint angles for controller 4 – Inverse dynamics control.

F Torques

The torque values during the simulations illustrates how badly the nonmodel–based controllers worked. Figure F.1 and F.2 shows these values which would not be possible for the crane to carry out. This is partly due to the missing joint angle limitations, but the simulations would have been worse if the limitations were implemented. The torque values of the last two controllers illustrated in Figure F.1 and F.1 shows that these torque values are fine.

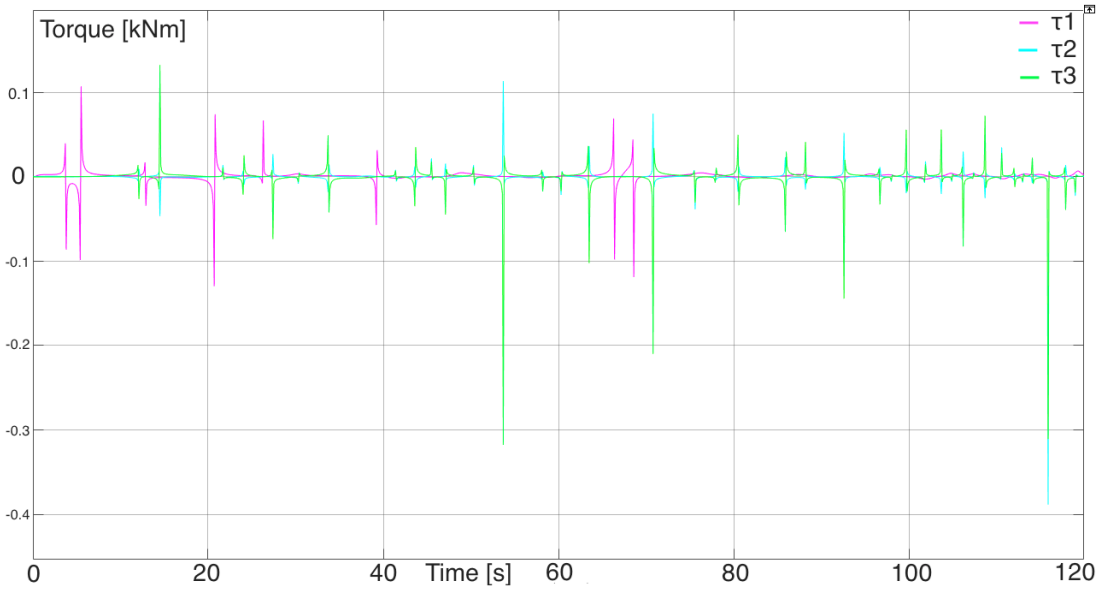

Figure F.1: Torques for controller 1 – Jacobian inverse control.

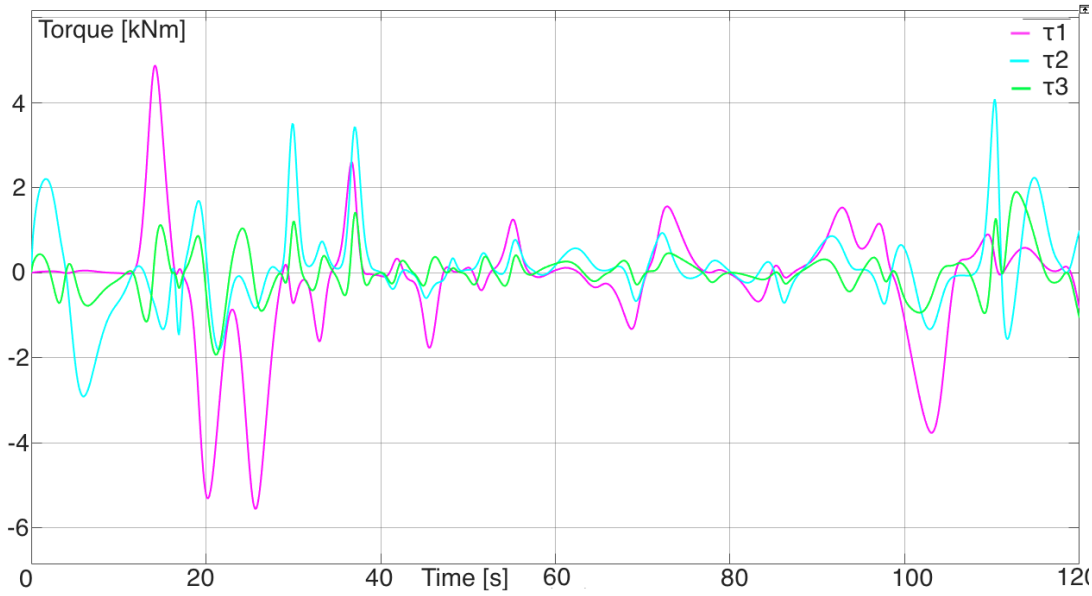

Figure F.2: Torques for controller 2 – Jacobian transpose control.

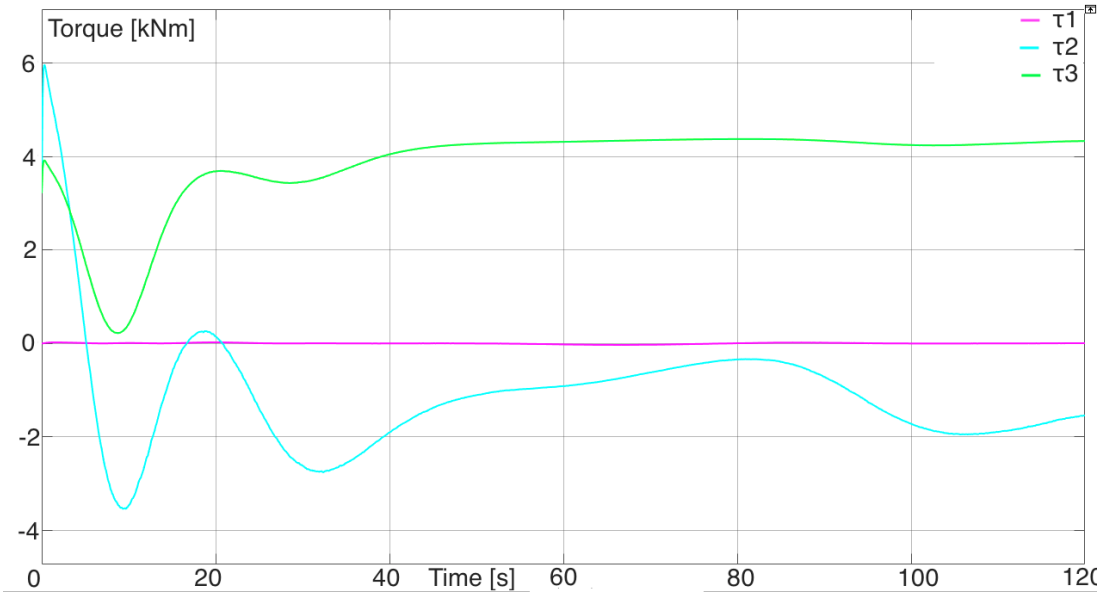

Figure F.3: Torques controller 3 – PD control with gravity compensation.

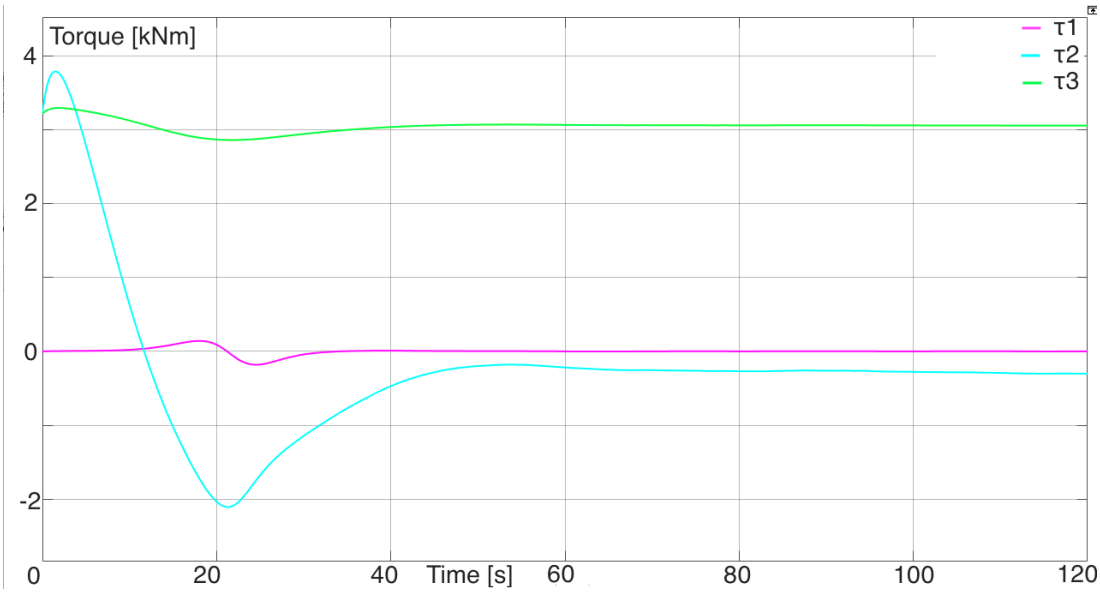

Figure F.4: Torques controller 4 – Inverse dynamics control.